

THE APPLICATION OF MICROELECTRODES TO THE STUDY

OF THE Li/Li<sup>+</sup> COUPLE IN ETHER SOLVENTS

by

William Michael Hedges

A thesis submitted for the degree of

MASTER OF PHILOSOPHY

November, 1984

Department of Chemistry,  
University of Southampton.

*TO MY PARENTS*

UNIVERSITY OF SOUTHAMPTON

ABSTRACT

FACULTY OF SCIENCE

CHEMISTRY

Master of Philosophy

THE APPLICATION OF MICROELECTRODES TO THE  
STUDY OF THE Li/Li<sup>+</sup> COUPLE IN ETHER SOLVENTS

by William Michael Hedges

Copper, nickel, carbon and aluminium disc microelectrodes (radii 5-50  $\mu\text{m}$ ) have been used to study the deposition and dissolution of lithium metal in ether solvents (tetrahydrofuran, 2-methyltetrahydrofuran, diethyl ether and dioxolane) each containing LiAsF<sub>6</sub> or LiBF<sub>4</sub>. It has been shown that high quality, reproducible data, free of effects due to IR drop may be obtained even in these low dielectric constant solvents.

Cyclic voltammetric and potential step techniques have been used to study the kinetics of the Li/Li<sup>+</sup> couple on a freshly deposited lithium surface. At room temperature and in THF/LiAsF<sub>6</sub> (0.56 mol dm<sup>-3</sup>) the data shows the couple to be quite rapid and the exchange current density was estimated to be 5.4 mA cm<sup>-2</sup>. The kinetics depend unusually strongly on the temperature.

It is suggested that a freshly deposited lithium surface, maintained at negative overpotentials is free of any surface films because it is continually being covered by fresh lithium layers. However, double potential step experiments have shown that a film does form on the lithium surface relatively quickly as soon as the electrode is allowed to stand on open circuit.

The mechanism and kinetics of the nucleation and growth of lithium metal on a copper substrate was probed by potential step experiments and well defined rising I-t transients were recorded. Analysis of the shape of these transients suggests that the lithium deposition occurs via the progressive nucleation of metal centres which grow three dimensionally under diffusion control.

The electrochemical alloying of lithium in aluminium has also been studied using cyclic voltammetric and potential step techniques. The low rate of diffusion of lithium atoms in the aluminium lattice is shown to be a determining factor of the kinetics of the LiAl/Li<sup>+</sup> couple. The nucleation and growth of lithium centres has been shown to be the initial step in the deposition of lithium onto aluminium.

The deposition of relatively thick lithium deposits, 50  $\mu\text{m}$ , onto copper and nickel macroelectrodes has been studied as a function of plating current density.

### Acknowledgements

I wish to express my sincerest appreciation and gratitude to Dr. D. Pletcher to whom I am greatly indebted, not only for providing me with an opportunity to work within his research group, but also for his excellent supervision and constant encouragement throughout this work. His "speedy" advice, inspiration and, most importantly, help, especially during the later stages of this work, will never be forgotten.

Research, today, is an expensive pastime(!) and in this respect I would like to extend my gratitude once again to Dr. D. Pletcher along with Professor M. Fleischmann, Professor G. Luckhurst and the Chemistry Department for putting their faith in me and providing me with the financial support necessary to undertake this work.

I would like to express my many thanks to the staff at the G.E.C. Battery Group, Hirst Research Centre and, in particular, Dr. C. Gosden and Dr. M. Hayes. This is not only for their provision of the argon filled dry box (without which this work would have been impossible) but also for giving me a practical introduction and insight into the workings of lithium batteries during my short, yet pleasant, stay with them.

At this stage I wish to express my most heartfelt gratitude and respect to my parents for their continued love and support throughout my academic career so far. They have never ceased to encourage me, despite, what seems to me, the almost insurmountable problems faced when raising four boys, such as myself.

I would also like to thank Shirley for her continued support and the abundant love that she has shown me during my work in Southampton.

Many thanks are also extended to all of my friends and colleagues both in Southampton and at home with whom all of my "spare" time has been memorably spent.

Finally, I would like to express my many, many thanks to Mrs K. Welfare for transforming, in record time by her care and typing skills, a very grubby report into this epic manuscript.

*Bill Hedges, November, 1984.*

## CONTENTS

### Chapter One

#### Introduction

<u>Section</u>		<u>Page No.</u>
1.0	The need for new battery systems	1
1.1	Lithium batteries	3
1.1.1	Positive electrode materials	3
1.1.2	Electrolytes	6
1.1.3	Problems associated with lithium batteries	8
1.2	Introduction to the aims of this work	11
1.3	The theory of metal deposition	11
1.3.1	The early stages of growth	11
1.3.2	The later stages of growth	13
1.4	The electrochemical deposition and dissolution of lithium metal	15
1.4.1	Solvents and lithium salts	15
1.4.2	Cycling of the lithium electrode	21
1.4.3	Kinetics of the lithium metal/lithium ion couple	25
1.4.4	The lithium-aluminium electrode	27
1.4.5	Lithium metal underpotential deposition	30
1.5	Microelectrodes	31

### Chapter Two

#### Experimental

2.1	Cells	37
2.2	Electrodes	37
2.3	Electrode polishing	46
2.4	Sources and treatment of chemicals	47

<u>Section</u>		<u>Page No.</u>
2.5	Instrumentation	50
2.6	The argon filled dry box	51
2.7	Experimental procedure	55

### Chapter Three

#### Results and Discussion

3.1	Deposition and dissolution of lithium using a copper microelectrode in a solution of $\text{LiAsF}_6$ /THF at room temperature	58
3.1.1	Cyclic voltammetry	59
3.1.2	Underpotential deposition	66
3.1.3	Linear potential sweep to high negative overpotentials	69
3.1.4	Potential steps to negative overpotentials	71
3.1.5	Double potential steps to study the dissolution of lithium	77
3.1.6	Analysis of the steady state currents as a function of overpotential	86
3.1.7	The nucleation and growth of lithium	92
3.1.8	Film formation on a freshly deposited lithium surface	101
3.2	Variation of the electrode material and its effect on the THF/ $\text{LiAsF}_6$ system	107
3.2.1	25 $\mu\text{m}$ radius aluminium microelectrode	107
3.2.2	25 $\mu\text{m}$ radius nickel microelectrode	116
3.2.3	4 $\mu\text{m}$ radius carbon microelectrode	116
3.3	Influence of temperature on the THF/ $\text{LiAsF}_6$ system	119

<u>Section</u>		<u>Page No.</u>
3.3.1	40 $\mu\text{m}$ radius copper microelectrode	119
3.3.2	25 $\mu\text{m}$ radius aluminium microelectrode	120
3.4	Variation of solvent and electrolyte salt	126
3.4.1	Variation of solvent	126
3.4.2	Variation of lithium salt	128
3.5	Galvanostatic deposition of lithium onto copper and nickel macro- electrodes	128
<u>Chapter Four</u>		
	Conclusions	131

CHAPTER ONE

INTRODUCTION

## INTRODUCTION

### 1.0 The need for new battery systems

During the last thirty years, the electronics industry has undergone an unprecedented technical expansion resulting in a whole variety of military and commercial products, many of which are in constant use in our lives and are now taken for granted. In particular, the tendency towards ever smaller devices has led to a vast range of portable electronic instrumentation, all of which requires some form of stored power, usually a battery. Conventional dry cells are too large and their performance decays on storage and hence do not meet the major requirements of these new devices; high energy density and long shelf life. The "ideal" battery system would have both of these properties with the additional property of being rechargeable.

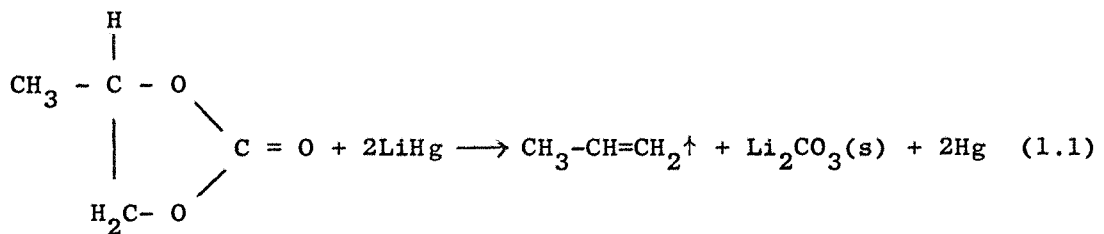
Although many theoretically interesting couples can be considered, thermodynamic data<sup>1</sup> suggests that lithium would be the best choice of negative electrode material. For example, a Li/F<sub>2</sub> cell has a theoretical voltage of 6.1V and an energy density of 6250 Wh kg<sup>-1</sup> compared to the realised voltage of 1.5V and energy density of 90 Wh kg<sup>-1</sup> for a Zn/MnO<sub>2</sub> cell. Beryllium offers an attractive energy density, although it has generally been ignored due to its toxic properties. Aluminium is another candidate but its dissolution and deposition present even more difficulties than lithium.

For a long time, however, no progress was made due to the non-availability of materials compatible with the lithium metal. The choice of electrolyte, in particular, presented many problems. Molten salt electrolytes were considered but for ambient temperature purposes these are obviously unsuitable. The problem stems from the high chemical reactivity of the lithium metal. Solvents containing any form of labile hydrogen are totally unsuitable due to the problem of hydrogen evolution. This criteria obviously

rules out water, organic acids, amines, amides and alcohols, but also solvents such as ketones due to keto-enol tautomerism. Studies were therefore directed to aprotic solvents, particularly ethers which were thought to be stable towards the alkali metals. It was also recognised, however, that their dielectric constants are low and therefore the conductivities of any electrolytes prepared from them were likely to be poor.

Interest in the development of high energy density lithium batteries was only rekindled after it had been demonstrated<sup>2</sup> that metallic lithium could be deposited from organic electrolytes comprising lithium salts dissolved in organic solvents such as propylene carbonate (PC). Cyclic esters (see table 1.2) such as PC and  $\gamma$ -butyrolactone (BL) were found to dissolve a variety of lithium salts to provide a reasonably conducting medium in which metallic lithium appeared to have some stability.

It was, however, shown by Dousek et al<sup>3</sup> that PC is unstable to Li amalgam, forming propene and lithium carbonate.



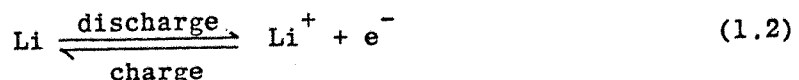
The apparent stability of lithium in PC was, in fact, found<sup>4</sup> to be due to a film on its surface, probably composed of  $\text{Li}_2\text{CO}_3$ , which protects the bulk metal from further chemical attack. In the case of the lithium amalgam a fresh surface of lithium is continually being exposed to the PC and so chemical reaction can occur. More recently, it has been suggested<sup>5</sup> that even on a purely thermodynamic basis, all of the aprotic solvents in use in lithium batteries can be reduced by Li. The importance of the anode film to the battery industry is thus stressed and has led Dey<sup>6</sup> to comment: "It is accurate to state that the success of all the commercially promising

(ambient temperature) liquid electrolyte lithium batteries (as opposed to solid electrolyte batteries) rests solely on this protective Li anode film". The evidence that lithium metal is thermodynamically unstable in ether solvents is, however, weak and the film which is undoubtedly formed may rather be due to reactions with the anion of the lithium salt or trace water in the solvent. This anode film, as well as a consideration of the anode kinetics and the influence of the film on them will be discussed later in more detail.

### 1.1 Lithium batteries

As soon as suitable, compatible components had been found, the development began of high energy density batteries, based on lithium electrodes. It quickly became apparent that a whole range of solvent/lithium salt combinations were possible and these will be discussed later. The choice of positive electrode materials is even broader and it is now possible to choose a cathode which is virtually tailor made to a particular requirement.

Despite the many possible positive electrode materials and electrode reactions that are available, the negative electrode reaction in Li batteries is always the dissolution of lithium metal during discharge (Equation 1.2)



The  $\text{Li}^+$  ions pass into the electrolyte whilst the electrons so released move around the external circuit, via a load, to the positive electrode. The reaction which occurs at the positive electrode obviously depends on the choice of electrode material.

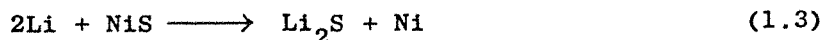
#### 1.1.1 Positive Electrode Materials

The range of positive electrode materials which may be used in lithium batteries is continually increasing. An excellent

review of many of these can be found in reference 1. It is possible to divide them into three main categories according to their corresponding cell reactions:

(i) Direct reduction of the cathode

An example is found in the Li/LiClO<sub>4</sub> in PC/NiS cell in which the NiS is reduced to give nickel metal and sulphide ion which associates with the Li<sup>+</sup> ions. The overall cell reaction is thus

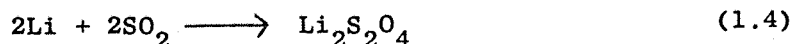


A quite different example is found in the use of poly-acetylene as the cathode material. It is normally used in an oxidised state, by doping it with an oxidising agent such as bromine or electrochemically so that the material is (CH)<sub>x</sub><sup>δ+</sup> X<sup>-</sup> where X<sup>-</sup> is AsF<sub>6</sub><sup>-</sup>, ClO<sub>4</sub><sup>-</sup>, etc<sup>7</sup>.

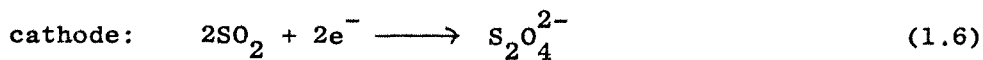
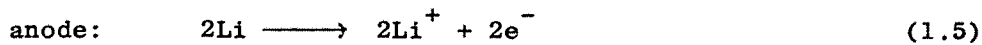
(ii) Reduction of a component of the electrolyte

This type of cell has proven to be the most popular choice for ambient temperature uses where medium to high current densities are required.

One such example is the Li/LiBr, acetonitrile, SO<sub>2</sub>/C cell. In this cell, liquid SO<sub>2</sub> is used as a co-solvent and also as the cathode depolarizer. To prevent SO<sub>2</sub> leakage the cell has to be pressurised. This cell illustrates the decisive importance of the protective film which prevents the strongly exothermic reaction between lithium and SO<sub>2</sub> occurring. Unprotected lithium would also react with the acetonitrile. The film is formed as a result of the spontaneous reaction of lithium with the SO<sub>2</sub> to give lithium dithionite which coats the lithium anode, equation 1.4.



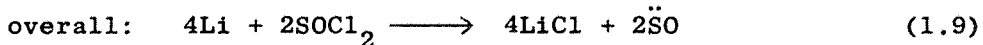
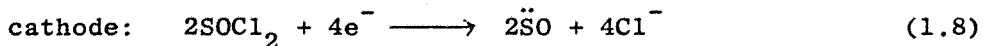
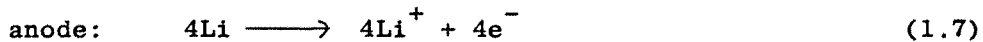
The cell reactions have been established<sup>6</sup> as:-



Thus the overall cell reaction is the same as equation 1.4. The  $\text{Li}_2\text{S}_2\text{O}_4$  is insoluble in the electrolyte and precipitates in the porous carbon cathode. Eventually the cathode itself becomes passivated by the  $\text{Li}_2\text{S}_2\text{O}_4$  and this marks the end of the useful life of the cell.

Another example is the  $\text{Li}/\text{LiAlCl}_4$ ,  $\text{SOCl}_2/\text{C}$  cell. In this case the anode film is probably composed of  $\text{LiCl}$ , a product of the reaction between lithium with the thionyl chloride. The cathodic reaction involves the reduction of  $\text{SOCl}_2$  at a porous carbon surface although the exact mechanism is unclear.

A proposed<sup>6</sup> cell reaction which conforms to all of the experimental results is:-



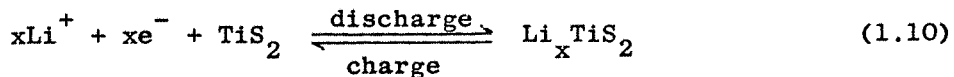
The reactive bi-radical,  $\ddot{\text{S}}\text{O}$ , is unstable and can decompose in one of several ways, the actual route apparently depending on the rate of discharge. Some of the observed discharge products are  $\text{S}$ ,  $\text{SO}_2$  and an  $(\text{S}_m\text{O}_n)_n$  polymer.

The  $\text{Li}|\text{SOCl}_2$  cell has, to date, provided the highest energy density of any known cell. With an operating voltage above 3.0V it has a practical energy density approaching  $700 \text{ Wh kg}^{-1}$ , although this is strongly dependent on the discharge rate.

### (iii) Intercalation electrodes

The use of these materials in rechargeable cells has attracted

much interest due to the reversible nature of the intercalation reaction. One such example is the Li/LiAsF<sub>6</sub>, 2-Me-THF/TiS<sub>2</sub> cell. In this cell the positive electrode reaction<sup>8</sup> can be represented by equation 1.10



where  $x < 1$ .

This is an example of an intercalation reaction. The TiS<sub>2</sub> has a layered structure and lattice expansion can occur to allow insertion of the intercalate; in this example Li<sup>+</sup>. This is a completely reversible process and the TiS<sub>2</sub> cathode can be cycled many hundreds of times.

The reduction of electrodes based on polycarbon monofluoride materials may be considered as further examples of intercalation reactions. These materials are made by fluorinating graphite and may be represented by (CF<sub>x</sub>)<sub>n</sub>, where x is usually one. It is postulated<sup>6</sup> that the Li<sup>+</sup> ions diffuse between the layers of the graphite lattice to form ternary compounds such as CLi<sub>z</sub>F, where z is less than one.

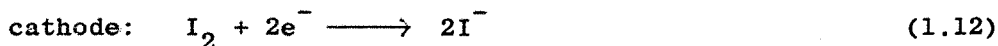
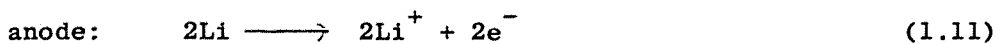
### 1.1.2 Electrolytes

Despite the many types of electrolyte that are now available it is possible to categorise them into four main groups:-

#### (I) Solid electrolytes

Solid electrolytes (ionic conductors but electronic insulators) started to be developed around 1960, particularly for use in fuel cells<sup>9</sup>. Today they have found use in the "All solid state" lithium battery, a battery suitable for low current applications, such as in a heart pacemaker. Such an example is the Li/LiI/I<sub>2</sub>-polyvinylpyridine cell. As soon as the lithium is brought into contact with the iodine a film of LiI is formed which acts as the solid electrolyte. The

probable cell reactions are:-



The low current densities realised are due to the low mobility of the  $\text{Li}^+$  ions in the  $\text{LiI}$  electrolyte. The polyvinylpyridine is used to increase this conductivity, so reducing the internal resistance of the cell. Being an all "solid state" battery the danger of electrolyte leakage is removed so making it an ideal system for implantation in the human body! The possibility of all solid state batteries for use in electric vehicle propulsion<sup>10</sup> and as secondary systems offer exciting prospects for this type of cell.

#### (II) Molten Salt electrolytes

These cells offer the possibility of extremely fast discharge rates due to the high mobility of  $\text{Li}^+$  ions in the melt. Interest in them is limited because of the need to use elevated temperatures. They do, however, have possible applications for secondary systems, e.g. for automobiles or load levelling.

#### (III) Inorganic electrolytes

These cells usually involve an oxyhalide such as  $\text{SOCl}_2$ ,  $\text{SO}_2\text{Cl}_2$  or  $\text{POCl}_3$ ; the  $\text{SOCl}_2$  cell having been considered earlier. Originally they were considered as possible solvents for  $\text{Cl}_2$  and  $\text{Br}_2$  cells but it soon became apparent that they were themselves cathode reactants and offered the possibility of high energy density systems.

#### (IV) Organic electrolytes

It has already been stated that interest in lithium batteries only re-developed once it had been shown that lithium could be deposited from certain organic electrolytes. A whole range of organic electrolytes are now available and some of these will be

considered in more detail later. To date, the most successful commercial high energy density and high discharge rate battery is the Li/SO<sub>2</sub> cell which contains an organic electrolyte based on acetonitrile.

It can be seen that the correct combination of lithium anode, electrolyte and cathode provides an almost infinite number of high energy density cells for a whole variety of applications. The performance of some of these cells as compared to the more conventional dry cells is displayed in figure 1.1. The advantages of the lithium cells are obvious and there are many reviews<sup>1,6,8,12,13,14,15</sup> in the literature which discuss the particular advantages (and disadvantages) of various systems.

### 1.1.3 Problems associated with lithium batteries

Today, virtually all of the problems associated with both primary and secondary lithium batteries relate to the properties of the anode protective film.

#### (i) Primary Lithium batteries

The most serious problem with the high energy density primary systems is the possibility of explosion whilst in use or when stored or abused (e.g. short circuiting). This is a particular problem for the Li/SO<sub>2</sub> and Li/SOCl<sub>2</sub> based cells. Dey<sup>6</sup> has reported on the unpredictable explosion of cells whilst on resistive loads and/or the casual storage of discharged cells. The mechanisms for such random cell explosions are not, as yet, understood. Discharge at high rates is thought to cause a build up of heat energy in the lithium surface film, which can lead to the anode melting which then causes the cell to explode due to the spontaneous, highly exothermic, chemical reaction of the molten lithium and electrolyte. It is also postulated<sup>6</sup> that the presence of sulphur in a discharged cell together with metallic lithium may act as a trigger for such explosions, although the participation of the SO bi-radical and other intermediates cannot be ruled out.

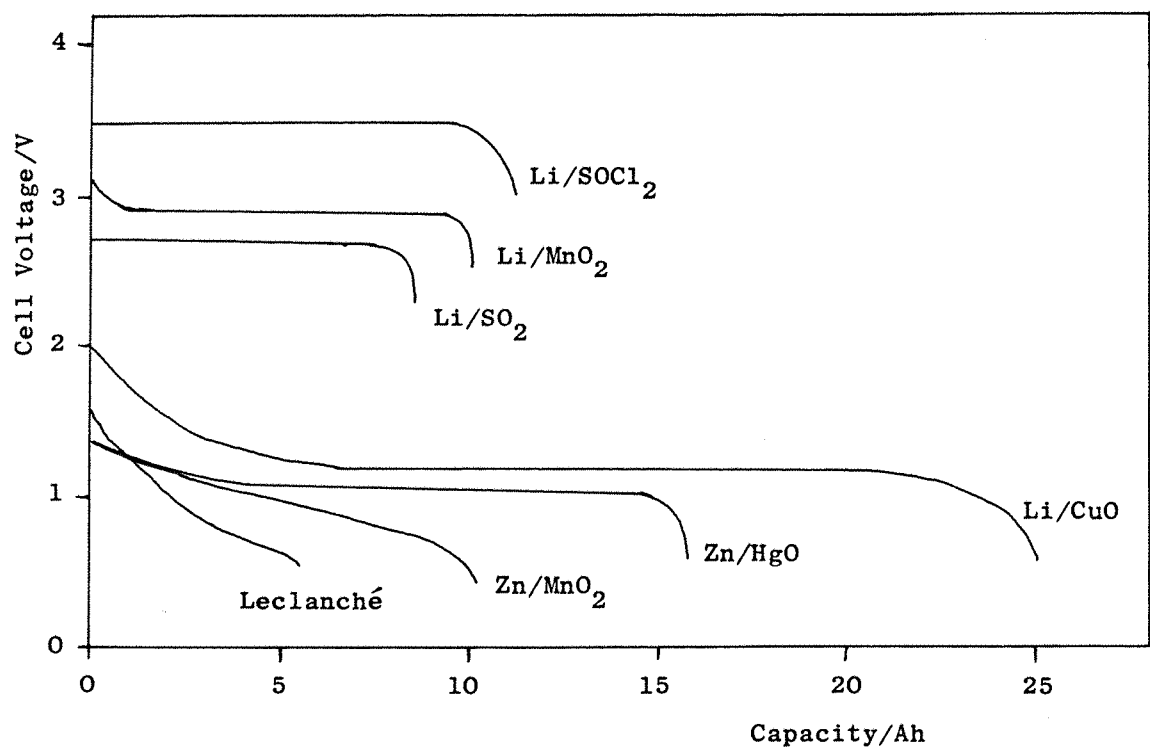


Figure 1.1 Discharge characteristics of some primary lithium and conventional dry cells<sup>11</sup>.

(ii) Secondary lithium batteries

At first sight, there are no theoretical obstacles to the realisation of a rechargeable lithium battery. Lithium can be efficiently deposited from organic electrolytes and a variety of reversible cathode reactions are known, e.g. intercalation electrodes. In practice the performance of secondary batteries is limited by the poor cyclability of the lithium electrode. It is this adverse cycling behaviour of the negative electrode which has been the topic of many recent investigations. Many attempts have been made to gain a better understanding of the chemical and electrochemical behaviour of the lithium electrode, especially in organic electrolytes, and these will be discussed in a later section. The results obtained, however, vary considerably. They appear to be dependent on the type of experiment performed and, in many cases, authors reporting identical experiments have obtained unacceptably differing data<sup>16</sup>. Recently, Moshtev has commented<sup>16</sup> with regard to our lack of knowledge concerning the true kinetics of the Li/Li<sup>+</sup> couple: "In our opinion more systematic work is still needed in order to determine the real kinetic parameters of the electrochemical reaction (equation 1.13)".



There are two fundamental problems concerned with the study of this reaction:

- (i) The Li metal surface is rapidly covered with a film which affects the kinetic parameters.
- (ii) The studies are usually carried out in organic electrolytes which, as will be seen later, have a low electrical conductivity. This results in large ohmic losses (IR drop) in the electrolyte which distorts the electrochemical data.

It is this second aspect which has prompted the work in this project.

## 1.2 Introduction to the aims of this work

The fundamental aim of this work was to study the electrochemical deposition and dissolution of lithium metal and to provide information concerning the kinetics of the lithium metal/Li<sup>+</sup> ion couple, in aprotic, organic solvents, free from distortion due to IR drop. This was to be achieved by the use of microelectrodes, the advantages of which will be discussed below. In addition, it was hoped to see how changes in various parameters, such as temperature, electrode material and electrolyte composition would alter the kinetics.

## 1.3 The theory of metal deposition

The electrochemical deposition of metals has found widespread industrial and commercial application, ranging from the removal of trace quantities of toxic metals in solution to the electroforming of intricate machine parts. Metal deposition corresponds to a phase transformation in which metal ions in solution are converted to metal atoms in a solid lattice. The growth of a metal layer on a foreign substrate is best discussed in two stages; the formation of the new phase and then the processes by which the deposit thickens or completes.

### 1.3.1 The early states of growth

Two distinct processes, each with characteristic thermodynamic and kinetic parameters, are essential in order for a new phase to form. These are the nucleation and then growth of centres of the new phase. Nucleation is typically the more difficult step and in electrodeposition it is necessary to supply free energy in the form of an overpotential. Once the nuclei have formed they will normally grow rapidly at the potential required to force nucleation.

The electron transfer process converts metal ions in solution into metal adatoms, adsorbed on the surface of the substrate. In the first stages of phase formation these adatoms move about the

surface and collect together into clusters; small clusters are prone to redissolve but if they reach a critical size they become stable and nucleation is said to have occurred. It is because the formation of such stable nuclei is statistically unlikely that nucleation is difficult and commonly requires a substantial overpotential.

In practice two limiting forms of the kinetics of nucleation are commonly observed.

(i) Instantaneous nucleation

Once a critical overpotential is applied to the cathode, nuclei form immediately at all sites where nucleation is possible. Thereafter the number of growing centres,  $N$ , is constant, and is given by:-

$$N = N_0 \quad (1.14)$$

where  $N_0$  is the number of sites available for nucleation.

(ii) Progressive nucleation

If the kinetics of nucleation are slow, then the number of growing nuclei will increase with time. If this process is first order, the number of nuclei will be given by:-

$$N = N_0 At \quad (1.15)$$

where  $N_0$  is as defined above and  $A$  is the nucleation rate constant.

Once formed, the stable nuclei will grow with a characteristic geometry. This may be two dimensional (i.e. the deposit will grow as a monolayer and the formation of additional layers requires further nucleation) or three dimensional, where the deposit grows out into the solution as a hemisphere or cone. Moreover, the rate determining step in this growth process may be the electron transfer step at the surface of the expanding centre or the diffusion

of ions in solution to the growing centres.

Phase formation is probably best studied by potential step techniques, where the current is monitored as a function of time following the imposition of a potential at which nucleation occurs. The phase formation process is always characterised by a transient in which the current increases with time. Two factors are responsible for this increase: (i) the number of nuclei may increase with time and (ii) the surface area available for electron transfer will increase as each nucleus grows. The exact form of the  $I-t$  dependence depends on the kinetics of nucleation, the geometry of growth and the rate determining step in the growth process. The exact form of the  $I-t^n$  relationships are available in several texts<sup>17,18,19</sup> and table 1.1 summarises some commonly encountered values of  $n$ .

It is common for the  $I-t$  response at short times to be complicated further by underpotential deposition. This occurs when the metal-substrate bond is stronger than the metal-metal bond in the lattice (common because of the polarisability of the former bond). Underpotential deposition is given its name because the first monolayer can be deposited at a potential, positive to the reversible potential of the  $M/M^{n+}$  couple. During a potential step to negative overpotentials, this first monolayer deposits rapidly and is seen as a sharp peak in the  $I-t$  transient. Nucleation of the bulk phase then occurs on top of this monolayer.

### 1.3.2 The later stages of growth

The relationships discussed above are only appropriate while the nuclei grow independently, i.e. there is no overlap of centres or their diffusion fields. Hence they only apply over a limited time regime. In many situations it is possible to derive an expression which to some extent takes overlap into account and will therefore apply over a longer time range. Eventually, complete overlap will occur and it is then necessary to consider how further growth occurs. For two dimensional growth, further nucleation is

Nucleus Geometry	Growth Type	Rate determining step in nuclei growth	Nucleation Type	Time dependence of current ( $i \propto t^n$ )
Hemispherical	3-dimensional	diffusion	Instantaneous	$t^{\frac{1}{2}}$
Cylindrical	2-dimensional	electron transfer	Instantaneous	$t^0$
Cylindrical	2-dimensional	diffusion	Progressive	$t^{\frac{3}{2}}$
Hemispherical	3-dimensional	diffusion	Progressive	$t^2$
Cylindrical	2-dimensional	electron transfer	Progressive	$t^2$
Hemispherical	3-dimensional	electron transfer	Instantaneous	$t^2$
Hemispherical	3-dimensional	electron transfer	Progressive	$t^3$

Table 1.1 The dependence of current on time, for isolated nuclei of various geometries<sup>18</sup>.

essential, whilst for three dimensional growth the "complete" layer, formed by overlap of many centres, can grow linearly into solution (again, either under diffusion or kinetic control).

Here it is only necessary to stress that the  $I-t^n$  relationships in table 1.1, only apply at short times. The total shape of the transient, however, should be compatible with the mechanism of growth proposed. Some limiting forms of complete transients are shown in figure 1.2. It should also be recognised that the current at short times may be distorted by the charging current (a falling  $I-t$  transient) and this reinforces the need to look at the complete shape of the transient.

During the thickening process the metal is being deposited onto its own lattice and this is a much more favourable electrode reaction than the deposition onto a foreign substrate without nuclei.

#### 1.4 The electrochemical deposition and dissolution of lithium metal

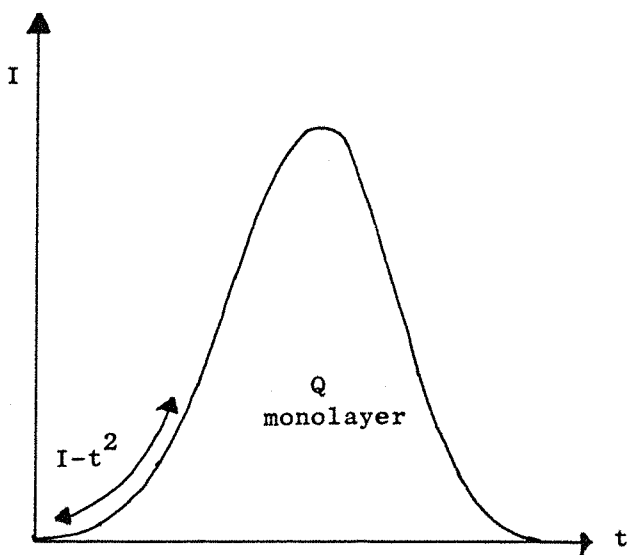
For many years now, the study of lithium deposition and dissolution has attracted attention; much of it being focussed on the development of a high energy density, secondary battery. Virtually all of this work has been thoroughly reviewed<sup>8,12,14,15,16,20</sup>.

##### 1.4.1 Solvents and lithium salts

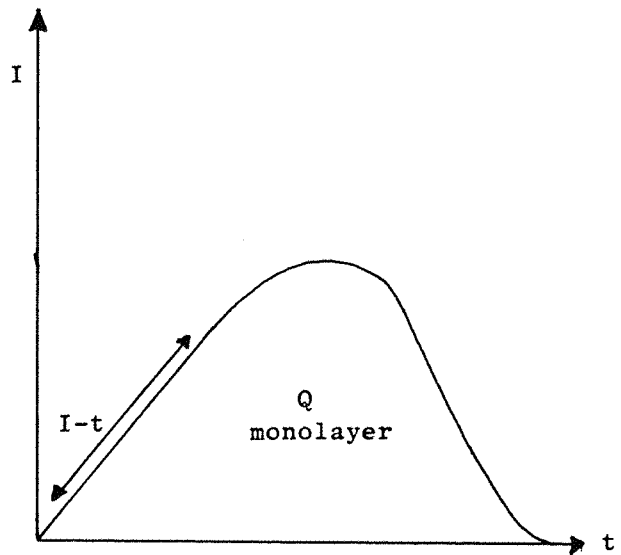
###### (i) Solvents

Since the thesis work of Harris<sup>2</sup>, organic solvents in particular have found widespread use in the electrochemical study of lithium. This is probably due to their ease of handling and low reactivity, as compared to inorganic solvents such as thionyl chloride ( $SOCl_2$ ).

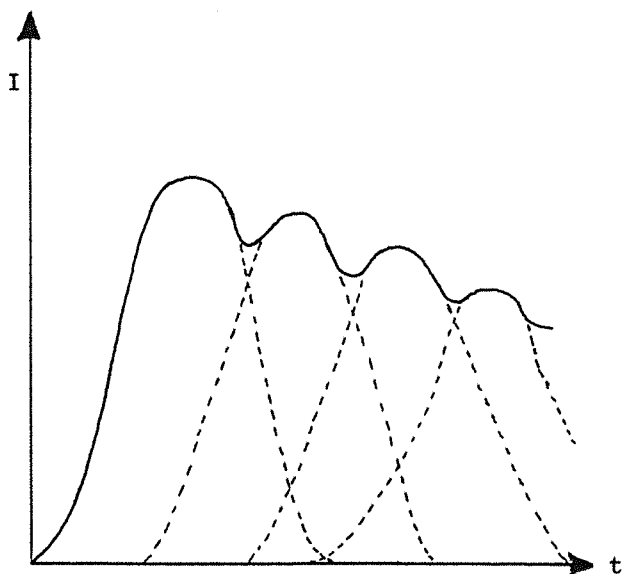
Due to the high reactivity of lithium, only aprotic organic solvents, such as ethers and esters, may be used. However, there is often uncertainty as to the stability of the solvent to lithium metal, the rôle of water and other impurities in the solvent in film



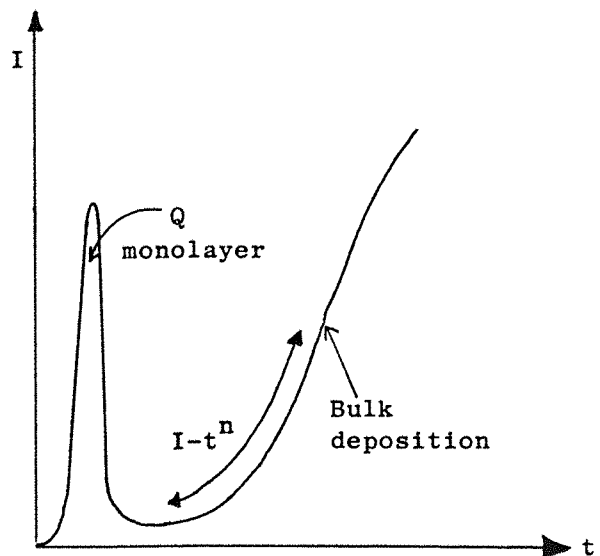
Deposition of a monolayer:  
progressive nucleation,  
2-dimensional growth.



Deposition of a monolayer:  
instantaneous nucleation,  
2-dimensional growth.

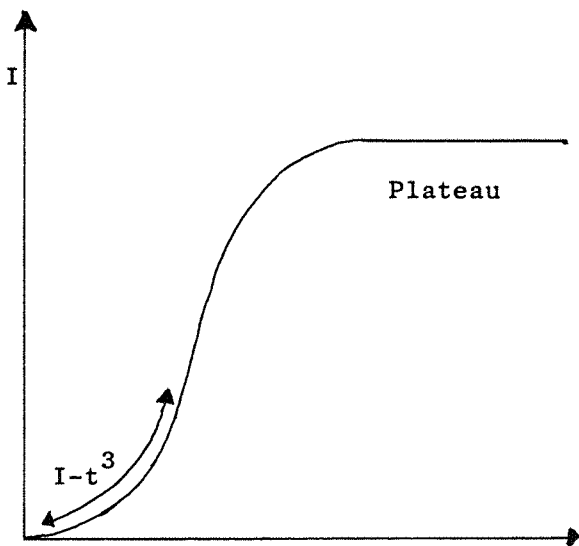


Layer by layer growth:  
area under each peak corresponds  
to the charge of a monolayer.

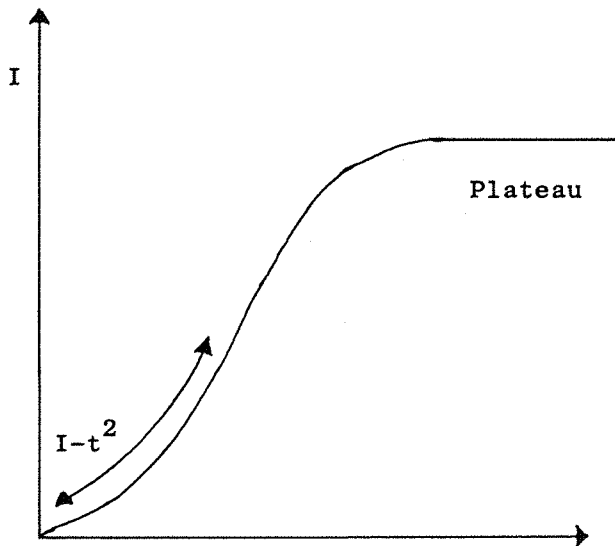


Initial peak due to under-  
potential deposition.

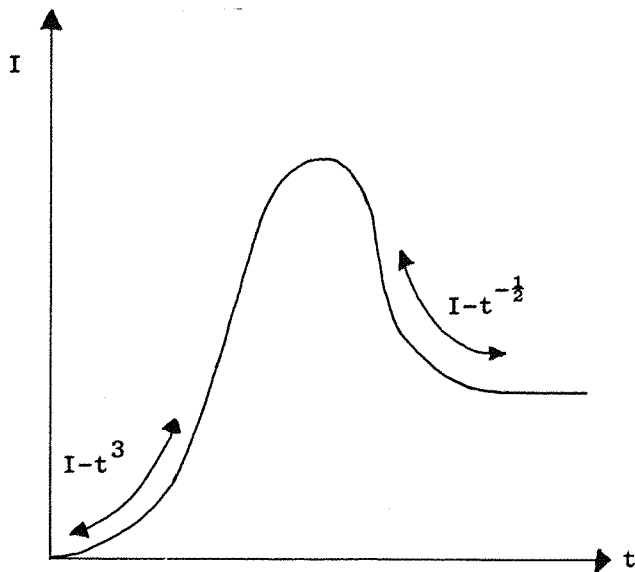
Figure 1.2 Some limiting forms of complete transients in response to a potential step.



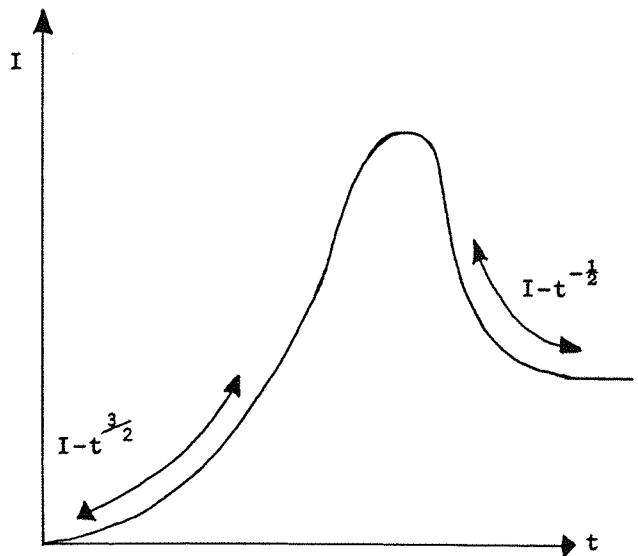
Progressive nucleation,  
3-dimensional growth with  
 $e^-$  transfer control.



Instantaneous nucleation,  
3-dimensional growth with  
 $e^-$  transfer control.



Progressive nucleation,  
3-dimensional growth with  
 $e^-$  transfer control  $\rightarrow$  linear  
diffusion.



Progressive nucleation,  
3-dimensional growth  
always diffusion control.

**Figure 1.2** Some limiting forms of complete transients in response to a potential step.

formation, and the nature of surface films which may be formed on the lithium. In fact solvents have generally been chosen empirically on the basis of lithium cycling efficiency, as measured by the repetitive galvanostatic deposition and dissolution of lithium metal in the solvent. Koch and co-workers have been particularly active in this field and have investigated the use of propylene carbonate (PC)<sup>21</sup>, tetrahydrofuran (THF)<sup>22,23</sup>, 2-methyltetrahydrofuran (2-Me-THF)<sup>24-27</sup>, and solvent mixtures of THF, 2-Me-THF and diethylether (DEE)<sup>28-30</sup>. Propylene carbonate has found widespread use due to its many favourable advantages (high dielectric constant, high solvating power, wide temperature range) all of which have been reviewed by Jasinski<sup>31</sup>. However, its use in battery systems is limited due to the phenomenon of voltage delay - attributed to the Li-PC film<sup>1</sup>. Other solvents are available in which metallic lithium is apparently stable and which will dissolve a variety of lithium salts to provide a "reasonably" conductive medium. Table 1.2 lists some important properties of the most commonly encountered solvents.

(ii) Lithium salts

There are only a few inorganic lithium salts which show good solubility in organic solvents, the most common being:  $\text{LiClO}_4$ ,  $\text{LiBF}_4$ ,  $\text{LiPF}_6$ ,  $\text{LiAsF}_6$ ,  $\text{LiAlCl}_4$  and sometimes  $\text{LiCl}$  and  $\text{LiBr}$ .

Plots of conductivity versus salt concentration usually pass through a maximum. This is because viscosity, as well as the number of charge carriers, increases with increasing salt concentration. The maximum conductivity for lithium salt/aprotic organic solvent systems generally occurs at salt concentrations of about 1 mole  $\text{dm}^{-3}$ . Some maximum conductivities are shown in table 1.3.

It can be seen that the maximum conductivity of these organic electrolytes is at least one order of magnitude lower than that of aqueous solutions. Special precautions must therefore be taken to ensure that electrochemical data, obtained in these electrolytes,

Solvent (abbreviation)	Formula	Boiling point/°C	Melting point/°C	Relative Permittivity (dielectric constant)	Density g cm <sup>-3</sup>	Viscosity 10 <sup>-3</sup> K g m <sup>-1</sup> s <sup>-1</sup>
Propylene Carbonate (PC)		242	-48	65.1	1.2	2.5
Acetonitrile (AN)	$\text{H}_3\text{C}-\text{C}\equiv\text{N}$	81.6	-45.7	35.9	0.78	3.39
Diethylether (DEE)	$\text{CH}_3-\text{CH}_2-\text{O}-\text{CH}_2-\text{CH}_3$	34.6	-116.2	4.3	0.71	0.22
Tetrahydrofuran (THF)		65	-108	7.4	0.88	0.46
2-Methyltetra hydrofuran (2-Me-THF)		80	-	6.2	0.85	0.46
Dioxolane		78	-93	7.1	1.06	0.59
γ-Butyrolactone		202	-43	39.1	1.13	17.5

Table 1.2 Properties of some solvents used in lithium batteries.

Solvent	Solute	Solute Concentration mol dm <sup>-3</sup>	Specific Conductivity Maximum $\Omega^{-1} \text{ cm}^{-1}$
PC	$\text{LiClO}_4$	0.66	$5.4 \times 10^{-3}$
	$\text{LiCl}$	1.00	$3.4 \times 10^{-4}$
	$\text{LiBF}_4$	1.00	$4.0 \times 10^{-3}$
	$\text{LiPF}_6$	0.86	$5.4 \times 10^{-3}$
THF	$\text{LiClO}_4$	2.20	$7.0 \times 10^{-3}$
	$\text{LiCl}$	0.16	$1.6 \times 10^{-4}$
	$\text{LiAlCl}_4$	1.20	$1.6 \times 10^{-2}$
	$\text{LiAsF}_6$	1.50	$1.7 \times 10^{-2}$
2-Me-THF	$\text{LiAsF}_6$	1.50	$4.0 \times 10^{-3}$
DEE	$\text{LiAsF}_6$	1.50	$1.0 \times 10^{-3}$

Table 1.3 Conductivity maxima<sup>8</sup> of lithium salts in some aprotic media.

is not distorted by ohmic losses (IR drop). Work done during the course of this report has led us to believe that many authors have not overcome this problem. Consequently, many ambiguous conclusions, concerning the lithium electrode, have been drawn from electrochemical data grossly distorted by IR drop.

#### 1.4.2 Cycling of the lithium electrode

The term "cycling" refers to the repeated deposition and dissolution of lithium onto a conducting substrate such as copper nickel or lithium itself. The most commonly employed technique for studying this has been the galvanostatic method (as used by Koch<sup>21-30</sup>) in which lithium is plated and stripped at a constant current. Cyclic voltammetry and, to a lesser extent, constant potential techniques have also been used by some authors as will be seen later.

The cycling efficiency (E%) of a particular cycle is defined as the ratio of the charge passed during the stripping stage ( $Q_s$ ) to the charge passed during the deposition stage ( $Q_d$ ), equation 1.16.

$$E\% = \frac{Q_s}{Q_d} \times 100 \quad (1.16)$$

For an experiment involving many cycles it is desirable to have a value for the average cycling efficiency ( $\bar{E}\%$ ). This may be found by using equation 1.17.

$$\bar{E}\% = \frac{1}{n} \sum^n E\% \quad (1.17)$$

where E% is the cycling efficiency of each cycle and n is the number of cycles. This becomes tedious for large numbers of cycles and a more convenient method for calculating  $\bar{E}\%$  is that due to Koch<sup>25</sup>. It consists of initially depositing a known amount of lithium (equivalent to a charge,  $Q_{ex} + Q_s$ ) onto an electrode (not lithium) and then sequentially stripping and plating a fraction of the lithium,  $Q_s$ . If each cycle were 100% efficient then the lithium remaining,

equivalent to an excess charge ( $Q_{ex}$ ), would remain constant. If each cycle is not 100% efficient then each strip cuts into the remaining lithium. The average cycling efficiency can then be calculated from equation 1.18.

$$\bar{E}\% = \frac{Q_s - Q_{ex}}{n} \times 100 \quad (1.18)$$

where  $Q_s$  is the charge of lithium stripped per cycle and  $n$  is the number of cycles before there is insufficient lithium remaining for the stripping process. The term "stripping efficiency" is often used instead of "cycling efficiency".

Many battery chemists are not concerned with the kinetics or mechanism of the deposition and dissolution process but concentrate their efforts into making  $\bar{E}\%$  as high as possible. This is because efficiencies above 99% are required to achieve a cycling capacity greater than 250 cycles. Another requirement of a practical lithium cell is that quantities of lithium corresponding to charges of  $50-100 \text{ C cm}^{-2}$  be cycled. For experimental reasons this is often impractical and much thinner plates, usually  $1 \text{ C cm}^{-2}$ , are cycled. In fact, Koch<sup>24</sup> has claimed that the cycling of thin plates more rapidly tests the criteria for electrode failure by exaggerating the conditions which cause the decline in performance. Thus a typical experiment would involve the cycling of  $1.1 \text{ C cm}^{-2}$  lithium plates at various current densities, usually in the range  $0.1 - 10 \text{ mA cm}^{-2}$ .

Low cycling efficiencies are not associated with the deposition process, as lithium may be plated from a variety of organic electrolytes with 100% efficiency<sup>32,33</sup>. In many cases, however, the subsequent anodic dissolution is invariably less efficient<sup>32,33,21-30</sup>. This is particularly noticeable if the deposit is allowed to stand on open circuit before being electrochemically stripped. For example, Selim and Bro<sup>32</sup> found that the stripping efficiency for a plate of lithium, deposited from a  $\text{LiClO}_4$ /propylene carbonate electrolyte, fell from 60% to 0% if the deposit was allowed to stand in the electrolyte

on open circuit for forty hours.

The proposed explanation of this was that some of the lithium was chemically reacting with one or more components of the electrolyte to produce insulating films which isolated the deposited lithium from the electrode. This idea led to many studies of these insulating films and it is now widely believed that two types of film exist:

(i) Solid electrolyte film

This is the type of film which has made possible the realisation of a number of lithium batteries. It is an electronic insulator but a lithium ion conductor. It is formed by the rapid reaction of the lithium with impurities in the electrolyte; particularly water, but also oxygen, nitrogen, carbon dioxide, etc. The reaction products so formed, coat the lithium surface and protect the bulk metal from further reaction. Being lithium ion conductors, these films allow the deposition and dissolution of lithium metal to occur via the diffusion of lithium ions through them. Peled has described this type of film as a solid electrolyte interphase (SEI) and has suggested how this might be responsible, under certain conditions, for low stripping efficiencies<sup>34</sup>.

(ii) Insulating film

This arises from the reaction of the lithium with the solvent or lithium salt in the electrolyte. These reactions give rise to a film which is an electronic insulator and which will not conduct lithium ions. Koch<sup>23</sup> has made an extensive study of this film on lithium in a LiAsF<sub>6</sub>/THF electrolyte. He concluded that it was a polymer formed by the reaction of the AsF<sub>6</sub><sup>-</sup> anion with the reduction products of THF (lithium butoxide).

While the intimate chemical and electrochemical details of the film forming processes are open to speculation, a wide variety of innovative strategies have been developed to cope with this

filming problem. The work of Muller<sup>35</sup> and Koch<sup>23</sup> has suggested that the solid electrolyte film is formed rapidly whilst the insulating film is formed at a much slower rate. With this in mind, two major approaches have been adopted to improve the lithium cyclability.

The first involves the use of additives which promote the formation of the solid electrolyte film. This is based on the premise that this film can block the reaction between the lithium and the electrolyte by acting as a physical barrier between them. Rauh and Brummer<sup>21</sup> were the first to adopt this approach and they found that the deliberate addition of certain reactive impurities ( $H_2O$ ,  $SO_2$ , nitromethane) afforded higher cycling efficiencies in a propylene carbonate based electrolyte. More recently, Glugla<sup>36</sup> found that the addition of certain alcohols (e.g. 2-methoxyethanol) to electrolytes based on 2-Me-THF gave improved cycling efficiencies. Koch<sup>23</sup> and Abraham et al<sup>30</sup> have observed a reduction in cycling efficiencies of THF based electrolytes when all of the reactive impurities are removed, indicating that it is in fact the impurities which are beneficial to the cycling behaviour. It is interesting to reflect that additives have been used for many years in industrial electroplating processes to obtain smoother deposits.

The second approach involves trying to reduce the rate of the reaction between the lithium and the electrolyte. One way of doing this is to structurally modify the solvents and Koch has again been very active in this area<sup>24,25</sup>. More recently Foos and McVeigh<sup>37</sup> showed that the open chain analogues of dioxolane (namely  $CH_2(OMe)_2$  and  $CH(OMe)_3$ ) had better stability towards lithium than dioxolane itself and consequently afforded higher cycling efficiencies. They attributed this to the absence of ring strain in these solvents.

The use of an alloy containing lithium, e.g. AlLi has also been considered. The lithium may be sequestered within the alloying host, thereby preventing physical contact between the lithium and the electrolyte. The problem of dendrite formation may also be reduced.

The use of aluminium as an electrode will be discussed below.

Other approaches have been adopted, such as the use of "in-situ" generated lithium scavengers such as bromine, and these have been fully reviewed<sup>15,20</sup>.

#### 1.4.3 Kinetics of the lithium metal/lithium ion couple

Despite the active interest in the cycling behaviour of the lithium electrode, very little work has been reported aimed directly at the kinetics of the Li/Li<sup>+</sup> couple, equation 1.19.



The reasons for this have already been discussed: low conductivity solutions, surface films and limited interest by battery chemists.

Table 1.4 considers some of the results obtained during kinetic studies of the Li/Li<sup>+</sup> reaction in propylene carbonate. There are obvious discrepancies between these results which limits their usefulness.

Cyclic voltammetry has been used to obtain a qualitative insight into the deposition and dissolution processes. Besenhard<sup>42</sup>, Frazer<sup>43</sup> and Dinkevich<sup>44</sup> have all obtained cyclic voltammograms showing the deposition and dissolution of lithium metal onto an inert substrate from propylene carbonate. Those due to Besenhard and Frazer have the expected shape; showing the nucleation overpotential, eventual nucleation and growth of the deposit and subsequent anodic dissolution. However, the results do appear to be affected by IR drop, as seen by the low current densities even at high overpotentials. The results of Dinkevich appear to defy thermodynamics, with nucleation of the lithium occurring positive to the reversible potential of the Li/Li<sup>+</sup> couple.

These results have limited interest due to the minimal use that propylene carbonate finds in lithium batteries. However,

Measurement technique	Exchange current density, $I_o$ . (mA cm $^{-2}$ )	Ref.
Galvanostatic	10.2	38
Tafel plot	2.7	39
Galvanostatic	0.95	40
Galvanostatic	3-6	41
A.C. impedance	2.8 <sup>a</sup>	16
A.C. impedance	3.3 <sup>a</sup>	16
A.C. impedance	1.3 <sup>a</sup>	16

Table 1.4 Values of the exchange current density for the Li/Li<sup>+</sup> couple in 1M LiClO<sub>4</sub>/Propylene carbonate at 25°C. (from reference 16).

(a) Results for different lithium surface treatments.

the study of the kinetics in ethereal solvents is much more difficult due to the low conductivity of the electrolytes. Takei<sup>45</sup> was unable to deposit lithium at all from electrolytes based on THF; almost certainly a consequence of IR drop. More recently, Matsuda<sup>46</sup> obtained a current-potential curve (Tafel plot) for a lithium electrode in a THF/dioxolane electrolyte. Even at overpotentials of 1.0V the current densities that he obtained were below  $10 \text{ mA cm}^{-2}$ . During this work we have shown that at true overpotentials of even 0.3V the limit of mass transfer in THF based electrolytes has been reached, corresponding to steady state current densities greater than  $400 \text{ mA cm}^{-2}$ .

Baranski and Fawcett<sup>47,48</sup> have studied the kinetics of the reduction of lithium and other alkali metal ions in various aprotic solvents and have shown them to be strongly dependent on the solvation properties of the solvent.

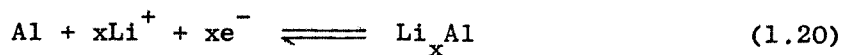
#### 1.4.4 The lithium-aluminium electrode

Since Dey<sup>49</sup> showed that lithium could be electrochemically alloyed with many metals, there has been considerable interest in the lithium-aluminium electrode<sup>50-57</sup>. Fawcett has summarised much of the work in a recent review<sup>8</sup>. There are two major advantages of using aluminium as an electrode material in secondary lithium batteries: (i) lithium deposited into aluminium does not grow dendrites<sup>52</sup> and (ii) the alloy exhibits high rechargeability in many aprotic solvents due to the limited contact of the lithium with the solvent<sup>50-52,57</sup>. The major disadvantages are that the "atomic weight" of LiAl is almost five times greater than that of lithium and the equilibrium potential is 0.38V more positive<sup>50</sup>. However, Fawcett<sup>57</sup> has estimated that the theoretical energy density of a LiAl/TiS<sub>2</sub> cell is only about 33% lower than that of a Li/TiS<sub>2</sub> one. This would be quite acceptable providing that a longer cycle life is achieved.

Rao and Francis<sup>50</sup> used the galvanostatic cycling technique

(current densities: charging  $2.5 \text{ mA cm}^{-2}$ , discharge  $10 \text{ mA cm}^{-2}$ ) to study the LiAl electrode. They found that as they cycled a  $\beta$ -LiAl electrode, its potential moved more negative towards that of a pure lithium electrode. They explained this in terms of the rate of diffusion of lithium in the alloy. As the  $\beta$ -LiAl electrode (46-56 atom percent lithium) is discharged, it becomes depleted in lithium and forms the  $\alpha+\beta$  phase. The  $\alpha$  phase can contain much less lithium (15-50 atomic %) and the mobility of lithium in it is much lower. Thus, during the charging process, lithium tends to accumulate on the electrode surface, moving the potential of the electrode towards that of pure lithium. Given time, the lithium does diffuse into the electrode to give the  $\beta$ -LiAl phase only.

Besenhard<sup>51</sup> used cyclic voltammetry to compare the rate of lithium dissolution from an inert (nickel) and an alloying (aluminium) electrode. Under the same conditions, he showed that the dissolution of lithium from the aluminium electrode was much slower and he also attributed this to the reduced mobility of lithium in the lithium-aluminium alloy. He also observed the nucleation and deposition of lithium onto the aluminium at a potential positive to the  $\text{Li}/\text{Li}^+$  reversible potential. This can be explained by considering the energetics of the alloy formation. Equation 1.20 represents the electrochemical process.



This alloying process occurs when it becomes energetically more favourable to form the alloy lattice than the pure lithium metal lattice. In electrochemical systems, this energy saving is seen as a shift in the equilibrium potential to a more positive potential and sometimes as a decrease in the overpotential required for the metal ion reduction.

Epelboim et al<sup>52</sup> have made a very detailed study of the LiAl electrode. Using a pure aluminium electrode with an initial lithium incorporation of  $50 \text{ C cm}^{-2}$  they obtained more than 1500 cycles, using  $1 \text{ C cm}^{-2}$  plates cycled at  $2 \text{ mA cm}^{-2}$ . They also observed that den-

driftic growth of lithium did not occur providing that the deposition charge,  $Q_d$ , was kept below a certain threshold value which was dependent on the current density used, (e.g.  $Q_d = 50 \text{ C cm}^{-2}$  at  $I = 10 \text{ mA cm}^{-2}$ , while  $Q_d = 100 \text{ C cm}^{-2}$  at  $I = 1 \text{ mA cm}^{-2}$ ). Again this is linked to the rate of lithium transport in the alloy.

Jow and Liang<sup>55</sup> used a potentiostatic technique to obtain values for the diffusion coefficients of lithium in the  $\beta$ -LiAl alloy of approximately  $5.0 \times 10^{-9} \text{ cm}^2 \text{ s}^{-1}$ . This value can be used to qualitatively explain the broadening of the stripping peak in Besenhard's<sup>51</sup> cyclic voltammogram noted earlier.

During the cycling of LiAl electrodes, several authors<sup>51-54</sup> have noted that the cycling efficiencies of the first few cycles are considerably lower than later cycles. Two explanations have been put forward to explain this. Besenhard<sup>51</sup> has suggested that initially some of the lithium is retained in the alloy lattice. After a few cycles, however, this "retention capacity" is filled up and further cycles show an increased efficiency. Fawcett<sup>54</sup>, however, has suggested that the low efficiency is due to the consumption of charge during the deposition process, to reduce the oxide layer which is always present on the aluminium surface.

The major problem associated with the LiAl electrode is its tendency to decompose during continued cycling or cycling with high charge densities ( $50 \text{ C cm}^{-2}$ ).<sup>51-55</sup> This is attributed to the differences in molar volumes of the various Li-Al phases which are formed. Continued cycling thus causes the alloy lattice to be repeatedly expanded and contracted. This leads to severe roughening and eventual disintegration of the electrode. Recently<sup>57</sup>, Fawcett claimed to have overcome this problem by the use of a separator which holds the alloy together. Peled<sup>58</sup> has demonstrated the advantage of using very high lithium concentration alloys (95 atomic %) in thionyl chloride cells.

Recently, Geronov<sup>56</sup> has studied the nucleation and growth

of the  $\beta$ -LiAl alloy. He obtained current/time transients which he was able to fit to  $i-t^3$  plots, indicative of progressive nucleation with three dimensional growth. Again, all these experimental data were obtained with PC (or similar solvents) as the electrolyte. Relatively few studies of LiAl in ether solvents have been reported.

#### 1.4.5 Lithium metal underpotential deposition

The deposition of a monolayer amount of metal atoms onto a foreign metal electrode at potentials positive to the reversible Nernst potential is widely recognised and has been extensively reviewed<sup>17,59</sup>. This phenomenon is associated with the difference in bond energies of the metal-substrate bond and the metal-metal bond. Thus the energetically favourable deposition of the first monolayer can be related to the ionic contribution in the metal-substrate bond. Fried and Barak<sup>60</sup> related the potential at which the underpotential deposition occurred to the differences in sublimation energies and lattice energies of the metal lattices. More recently, Kolb<sup>61,63</sup> interpreted underpotential deposition in terms of the differences of the work function of the electrode material and the metal lattice.

Several authors<sup>60-62</sup> have studied the reduction of lithium ion on various substrates and claim to have observed underpotential lithium metal deposition.

All of these studies have involved the use of cyclic voltammetry in either propylene carbonate or acetonitrile based electrolytes. The results shown are by no means convincing. None of the results show both the deposition and stripping of the monolayer in the same voltammogram. The stripping peak shown by Kolb<sup>61</sup> for lithium on copper and by Morcos<sup>62</sup> for lithium on graphite are very broad, extending for almost 1.0V. Kolb<sup>61</sup>, however, does show a reasonable correlation between the values of the underpotential for lithium on copper (+1.05V vs Li/Li<sup>+</sup>)

and the work function differences. The measured charge under the peak is larger than the expected value for a monolayer ( $210 \mu\text{C cm}^{-2}$ ) although he suggests that there is a significant roughness factor associated with the electrode surface which would explain this.

A much simpler approach to estimating the value of the under-potential can be taken by considering the data<sup>64</sup> in table 1.5. From this data, it can be seen that the Li-Cu bond is stronger than the Li-Li bond by a factor of  $87 \text{ kJ mole}^{-1}$ . The use of equation 1.21 (from the Vant Hoff isotherm) suggests that, on the basis of these values, the formation of a lithium monolayer on copper should be favourable at +0.87V.

$$\Delta G = -nFE \quad (1.21)$$

During this work, an attempt was made to observe this monolayer formation.

### 1.5 Microelectrodes

The use of microelectrodes (typically electrodes with a surface area in the range  $10^{-8} - 10^{-4} \text{ cm}^2$ ) for electrochemical studies is on the increase and has been reviewed<sup>65,66</sup>.

Microelectrodes were originally developed for use in in-vivo electrochemical studies, such as the detection of species in biological cells or the mammalian brain<sup>65</sup>, where a small electrode is obviously essential. They do, however, have additional properties which make them extremely attractive for application in other areas of electrochemistry. The most important properties are:

#### (i) High steady state rates of diffusion

In many circumstances, the mass transport of species to the electrode can be the rate determining step in the overall

Diatomic	Dissociation energy at 298K (kJ mole <sup>-1</sup> )
Cu-Li	193
Li-Li	106

Table 1.5 Dissociation energies of the diatomic molecules Li-Li and Cu-Li at 298K.

process and so prevents the characterisation of fast electron transfer reactions and coupled chemical reactions. This problem is sometimes overcome by the use of a rotating disc electrode which increases the rate of mass transport by the introduction of convection into the system.

The steady state rate of diffusion may also be increased by the use of a microelectrode. This is a consequence of the so-called "edge effects", which for a normal macroelectrode are insignificant but which for a microelectrode are not only important but may become dominant. No analytical solution exists which accurately describes the mass transport to such an electrode although it has been shown to have some similarity to the mass transport to a spherical electrode. In the case of a spherical electrode, mass transport occurs in a spherical diffusion field and the current-time response to a potential step is given by:

$$I = \frac{nFD^{\frac{1}{2}}C}{(\pi t)^{\frac{1}{2}}} + \frac{nFDC}{r} \quad (1.21(a))$$

where  $r$  is the radius of the sphere,  $C$  is the concentration of electroactive species and all other symbols have their usual meanings. It can be seen that for large values of  $r$  the second term in this equation becomes insignificant and the equation reduces to the first term - more commonly known as the Cottrell equation. For very small values of  $r$ , however, the second term becomes increasingly important and for all but the shortest time-scales, the equation can be approximated to:

$$I = \frac{nFDC}{r} \quad (1.22)$$

Thus, the rate of diffusion to a small spherical electrode rapidly becomes independent of time and is at a higher value than that to a large planar electrode. For example, at a spherical electrode of radius  $1 \mu\text{m}$  and a concentration of electroactive species of  $1 \text{ mmol dm}^{-3}$  the current density in the steady state will be

$10 \text{ mA cm}^{-2}$ . It has been shown that very small planar electrodes of radius  $r$  can be approximated to small hemispherical electrodes of radius  $r$  and so equation 1.22 may be applied to microelectrodes. This property of higher rates of steady state diffusion has resulted in microelectrodes being used to study fast electron transfer reactions<sup>67</sup> and fast coupled chemical reactions<sup>68</sup>.

(ii) Studies in resistive media

Papers are now appearing in the literature which show that the use of microelectrodes allows good quality data to be obtained even from highly resistive media<sup>69,70</sup> and in the absence of supporting electrolyte<sup>71</sup>. The reason for this is that the total current flowing through the cell is very low and so the IR drop is also very low. This can be shown more quantitatively when we remember that a microelectrode behaves in a similar manner to a small spherical electrode. Ilkovich<sup>72</sup> showed that for a spherical electrode of radius  $r_1$ , the cell resistance,  $R$ , is given by:

$$R = \left( \frac{\rho}{4\pi} \right) \left( \frac{1}{r_1} - \frac{1}{r_2} \right) \quad (1.23)$$

where  $\rho$  is the specific resistance of the solution and  $r_2$  is the distance between the spherical electrode and the counter electrode. Thus for small values of  $r_1$  the  $1/r_2$  term becomes insignificant and we can write:

$$R = \frac{\rho}{4\pi r_1} \quad (1.24)$$

If the current density to the electrode is  $I$ , then the total current flowing into the spherical electrode will be:

$$i = 4\pi r_1^2 I \quad (1.25)$$

and the total  $iR$  drop in the cell can be expressed by multiplying equations 1.24 and 1.25 together:

$$iR = \rho r_1 I \quad (1.26)$$

Thus for a spherical electrode (which the use of a microelectrode approximates to) the  $iR$  drop is much less than at macroelectrodes.

(iii) Reduction in the double layer charging time

Microelectrodes show great potential for the study of very fast electrochemical events which may not be investigated with conventional macroelectrodes due to the interference of double layer charging current on the timescale where currents must be measured. It is, in fact, the charging current which determines the shortest time at which meaningful measurements of faradaic current can be made. For a potential pulse the charging current,  $I_c$ , is given by:

$$I_c = \frac{\Delta E}{R} \exp \left[ -\frac{t}{RC} \right] \quad (1.27)$$

where  $\Delta E$  is the amplitude of the pulse,  $R$  is the resistance of the cell,  $C$  is the double layer capacitance and  $t$  is the time measured from the application of the pulse. The charging current will thus decrease rapidly with the use of a microelectrode for two reasons:

- (a) the capacitance,  $C$ , is proportional to the electrode area. ( $r^2$ )
- (b) it has been seen in the previous section that the resistance of the cell also increases with the use of a microelectrode. (But only as  $1/r$ )

In fact, Wightman has suggested<sup>65</sup> that for a disk electrode of  $4 \mu\text{m}$  radius, the double layer should be 99% charged within  $3 \mu\text{s}$ , even assuming a  $100 \mu\text{F cm}^{-2}$  double layer capacitance and a cell resistance of  $100 \text{ k}\Omega$ , although he was not able to verify this prediction because of background currents with the carbon fibres used. The electrodes used in this work should be completely charged in  $115 \mu\text{s}$ .

The faradaic current, however, only decreases linearly

with electrode area. Thus the ratio of faradaic to non-faradaic current increases, allowing the earlier detection of faradaic processes.

Another more specialised property of micrelectrodes involves their use in the study of metal nucleation because they allow the growth and study of a single metal nucleus.

All of the properties (i) to (iii) make the use of micro-electrodes attractive for a study of the  $\text{Li}/\text{Li}^+$  couple in ether type solvents. It has been seen that previous studies on the kinetics of this couple in propylene carbonate have suggested that they are fast, with values of the exchange current density,  $I_o$ , as high as  $10 \text{ mA cm}^{-2}$  being reported<sup>38</sup>. Also, many of these studies, despite being performed in propylene carbonate (a relatively high conductive medium) appear to be distorted due to ohmic losses.

CHAPTER TWO

EXPERIMENTAL

## EXPERIMENTAL

### 2.1 Cells

#### (a) Microelectrode cells

All of the experiments with the copper, nickel, carbon and aluminium microelectrodes, performed at room temperature, were carried out in the cell in figure 2.1. This was an undivided cell, employing two electrodes with a volume of approximately  $10\text{ cm}^3$ . The counter electrode in all experiments was a lithium foil.

For experiments involving low or elevated temperatures, a cell (fig. 2.2) was used which could be immersed in a water or slush bath.

In both cells, the working electrode was held in a Quick-fit cone to screw thread adaptor by means of a rubber ring and PTFE washer which allowed the electrode to be pushed as close to the counter electrode as was desired.

#### (b) Macroelectrode cell

For the large scale deposition of lithium onto copper or nickel, the cell in figure 2.3 was used. This was also an undivided, two electrode cell with a volume of approximately  $20\text{ cm}^3$ . The working electrode was pushed to the desired distance from the counter electrode by sliding it down the syringe barrel.

### 2.2 Electrodes

#### (a) Copper, nickel and aluminium microelectrodes

These working electrodes are prepared (fig. 2.4(a)) by pushing the required metal wire, welded to a thicker nichrome wire (for electrical connection), into a capillary tube made of soda glass, as this melts at a lower temperature than other glasses and was found to seal the fine wires more efficiently. The glass was then

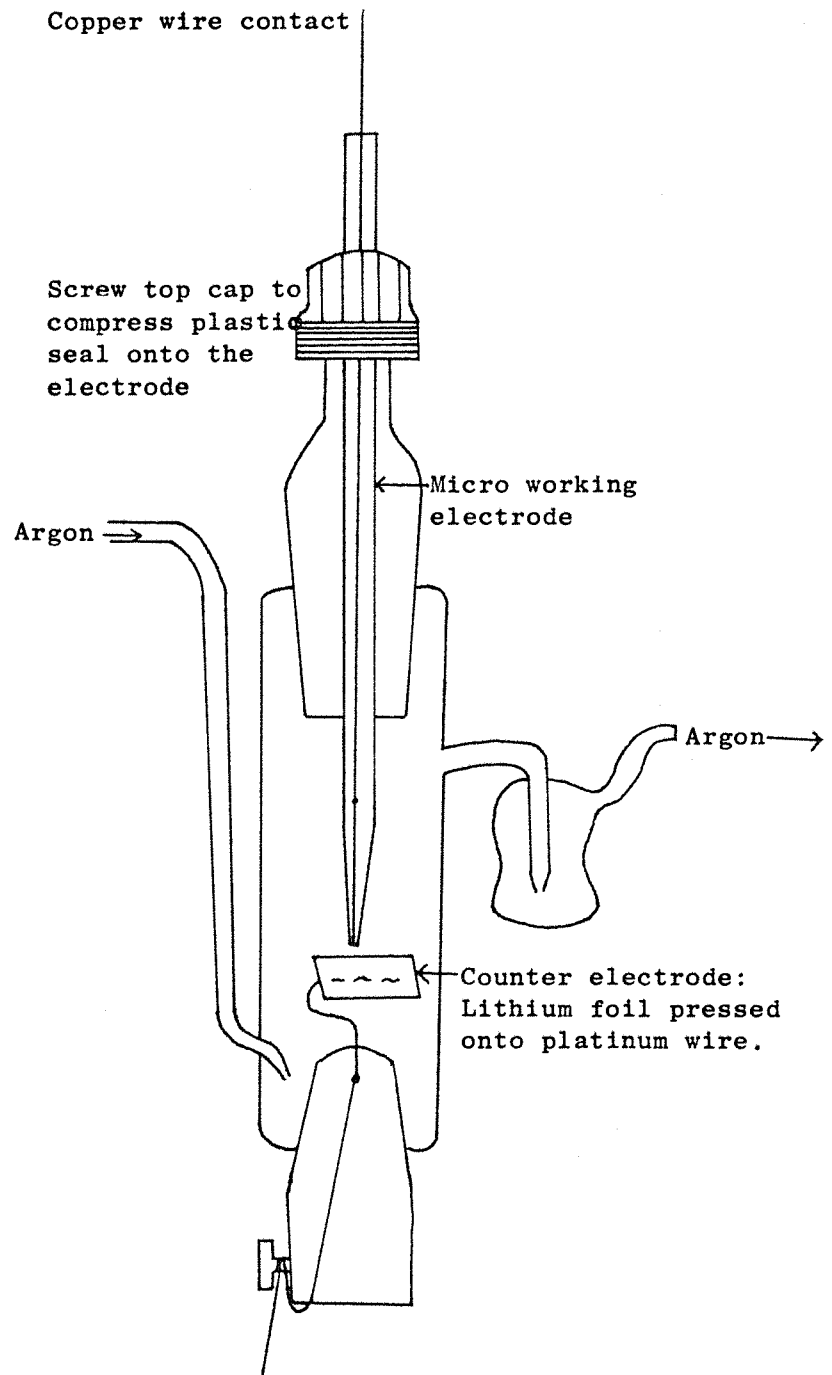
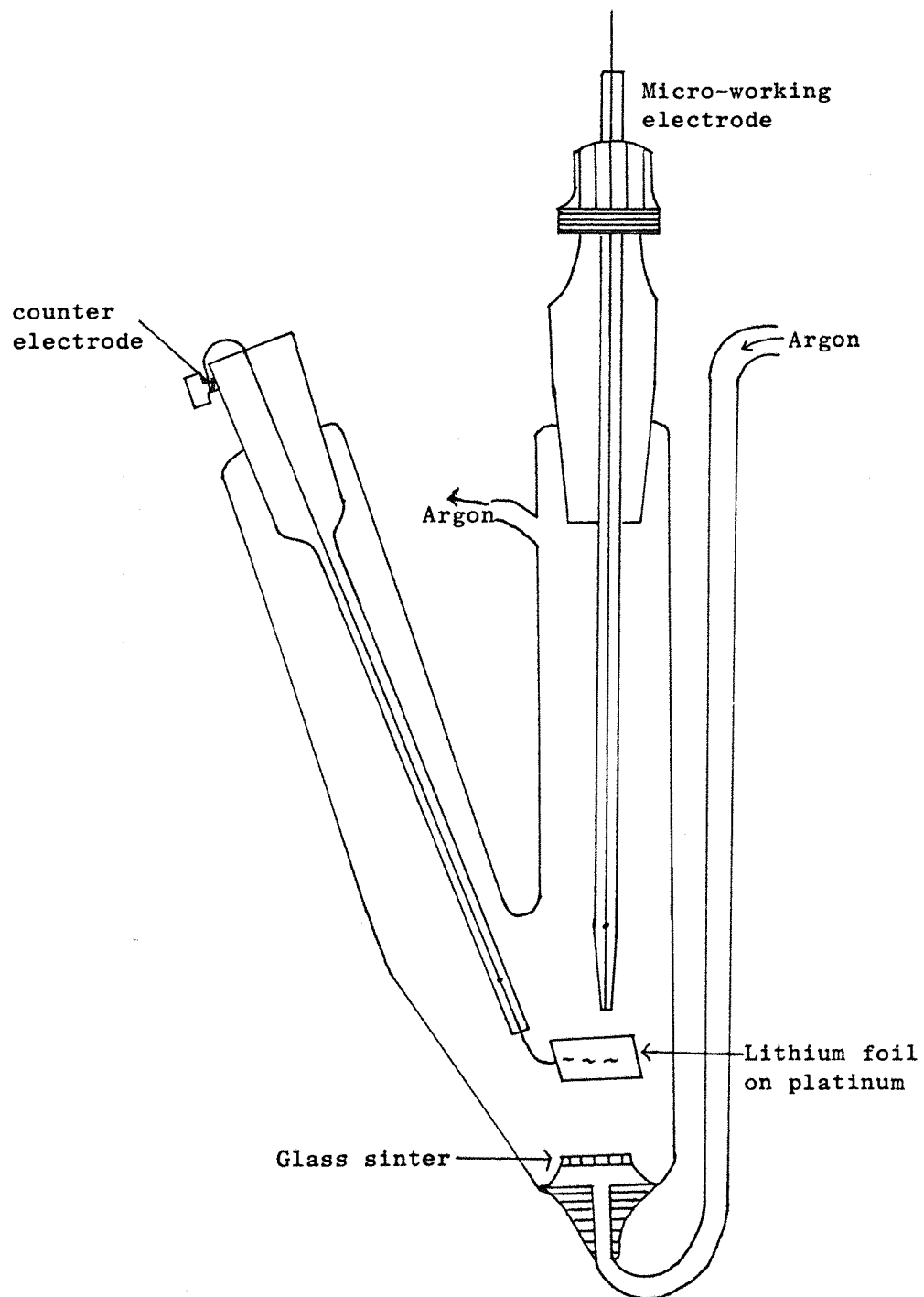


Figure 2.1 Cell used for the deposition of lithium onto microelectrodes at ambient temperatures.



**Figure 2.2** Cell used for the deposition of lithium onto microelectrodes at elevated or reduced temperatures.

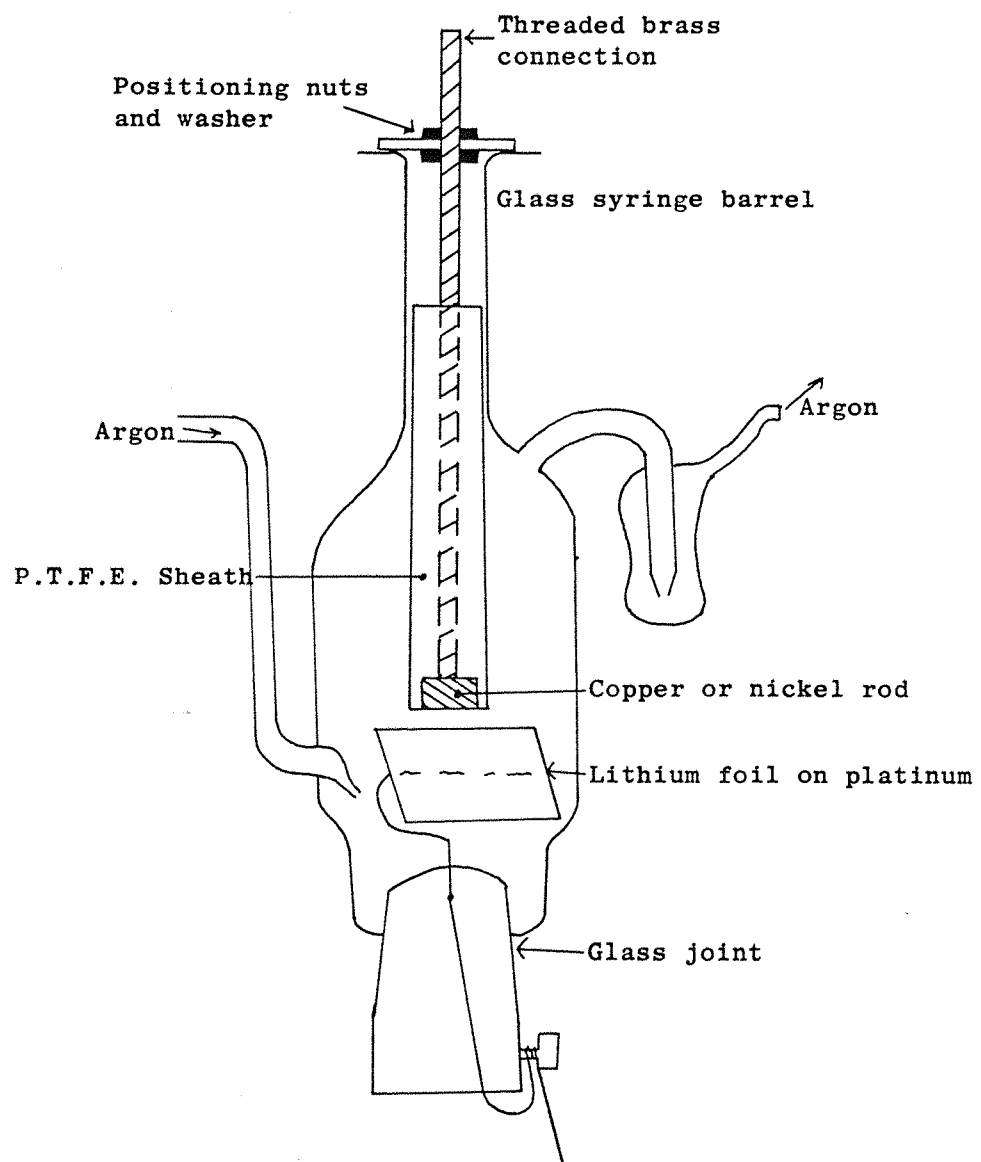


Figure 2.3 Cell used for the deposition of lithium onto copper and nickel macroelectrodes.

collapsed onto the wire by applying a vacuum along the capillary and heating it. The end of the electrode was then polished (see 2.3) to reveal a disc of metal surrounded by glass. To give the electrode mechanical strength, the thicker nichrome wire was also sealed to the glass. Details of the metal wires used can be found in table 2.1.

(b) Carbon microelectrodes

The carbon microelectrodes were made by sealing a carbon fibre into a glass capillary, under vacuum as described in 2.2(a).

Electrical contact was made by partially filling the capillary with lead beads, inserting a copper wire from the top and then heating the assembly until the lead melted, at approximately 100°C. Whilst the lead was molten, a slight vacuum was applied to the capillary to remove any air bubbles. The electrode was then allowed to cool. Details of the carbon fibre used can be found in table 2.1, while fig. 2.4(b) shows a finished electrode.

(c) Macro working electrodes

Copper and nickel macroelectrodes (fig. 2.5) were prepared by sealing a rod of the desired metal into PTFE, with a brass contact, to reveal a disc of metal exposed to the solution. The PTFE sheath is machined to fit the syringe barrel of the cell as tightly as possible.

Details of the metal rods used can be found in table 2.2.

(d) Secondary and reference electrodes

In all of the experiments, a two electrode cell was used in which the counter electrode acts as a secondary and reference electrode. The counter electrode used was a piece of lithium foil (Foote Mineral Co.) pressed onto a platinum wire sealed into glass, fig. 2.6. This process was carried out in the argon filled dry box (see 2.6).

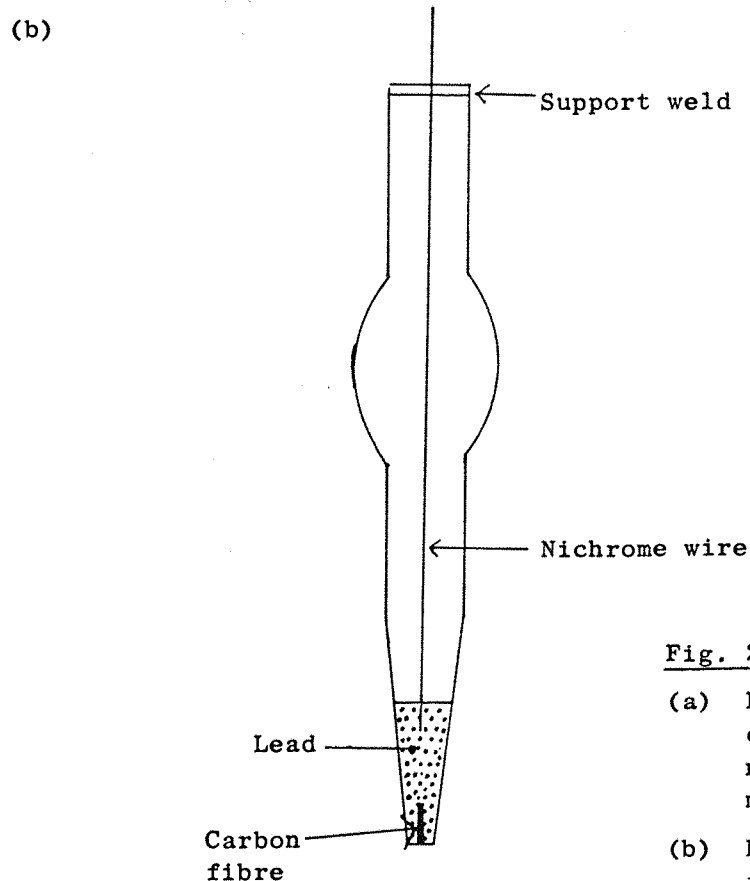
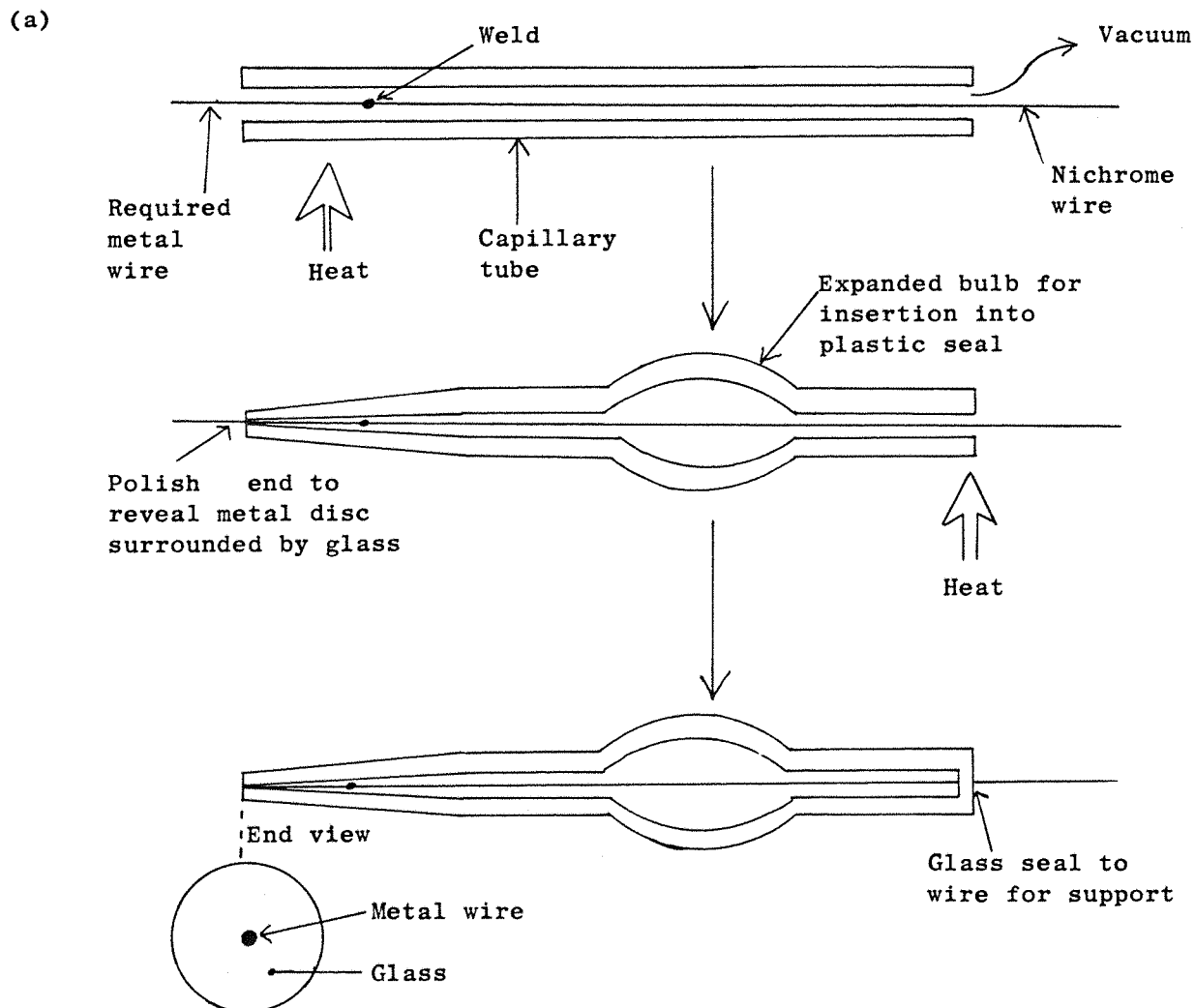


Fig. 2.4

(a) Flow diagram for the construction of the copper, nickel and aluminium microelectrodes.

(b) Diagram of a finished carbon fibre microelectrode.

Electrode material	Supplier	Purity (%)	Diameter ( $\mu\text{m}$ )	Disc of area ( $\text{cm}^2$ )
Copper	Single strand untwisted from mains cable	unknown	80	$5 \times 10^{-5}$
			40	$1.25 \times 10^{-5}$
Nickel	Goodfellow Metals	99	50	$2 \times 10^{-5}$
Aluminium	Goodfellow Metals	>99.99	50	$2 \times 10^{-5}$
Carbon fibre	Harwell	-	8	$5 \times 10^{-7}$

Table 2.1 Details of the metal wires and carbon fibres used in constructing the microelectrodes.

Metal rod	Supplier	Purity (%)	Diameter (mm)	Disc of area (cm <sup>2</sup> )
Copper	Johnson Matthey	Spectro-graphical standard	7.0	0.38
Nickel	Johnson Matthey	Spectro-graphical standard	5.0	0.20

Table 2.2 Details of metal rods used in constructing the macroelectrodes.

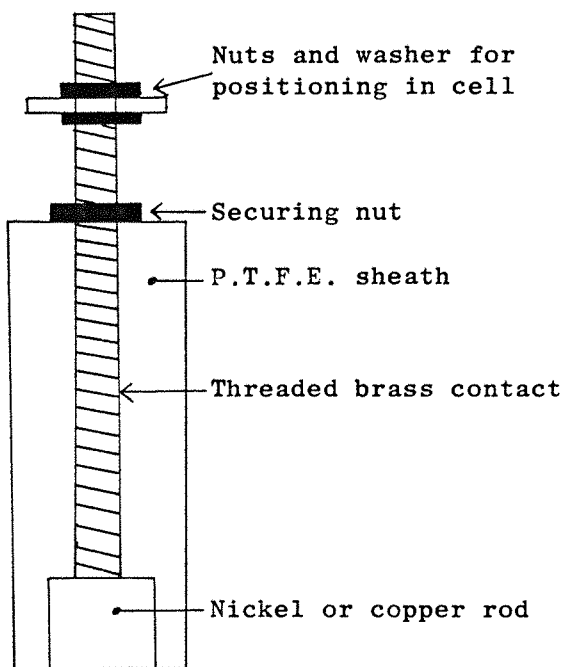


Figure 2.5 Finished macroelectrode.

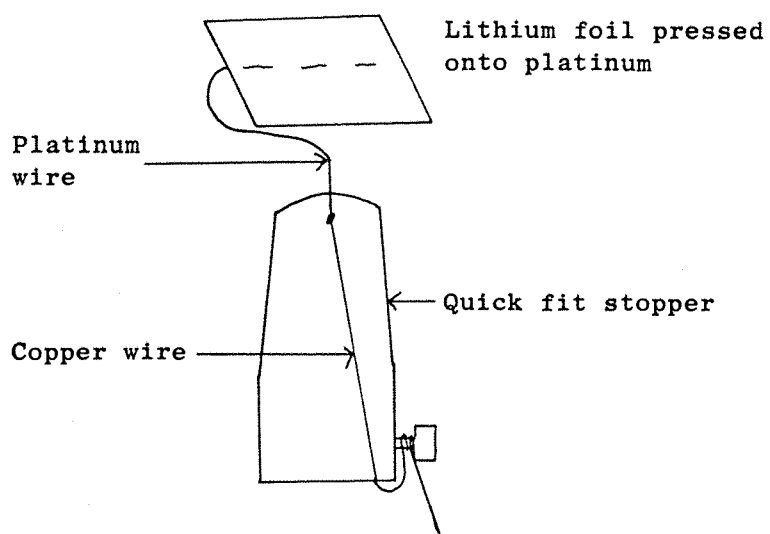
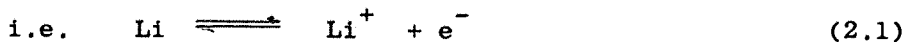


Figure 2.6 Combined secondary and reference electrode.

When placed in the same lithium ion solution as the working electrode, the lithium foil and hence the whole of the counter electrode adopts the potential characteristic of the lithium/lithium ion couple.



Thus, all the potentials quoted in this report are versus this equilibrium potential for lithium in the solution under study. Therefore, when considering the deposition and dissolution of lithium the applied potentials are, in fact, the overpotentials.

This choice of reference electrode is excellent while the solvent and lithium ion concentration are kept constant. It does not, however, allow ready comparison between experiments in different solvents. Throughout this study, the concentration of lithium ion was varied very little ( $0.5 \pm 1.1 \text{ moles dm}^{-3}$ ).

### 2.3 Electrode polishing

#### (a) Microelectrodes

After being sealed into glass, the electrode tip was ground on a grinding wheel until visually flat. It was then successively polished with fine emery paper and 12 micron polishing paper (3M, wet or dry production) until a flat background current was obtained during potential sweep experiments. Once this situation had been reached, any further polishing was done on the 12 micron polishing paper.

Water based polishing powders were not used so as to minimise the risk of contaminating the solution during experimental work.

#### (b) Macroelectrodes

Before each experiment, the electrodes were polished on fine emery paper until all of the previous deposit and large pits had

been removed. 3.0 micron polishing alumina (Banner Scientific Ltd.), supported on a polishing cloth with water as the lubricant was then used until the surface was visually smooth with a mirror finish. 0.05 micron alumina (Banner Scientific Ltd.) was then used in the same way for about 15 minutes.

The electrode was then rinsed and wiped dry with a tissue.

To remove water which had crept up the gap between the metal rod and PTFE sheath, the electrode was heated with a warm air dryer and placed under vacuum for approximately 15 minutes.

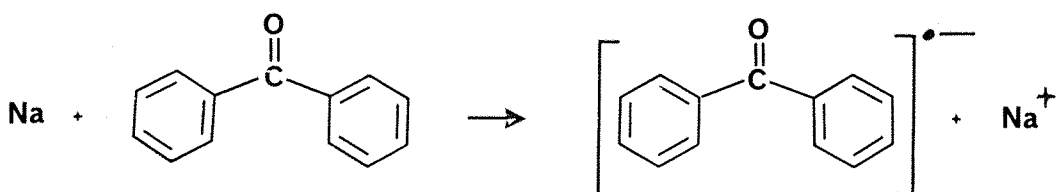
#### 2.4 Sources and treatment of chemicals

Table 2.3 lists the suppliers and grades of all the chemicals used.

With the exception of lithium bromide, which was heated at 160° centigrade in a vacuum oven overnight, all of the salts were used as received. All of the lithium salts and the lithium metal were stored in the argon filled dry box.

Initially, the ether type solvents; tetrahydrofuran (THF), 2-methyltetrahydrofuran (2-Me-THF), dioxolane and diethylether (DEE) were purified by distillation from sodium metal under a nitrogen atmosphere, only the middle fraction being collected. During the course of this work, however, it was found that a more satisfactory method was to distil the required ether from sodium metal and benzophenone, under a nitrogen atmosphere using the apparatus shown in fig. 2.7.

Equimolar amounts of freshly cut sodium and benzophenone are added to the ether to produce the benzophenone anion radical:-



Chemical	Grade	Supplier
Lithium hexafluoroarsenate	Electrochemical	USS Agri-Chemicals
Lithium hexafluorophosphate	Reagent	Aldrich
Lithium tetrafluoroborate	Reagent	Aldrich
Lithium bromide	Reagent	Koch-Light Labs. Ltd.
Lithium metal	High purity	Foote Mineral Co.
Sodium metal	Reagent	BDH
Calcium hydride	Reagent	Aldrich
Benzophenone	Reagent	BDH
Nitrogen	Reagent	BOC
Argon	High purity	BOC
Tetrahydrofuran	Reagent	Various
2-methyltetrahydrofuran	Reagent	Aldrich
Diethyl ether	Reagent	May and Baker
Dioxolane	Reagent	Aldrich
Propylene carbonate	Reagent	Aldrich
Acetone	Reagent	May and Baker
Nitric acid	Reagent	May and Baker
Liquid Paraffin	-	Evans Medical Ltd.
Polishing aluminas	-	Banner Scientific Ltd.
12 micron polishing cloth	-	3M

Table 2.3 Suppliers and grades of all chemicals used.

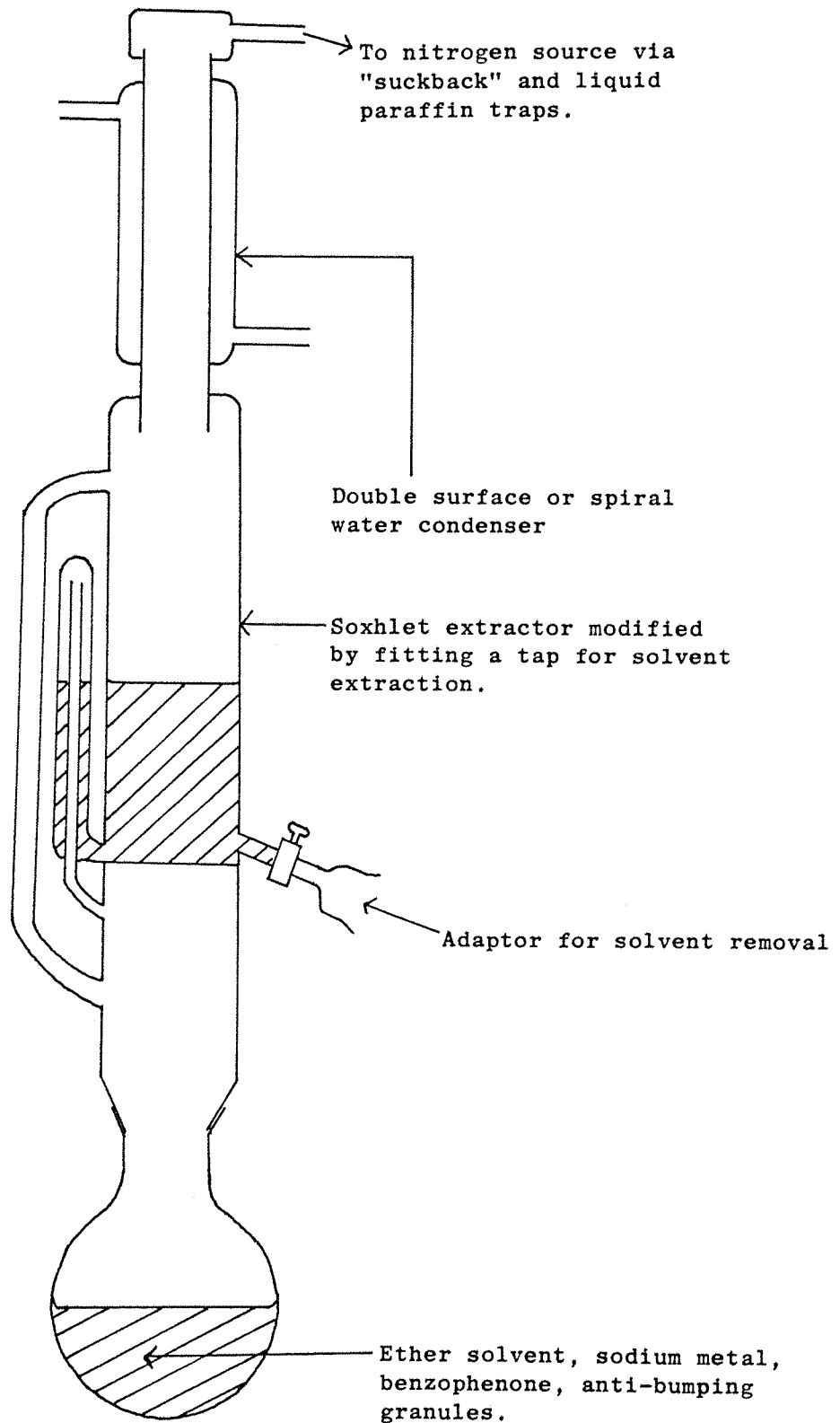


Figure 2.7 Apparatus for the continued distillation of ether type solvents.

This deep blue coloured anion radical acts as a scavenger for water and oxygen, so removing them from the solvent. The sodium metal also reduces any peroxides formed.

For the experiments reported in this thesis, THF and DEE were prepared in this way. The data obtained for dioxolane and 2-Me-THF, used solvent distilled only from sodium. Future work will use the Na/benzophenone method.

Immediately after distillation the solvent was transferred to the dry box and back flushed with argon to remove any dissolved nitrogen. Experiments with these solvents were always performed immediately after distillation.

Propylene carbonate (PC) was distilled from calcium hydride under reduced pressure, only the middle fraction being collected over alumina.

Deionised water, with  $K \leq 5 \mu\Omega^{-1}$ , was used for polishing electrodes and washing glassware.

## 2.5 Instrumentation

Experiments employing the microelectrodes involve very small currents (typically  $< 10^{-6}$  amps) and hence due to the virtual absence of IR drop, a two electrode cell may be used; the counter electrode serving as both reference and secondary electrode.

For the experiments with a microelectrode, the potentials were programmed using a Hi-Tek waveform generator, model PPR1 and no potentiostat was employed.

The currents flowing through the cell were amplified using a house built amplifier capable of the range  $10^{-4} \rightarrow 10^{-9}$  amps. The output, 10 volts full scale, was displayed either directly on a Farnell XY recorder, or stored in a Gould digital oscilloscope, type OS4100, or a BBC microcomputer and then transferred to the XY recorder.

Block diagrams of the instrumentation can be seen in figures 2.8(a) and 2.8(b).

For the constant current deposition of lithium onto a macroelectrode, a two electrode cell was again used in conjunction with a Hi-Tek, type DT2101, potentiostat and an electronic integrator to measure the charge passed (fig. 2.9). For the analysis of the short time current responses to potential step experiments, a BBC microcomputer was used in conjunction with an in-house built analogue-to-digital converter. A Solidisk<sup>75</sup> silicon disc drive was used to facilitate rapid data storage and analysis. The software used to collect and analyse the data was written by members of the Southampton electrochemistry group<sup>76</sup>.

## 2.6 The argon filled dry box

A continually circulating argon filled dry box system was used to store the air sensitive chemicals and to prepare the solutions. Photographs of the dry box can be found in fig. 2.10.

The glove box was a Faircrest Engineering Ltd. Mark 4B box with a small non-evacuable posting port and a large evacuable transfer port.

All of the pipework, the molecular sieve holders and the control electronics were designed and built by members of the Battery Research Group at the Hirst Research Centre (G.E.C.). The argon was pumped through activated molecular sieves and into the box at a rate of 50 litres per minute.

A piece of lithium foil, left exposed to the glove box atmosphere did not tarnish significantly over a six month period - a qualitative indication of the very low water, oxygen and nitrogen content of the box atmosphere. Typically in such dry box systems the water content is below 10 p.p.m.

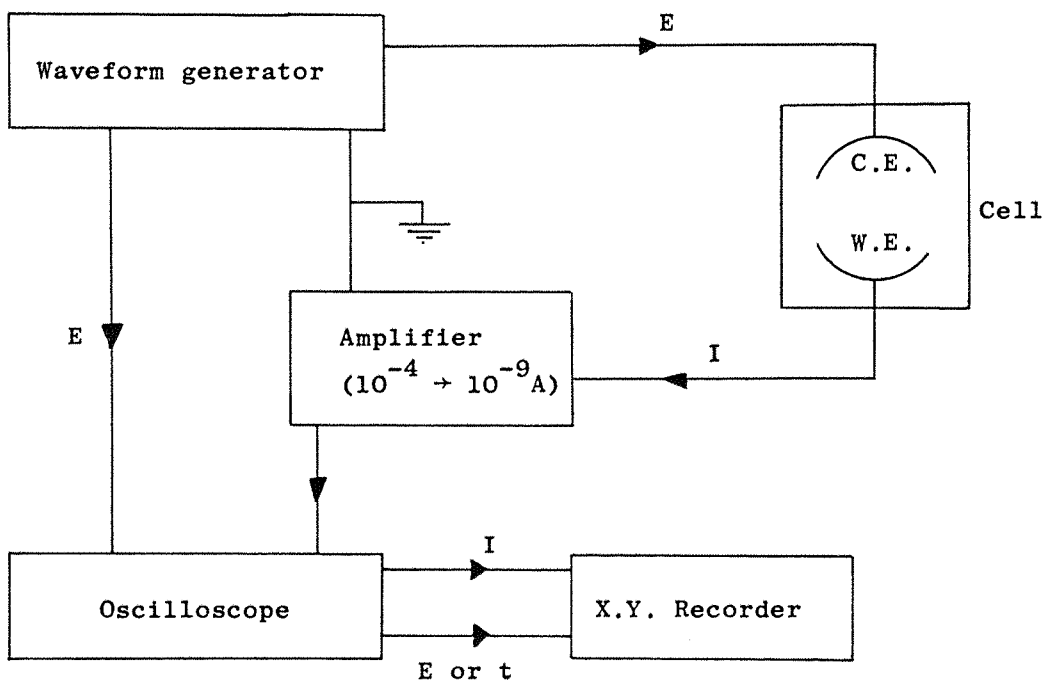


**Figure 2.8(a)** Block diagram of the instrumentation used for the cyclic voltammogram and potential step experiments employing microelectrodes.

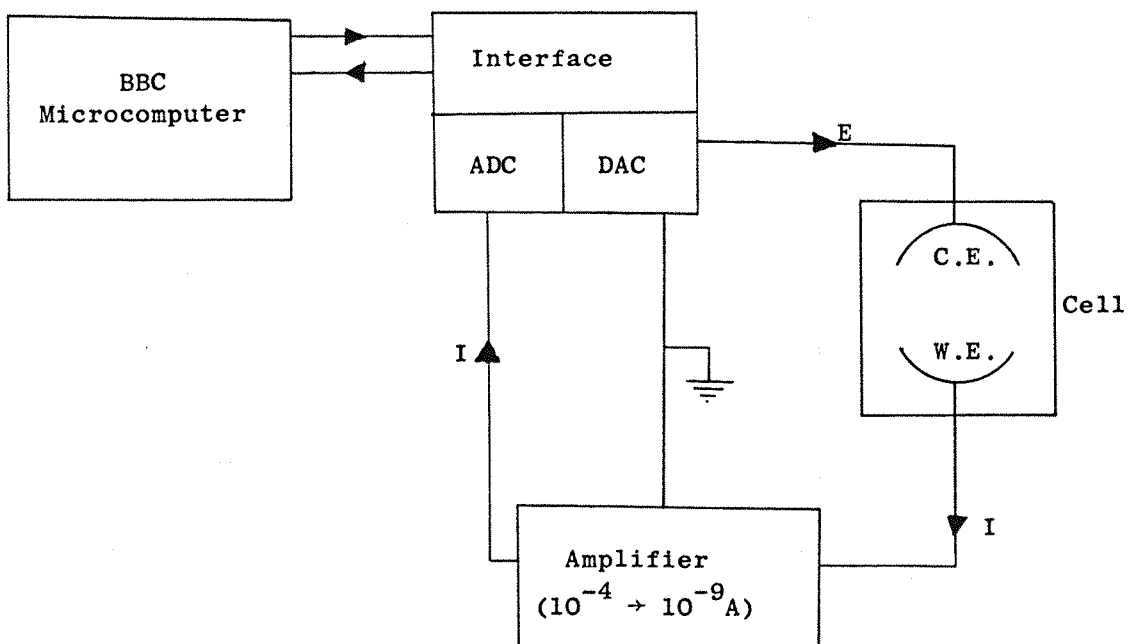


**Figure 2.8(b)** Block diagram of the instrumentation used when employing the BBC microcomputer for experiments involving the microelectrodes.

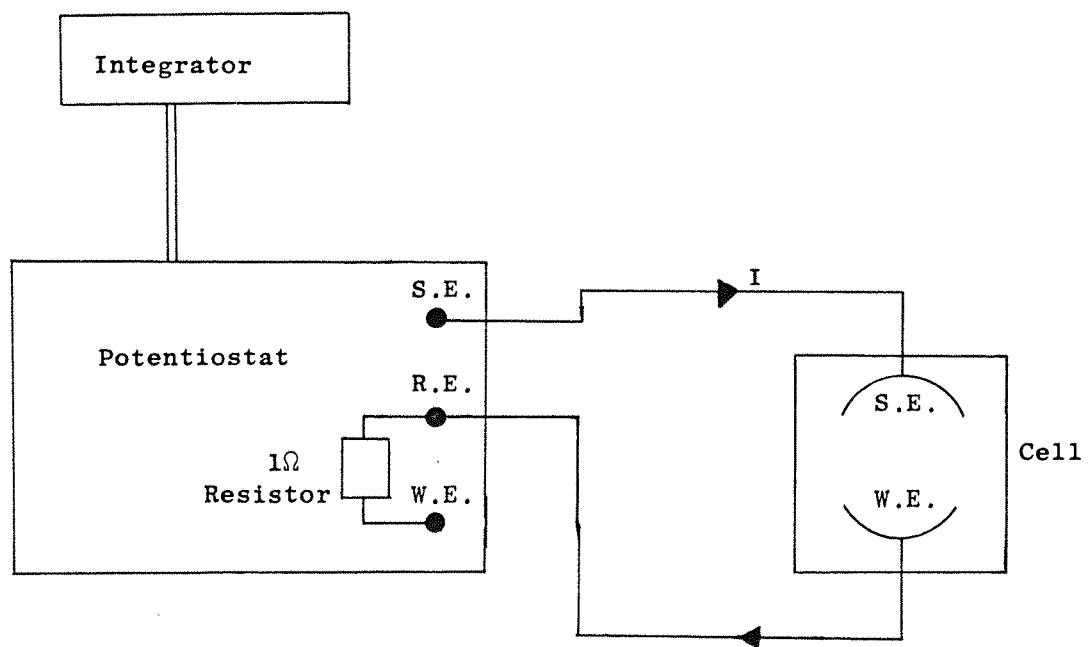


Figure 2.9 Block diagram of the instrumentation used for the constant current deposition of lithium onto a macroelectrode.

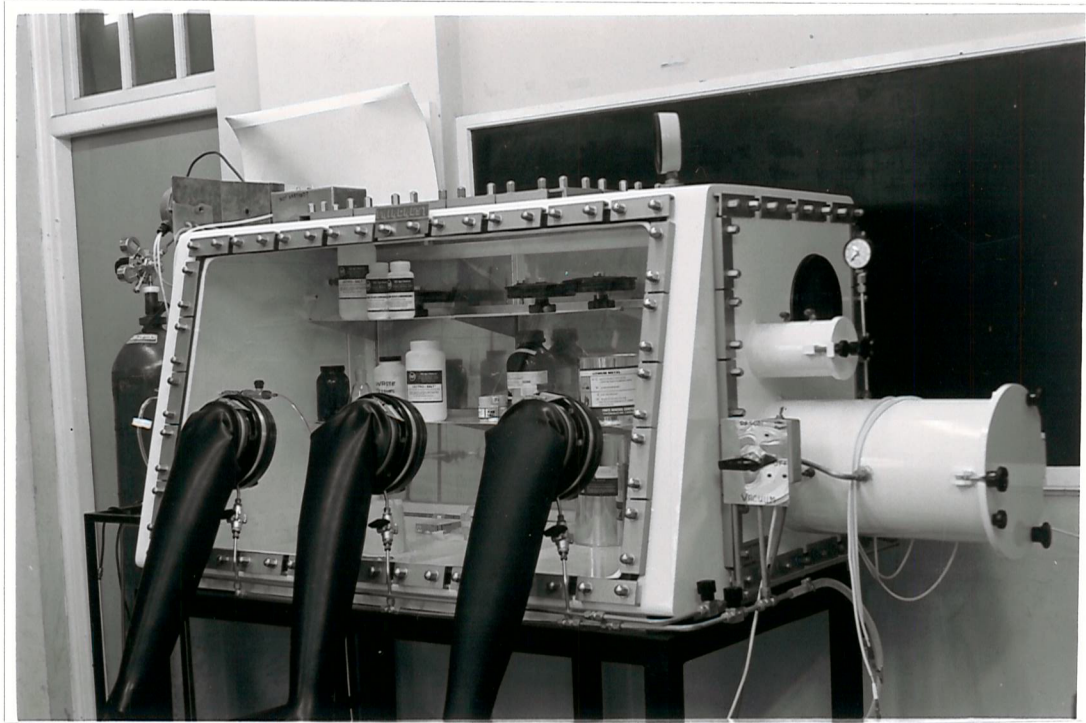
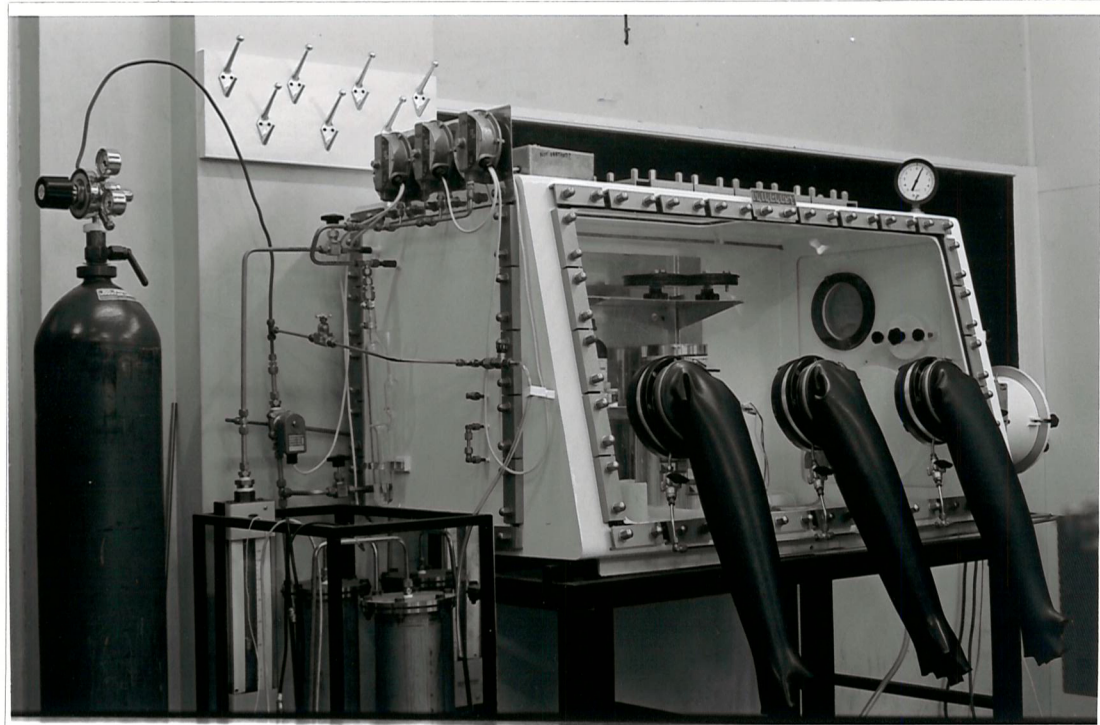


Fig. 2.10 Photographs of the circulating argon filled dry box system used during this study.



## 2.7 Experimental procedure

It was found during the course of this work that the results of similar experiments performed inside and outside the dry box did not differ significantly, providing that the experiments done externally were flushed regularly with argon. As the experiments were more conveniently performed externally, all of the results quoted, except where stated, were taken from experiments set up inside, but performed outside of the dry box.

Prior to use, all glassware including cells, was cleaned by immersion in dilute nitric acid, followed by continued rinsing in deionised water. It was then rinsed with acetone and dried with a hot air blower. Platinum wires, used as electrical contacts in the counter electrodes, were cleaned in the flame of a bunsen burner until the flame regained its usual colour.

The clean glassware and a flask of the freshly distilled solvent being used, were then placed in the dry box via the vacuum port where all of the outside atmosphere was removed and replaced with dry argon.

Once inside the box, the glassware was placed under a jet of argon to remove any traces of dust or air adhering to its walls and the solvent was flushed with argon to remove any dissolved nitrogen remaining from the still.

In the majority of the experiments the required lithium salt was made up to be approximately 0.5 moles  $\text{dm}^{-3}$  in the chosen solvent. Since the salts used are extremely hygroscopic and the ether solvents decompose quite readily, all of the solutions used were made up immediately before use.

Inside the dry box a given volume of the required salt was placed into a volumetric flask of known mass. This was then removed from the dry box, weighed, and the mass of salt used calculated by difference. Once back in the dry box the required

volume of solvent was added to make the solution.

The lithium counter electrode was made by sandwiching the platinum wire between a piece of folded lithium foil. The electrode was then placed in position in the cell and a glass stopper placed in the position of the working electrode.

The completed cell and the flask of solution were then removed from the box. Once outside the solution was quickly poured into the cell and argon bubbled through it.

(a) Experiments involving microelectrodes

Before each cyclic voltammogram or potential step experiment the electrode was polished on the 12 micron polishing cloth. For copper and nickel electrodes this could be done in approximately 30 seconds. For aluminium, however, where the lithium moves into the aluminium lattice, a longer period of polishing was required.

The I-E responses from cyclic voltammetry experiments were recorded directly onto the XY recorder.

The I-t responses from potential step experiments were recorded onto an oscilloscope or into the BBC microcomputer and then played back onto the XY recorder.

At the beginning of each series of experiments, it was necessary to set up the zero position of the current measurement system. This was best done by recording cyclic voltammograms and adjusting the amplifier until the current-potential curve on the reverse sweep passed exactly through zero. Once this adjustment had been made (which was anyway small) no further drift was observed.

Once the shape of the cyclic voltammogram for lithium being deposited on copper had been established, it was used as a "fingerprint" check for each new solution, i.e. before a set of experiments was carried out on a new solution, the cyclic voltammogram on copper

was recorded and data such as the nucleation potential, peak, currents and stripping efficiency were compared with the established result.

(b) Experiments involving macroelectrodes

The polished electrode was placed in the syringe barrel and moved to approximately 0.5 cm from the counter electrode. The desired, constant current was then selected on the potentiostat by placing a one ohm resistor between the reference and working electrode terminals (fig. 2.9) and dialling up the numerically equivalent voltage. An electronic integrator was used to measure the charge passed during the electrolysis.

When the experiment was finished the cell was transferred to the dry box where the working electrode was removed. The working electrode was then washed with pure solvent to remove any salt and dried in a stream of argon. The deposit was then visually inspected.

CHAPTER THREE

RESULTS AND DISCUSSION

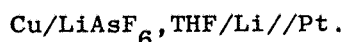
## RESULTS AND DISCUSSION

### ELECTRODEPOSITION AND DISSOLUTION OF LITHIUM IN ETHER

#### TYPE SOLVENTS

3.1 Deposition and dissolution of lithium using a copper microelectrode in a solution of  $\text{LiAsF}_6$ /THF at room temperature

The system chosen for the initial studies of lithium deposition and dissolution consisted of a copper working electrode in a solution of  $\text{LiAsF}_6$ /THF at room temperature. The reference and counter electrode consisted of a lithium foil supported on a Pt wire in the same solution and sited about 0.5 cm from the Cu microelectrode. Hence the cell was:-



Copper was chosen as the working electrode because it was known that lithium does not alloy with copper at room temperature.  $\text{LiAsF}_6$  was selected as the supporting electrolyte and  $\text{Li}^+$  ion source because it is available commercially as an anhydrous salt and it has a high solubility in ether type solvents. Tetrahydrofuran was chosen as the solvent due to its use in certain Li batteries and because of an interest within the Group in forming lithium alkyls in situ from freshly deposited lithium.

The resistance of the experimental cell filled with  $\text{LiAsF}_6$ /THF (0.6 moles  $\text{dm}^{-3}$ ) was measured using an AC bridge and was found to be  $5000\Omega$ . Therefore, when considering current densities as high as  $100 \text{ mA cm}^{-2}$ , the maximum ohmic drop is only 25 mV since the actual current flowing through the cell is only  $5 \mu\text{A}$  (in the majority of experiments the current densities were much lower). In many ways the better test of the absence of significant IR drops is to repeat the experiment with an electrode of different area where only the current should change and there should be no shift in peak potential or change in the shape of transients. During this work two electrodes whose areas differed by a factor of four were used

for such checks (see later).

### 3.1.1 Cyclic voltammetry

Figure 3.1 shows a cyclic voltammogram run at  $100 \text{ mV s}^{-1}$  using a copper microelectrode ( $r = 40 \mu\text{m}$  and area  $5 \times 10^{-5} \text{ cm}^2$ ) in  $\text{LiAsF}_6/\text{THF}$  (1.1 moles  $\text{dm}^{-3}$ ) recorded between +500 mV and -150 mV vs the  $\text{Li}/\text{Li}^+$  reference electrode in the same solution.

At the scan rate used, no current is observed until -90 mV at which point the cathodic current rises very steeply. At the negative potential limit the current is still rising and continues to do so at the beginning of the reverse sweep.

During the reverse sweep, at negative overpotentials, the cathodic current is always higher than on the forward sweep and reduction continues until 0 mV.

The current then crosses the potential axis at 0.0 mV and an anodic current is seen which increases with the applied overpotential until a peak is observed at  $E_p = 205 \text{ mV}$  after which the current falls sharply to zero. The "nucleation loop" seen at negative overpotentials is good evidence for a deposition process involving the formation of a new phase. Although it is thermodynamically favourable for  $\text{Li}^+$  ions to be reduced at all negative overpotentials, there is a kinetic barrier associated with the need to form the lattice of the new phase on the electrode surface. This barrier is overcome by supplying energy in the form of the nucleation overpotential, which for this system is seen to be 90 mV. Once the nuclei of lithium have formed they continue to grow in size, thus creating a larger surface area for electron transfer and so the current rises with time as well as with increasing overpotential.

On the way back the lithium continues to deposit at all negative overpotentials as this kinetic barrier does not exist when depositing lithium on lithium. The fact that the current crosses through the voltage axis, without a potential region of

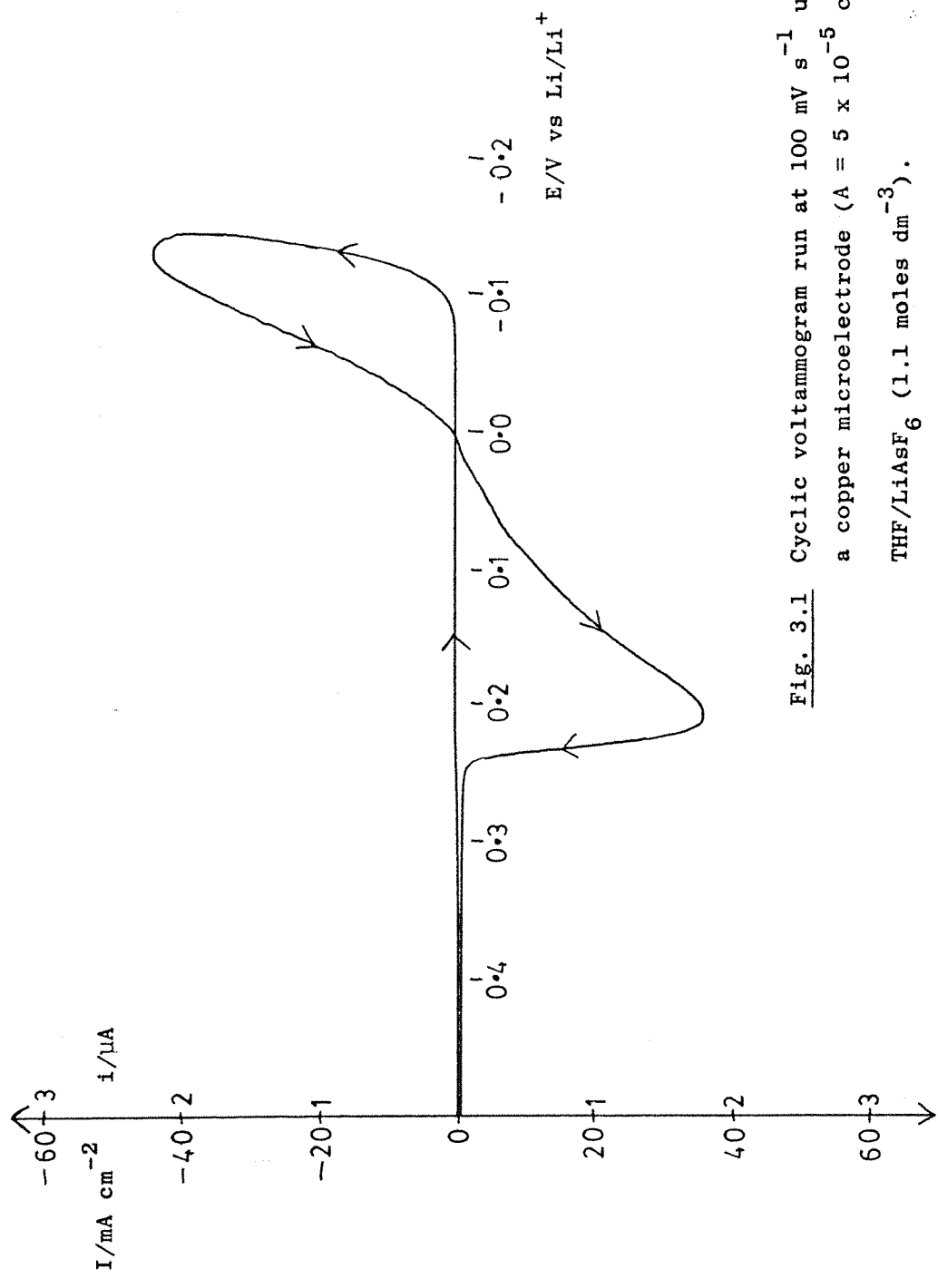


Fig. 3.1 Cyclic voltammogram run at  $100 \text{ mV s}^{-1}$  using a copper microelectrode ( $A = 5 \times 10^{-5} \text{ cm}^2$ ) in  $\text{THF}/\text{LiAsF}_6$  ( $1.1 \text{ moles dm}^{-3}$ ).

low or zero current, is a good indication that under these conditions, the kinetics of the  $\text{Li}/\text{Li}^+$  couple, on lithium, are fast (see later). As soon as the applied potential becomes positive with respect to the  $\text{Li}/\text{Li}^+$  couple, oxidation of the deposited lithium layer occurs and dissolution begins. The rate of dissolution increases as the potential is scanned positive but eventually the layer of lithium is depleted and the current falls sharply to zero.

The charge associated with the deposition process was measured by integrating the charge under the forward and reverse sweeps at negative overpotentials; for the voltammogram in fig. 3.1 it is  $79 \text{ mC cm}^{-2}$ . The stripping efficiency is almost 100%. Other features of the voltammogram to be noted are:-

- (i) The virtual absence of any background or charging currents prior to deposition.
- (ii) Despite the low measured currents the current densities are large and certainly within the technologically significant range.

Both illustrate the advantages of using microelectrodes for these investigations.

During the course of this work, this cyclic voltammogram was reproduced many times and it was normally the first experiment performed in any series to ensure the quality of the solutions, etc.

The effect of varying the potential sweep rate can be seen in fig. 3.2, which shows cyclic voltammograms run at 25, 100 and  $250 \text{ mV s}^{-1}$  for the same system as in fig. 3.1, from +500 mV to -150 mV vs the  $\text{Li}/\text{Li}^+$  reference.

Increasing the sweep rate causes nucleation to occur at more negative potentials and hence leads to a decrease in current

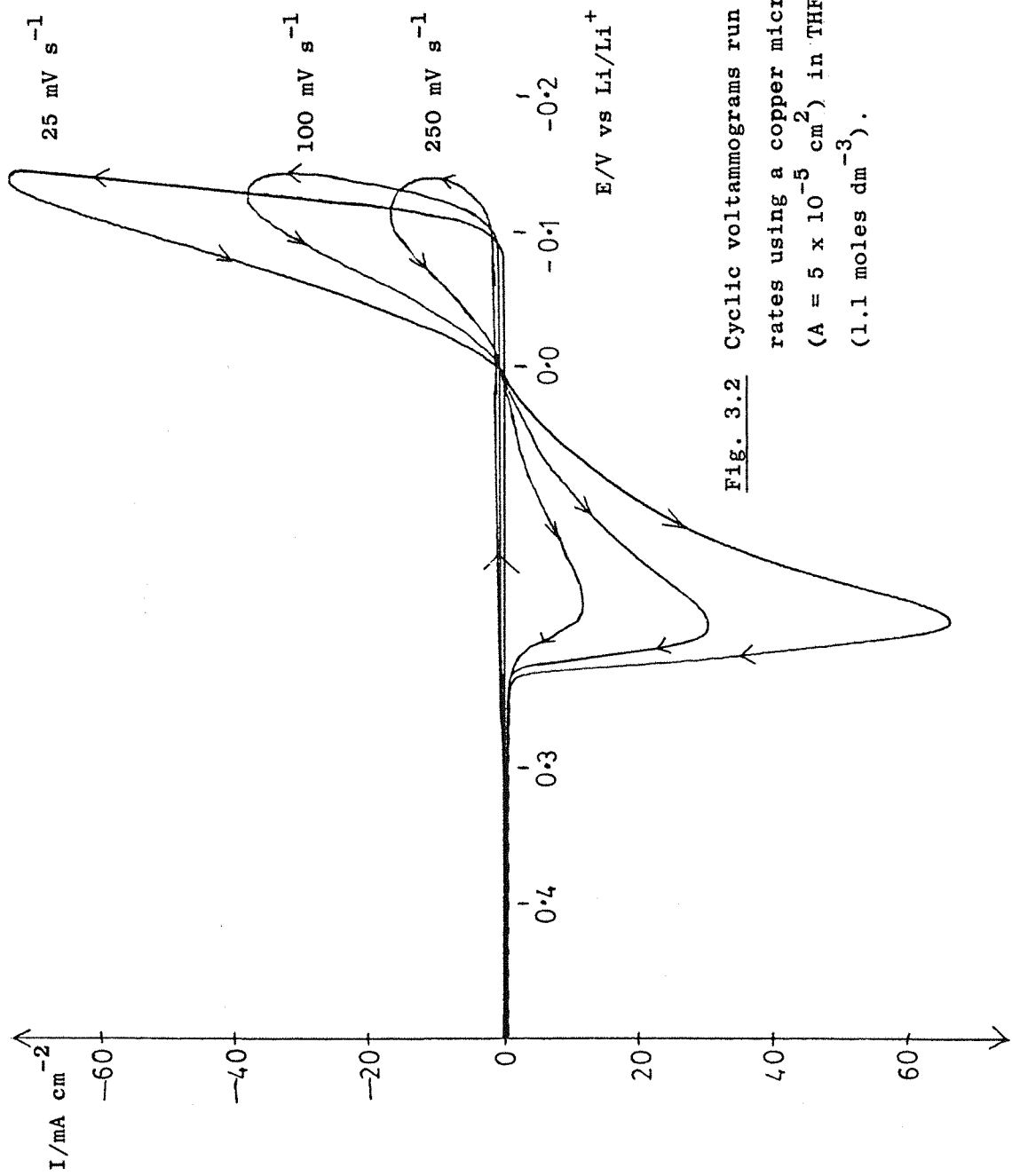


Fig. 3.2 Cyclic voltammograms run at various sweep rates using a copper microelectrode ( $A = 5 \times 10^{-5} \text{ cm}^2$ ) in  $\text{THF}/\text{LiAsF}_6$  (1.1 moles  $\text{dm}^{-3}$ ).

and charge for both the deposition and dissolution process. This result emphasises the fact that the number of nuclei formed under given conditions (e.g. temperature, composition, etc.) is a function of both potential and time. Another feature to notice is the slight increase in charging current associated with an increase in sweep rate.

Figure 3.3 shows the effect of varying the negative limit for cyclic voltammograms run at  $100 \text{ mV s}^{-1}$ , again with the same system as described for fig. 3.1. The background current and nucleation overpotential are virtually identical for the two sweeps but the charge associated with the nucleation loop for the sweep to the more negative limit is, as expected, greater, indicating that a larger amount of lithium has been deposited. The stripping peak is correspondingly larger reflecting the increased time required to remove all of the deposit.

As stated earlier, the best method of testing for the absence of significant IR drop is to use an electrode of reduced area. Figure 3.4 compares the results of cyclic voltammograms run from +500 to -150 mV at  $100 \text{ mV s}^{-1}$  in the same solution, for two electrodes whose areas differ by a factor of four; the radii being 40 and  $20 \mu\text{m}$  respectively. Despite the variation in electrode area the results are, within experimental error, identical. The stripping peak potentials are the same within 10 mV and the ratio of anodic to cathodic charge is 1.0 in both cases. Moreover, the ratios of the anodic peak current to cathodic current at -150 mV are very similar. This result confirms the absence of significant IR drop even at high current densities and so illustrates one of the major advantages gained by the use of microelectrodes.

The effect of cycling the copper electrode over the range +500 mV was also probed using cyclic voltammetry. Using a clean, freshly polished, electrode the potential was repeatedly scanned at  $100 \text{ mV s}^{-1}$  again using the same conditions as described for fig. 3.1. The first scan resulted in a cyclic voltammogram

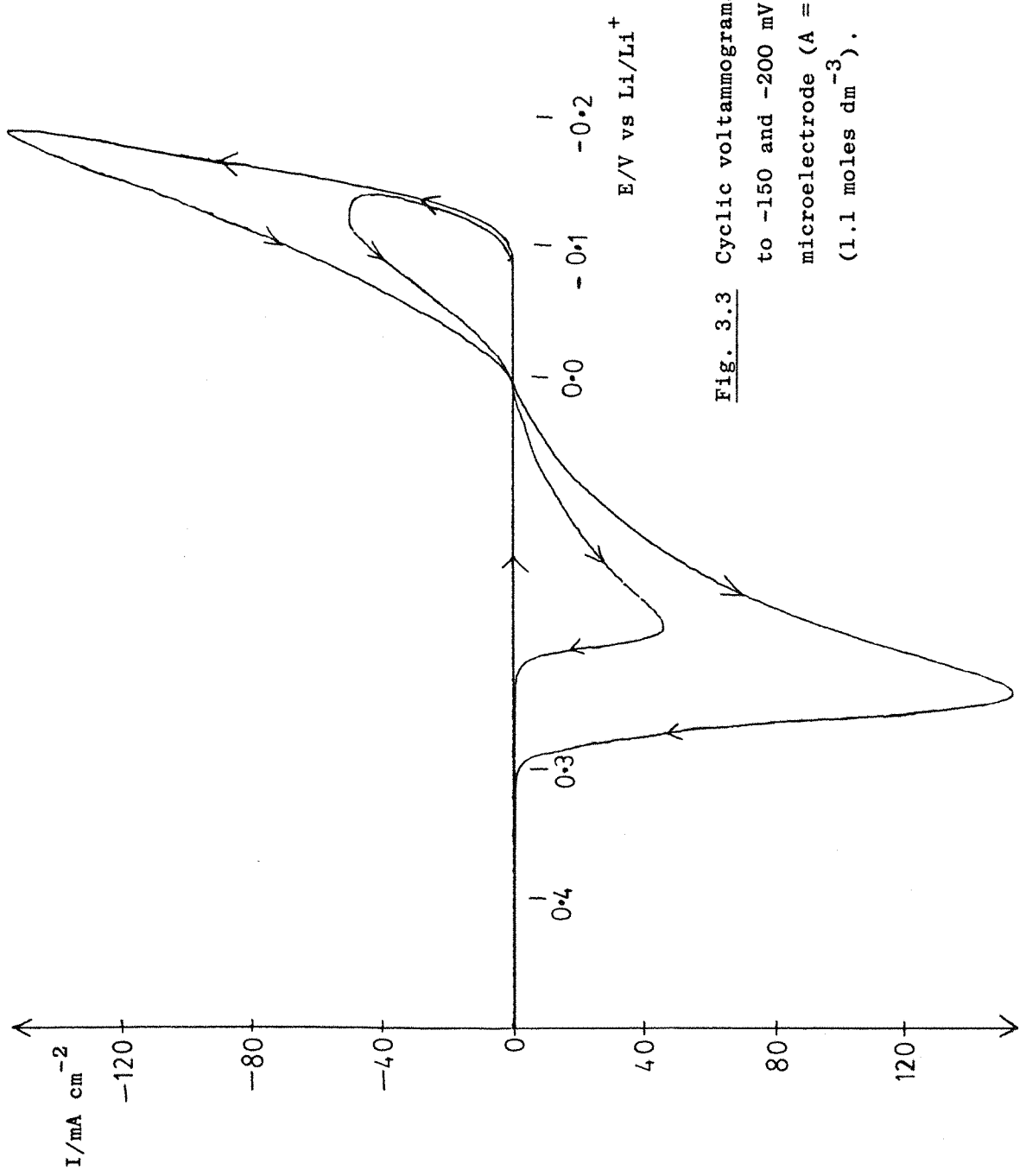


Fig. 3.3 Cyclic voltammograms run at 100  $\text{mV s}^{-1}$  to -150 and -200 mV using a copper microelectrode ( $A = 5 \times 10^{-5} \text{ cm}^2$ ) THF/LiAsF<sub>6</sub> (1.1 moles  $\text{dm}^{-3}$ ).

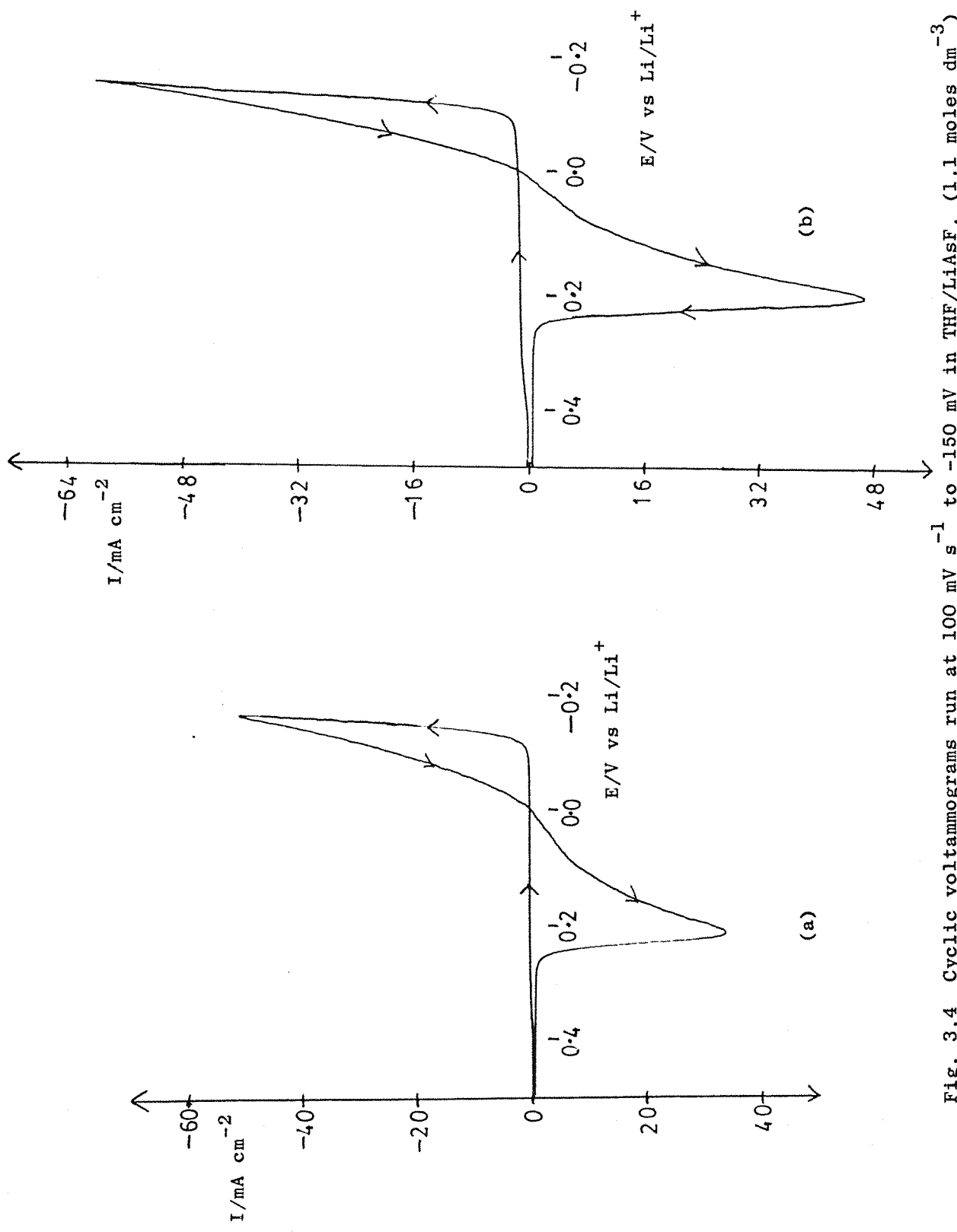


Fig. 3.4 Cyclic voltammograms run at  $100 \text{ mV s}^{-1}$  to  $-150 \text{ mV}$  in  $\text{THF/LiAsF}_4$  (1.1 moles  $\text{dm}^{-3}$ ) using copper microelectrodes of differing areas:  
 (a)  $A = 5 \times 10^{-5} \text{ cm}^2$ , (b)  $A = 1.25 \times 10^{-5} \text{ cm}^2$

identical to that of fig. 3.1. On the second sweep, however, nucleation occurred approximately 10 mV earlier at -80 mV but the peak current at the cathodic limit was about 15% lower. On the reverse sweep the current crossed the potential axis at zero and a stripping peak was observed although the peak current (and hence charge) was less than that on the first sweep. During successive cycles this trend continued until the twentieth cycle by which time nucleation was occurring at 50 mV and the peak cathodic current was only 50% (i.e.  $25 \text{ mA cm}^{-2}$ ) of that of the first cycle. The stripping peak was correspondingly smaller and the stripping efficiency had decreased to approximately 65% during each cycle. By the fiftieth cycle, the stripping peak ceased to be a smooth curve and became erratic, probably indicating that dissolution was no longer a simple process. Probably a film on the lithium or copper surface determines the results. Hence throughout this study, the results presented are for first sweeps on freshly polished surfaces.

When comparing these cyclic voltammograms to previous work in the literature<sup>44,51,53</sup> it is essential that the sensitivity of the measurements be noted. The scaling of the potential axis is particularly important. For the cyclic voltammograms presented here, parameters such as the nucleation potential, reversible potential and current densities at particular overpotentials may be clearly identified. For the data in the literature, potential scales are commonly 1V/cm and hence it is impossible to measure potentials with any accuracy and the peaks have been forced to appear to have a reasonable shape.

### 3.1.2 Underpotential deposition

Since reports on the underpotential deposition of lithium have appeared in the literature<sup>60-62</sup> it was considered of interest to briefly investigate whether this phenomenon could be observed using cyclic voltammetry at a microelectrode.

Cyclic voltammograms were run to  $-150$  mV at  $100 \text{ mV s}^{-1}$  in the same solution as described for figure 3.1. Initially, the starting potential was  $+800$  mV versus the  $\text{Li}/\text{Li}^+$  couple although this was systematically increased to  $+1.5\text{V}$ . The charge associated with the formation of a monolayer is usually of the order of  $200 \mu\text{C cm}^{-2}$ . Thus for a microelectrode of area  $5 \times 10^{-5} \text{ cm}^2$  the total charge expected is  $10 \text{ nC}$  which over a one second period would require a current of  $10 \text{ nA}$ . Thus, the sensitivity of the current scale was adjusted to be  $5 \text{ nA cm}^{-1}$ .

Figure 3.5 shows such a cyclic voltammogram run between  $+1.5\text{V}$  and  $-150$  mV. On the forward sweep, two peaks are clearly visible before the bulk deposition occurs. The first peak is very broad and occurs at  $+0.95\text{V}$  whilst the second is much more pronounced and occurs at  $+0.42\text{V}$ . The first, broad peak has an associated charge of  $1.2 \text{ mC cm}^{-2}$  and the second peak has an associated charge of at least  $1.2 \text{ mC cm}^{-2}$ .

During the remainder of the forward sweep, the expected bulk deposition of the lithium occurs. On the reverse sweep the current crosses the potential through  $0.0\text{V}$  and the dissolution process occurs as seen by the stripping peak. Dissolution of the bulk phase is completed by the time the potential has reached  $+0.22\text{V}$  where the current returns to zero. During the remainder of the reverse sweep, one more broad peak is seen which has its maximum at  $+0.85\text{V}$  and an associated charge of  $0.35 \text{ mC cm}^{-2}$ . Neither of the peaks on the forward sweep can be clearly attributed to the formation of a monolayer. If one assumes that the charge density of a monolayer is  $200 \mu\text{C cm}^{-2}$  then both of these peaks have at least five times the expected charge associated with them (although the roughness factor of the microelectrode surface may not be one). Moreover, peaks associated with monolayer formation are often very sharp whereas both of the peaks seen in figure 3.5 are broad. It is also possible that the peaks observed may be due to the reduction of trace quantities of oxygen and/or water.

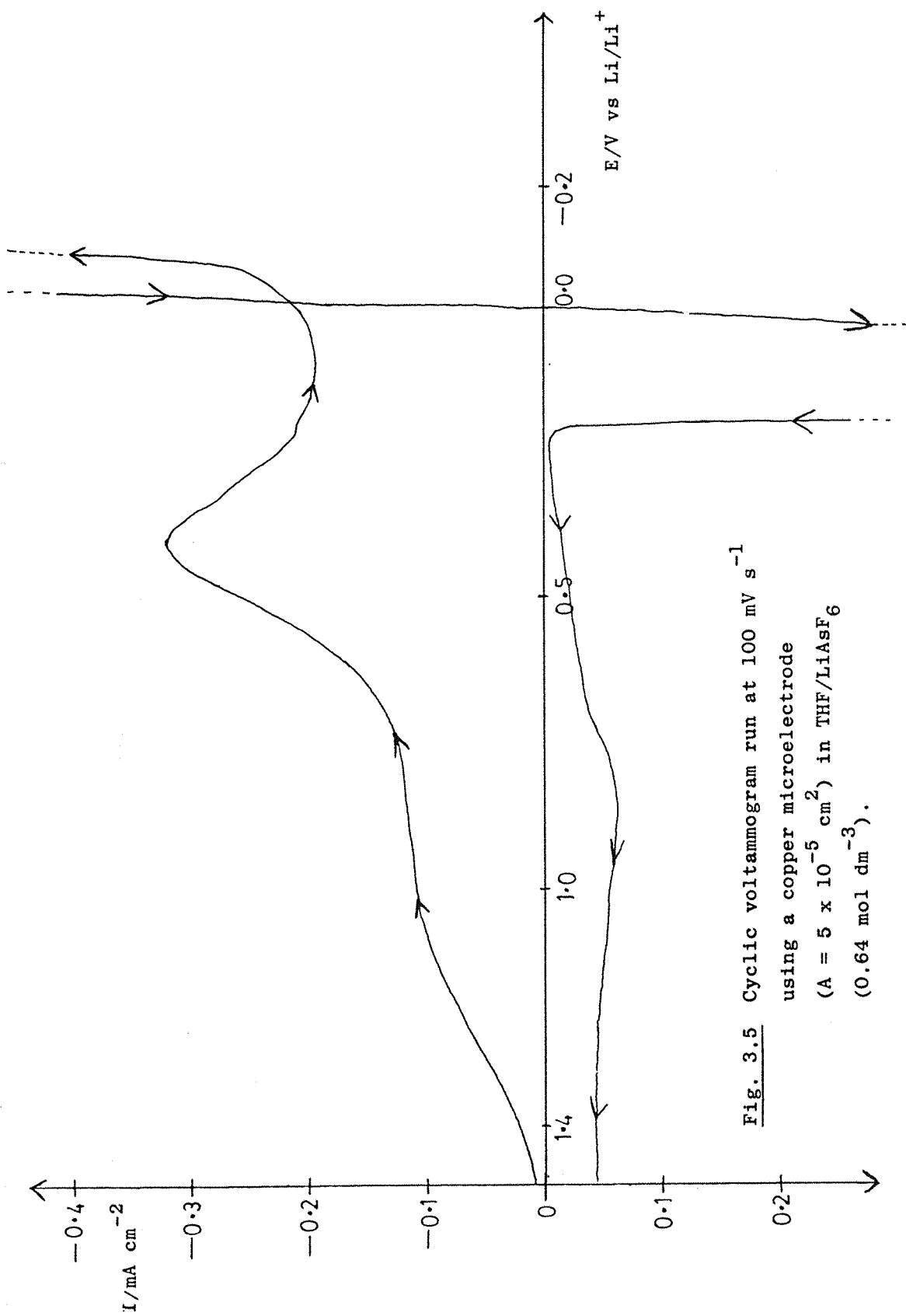


Fig. 3.5 Cyclic voltammogram run at  $100 \text{ mV s}^{-1}$  using a copper microelectrode ( $A = 5 \times 10^{-5} \text{ cm}^2$ ) in THF/ $\text{LiAsF}_6$  ( $0.64 \text{ mol dm}^{-3}$ ).

Irr<sup>77</sup> has recently shown that trace amounts of water in a lithium salt/acetonitrile electrolyte give rise to a peak in cyclic voltammograms at approximately +1.0V versus the deposition of lithium and he has suggested that this peak may be used to quantify trace amounts of water. The oxidative peak during the reverse scan does bear some resemblance to the peaks reported by Fried<sup>60</sup> and Kolb<sup>61</sup>, and the charge associated is close to that expected for a monolayer oxidation. However, it is unexpectedly broad and not conclusively that for the removal of a monolayer of lithium.

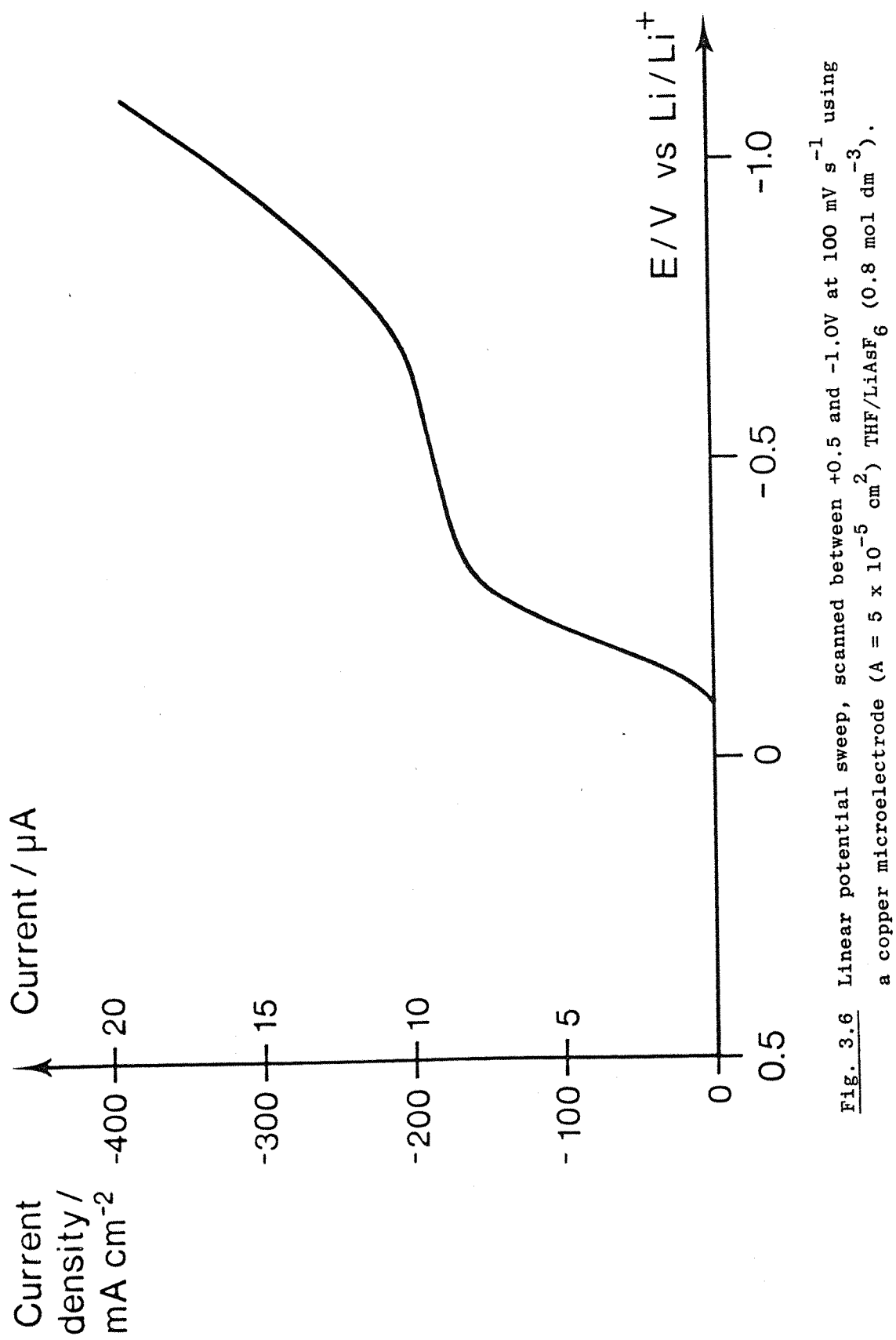
### 3.1.3 Linear potential sweep to high negative overpotentials

Figure 3.6 shows the I-E characteristic for a linear potential sweep experiment where the potential is scanned from +500 to -1000 mV at 100 mV s<sup>-1</sup>. A well formed reduction wave is observed with  $E_{1/2} = -210$  mV and a limiting current of  $0.18 \text{ A cm}^{-2}$ . At more negative potentials the further rise in current is presumably due either to direct cathodic reduction of the solvent, or an increase in the area of the lithium surface as it grows into the solution (see later).

An estimate of the expected mass transport limiting current can be made by assuming that the rate of steady state diffusion to the microelectrode is given by  $\frac{DC}{r}$ , where D is the diffusion coefficient ( $\text{cm}^2 \text{ s}^{-1}$ ), C the concentration of electroactive species (moles  $\text{cm}^{-3}$ ) and r is the radius of the electrode ( $\text{cm}^2$ ). Thus we have:-

$$I_{\text{Lim}} = \frac{DC}{r} \cdot nF \quad (3.1)$$

Assuming a value of D to be  $1 \times 10^{-5} \text{ cm}^2 \text{ s}^{-1}$  and with an electrolyte concentration of  $0.8 \text{ moles dm}^{-3}$  gives  $I_{\text{Lim}}$  to be  $0.19 \text{ A cm}^{-2}$ . The observed value is in reasonable agreement with the estimated current density, although some contribution from migration might also be expected.



### 3.1.4 Potential steps to negative overpotentials

Figures 3.7 to 3.9 show the current time responses to a series of potential steps from 0.0V to a value in the range of -70 mV to -400 mV. It can be seen that the currents start at zero (there is no background current) and rise over a period of time to a limiting, plateau current. The time taken to reach the limiting current and the size of the limiting current are dependent on the value of the applied overpotential: the larger the overpotential the faster the plateau is reached and the higher the limiting current is. At very high overpotentials, more than 250 mV, the current passes through a peak and then falls to a limiting value, corresponding to the maximum rate of steady state mass transport.

At overpotentials above approximately -300 mV the limiting currents tended to converge on the same value, presumably due to the limiting steady state rate of mass transport of  $\text{Li}^+$  ions to the electrode. However, this convergence could not be observed completely because after a certain amount of charge had been deposited, the current again started to rise. Figures 3.10 and 3.11 clearly show this secondary increase in current at both low and high overpotentials. It can be seen that at the lower overpotentials, fig. 3.10, more time is required to observe this secondary increase whilst at higher overpotentials, fig. 3.11, where the lithium is being deposited at a much faster rate, the secondary increase occurs relatively quickly and a plateau current may not be observed.

This second increase in current is probably a consequence of an increasing electrode surface area due to the lithium deposit growing three dimensionally over the glass surround. When the layer of lithium is thin it grows linearly into solution over the geometric area of the disc electrode, but when the deposit is thick enough, it may start to grow at the edges and hence three dimensionally over the insulating surround. This second, long

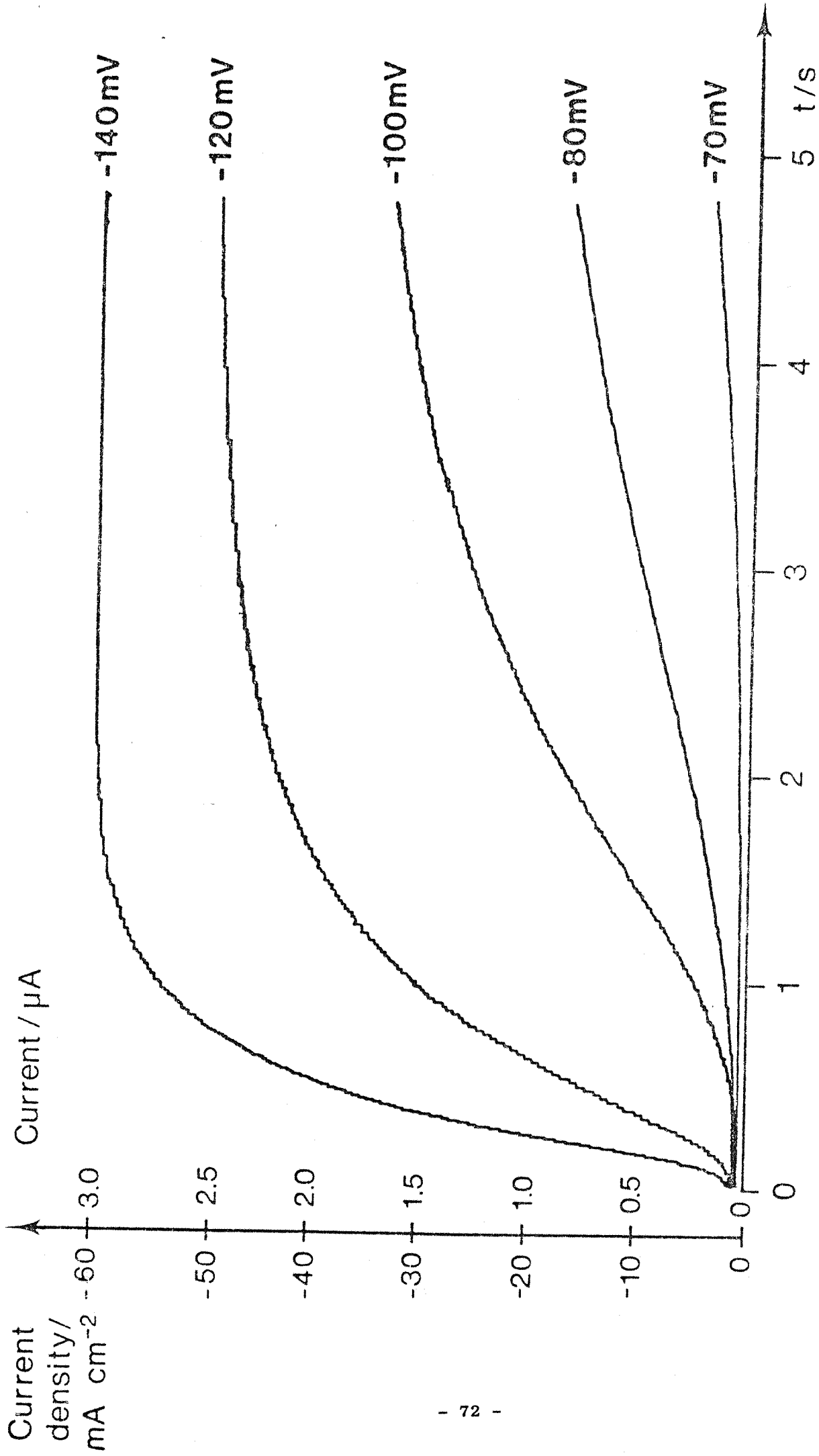
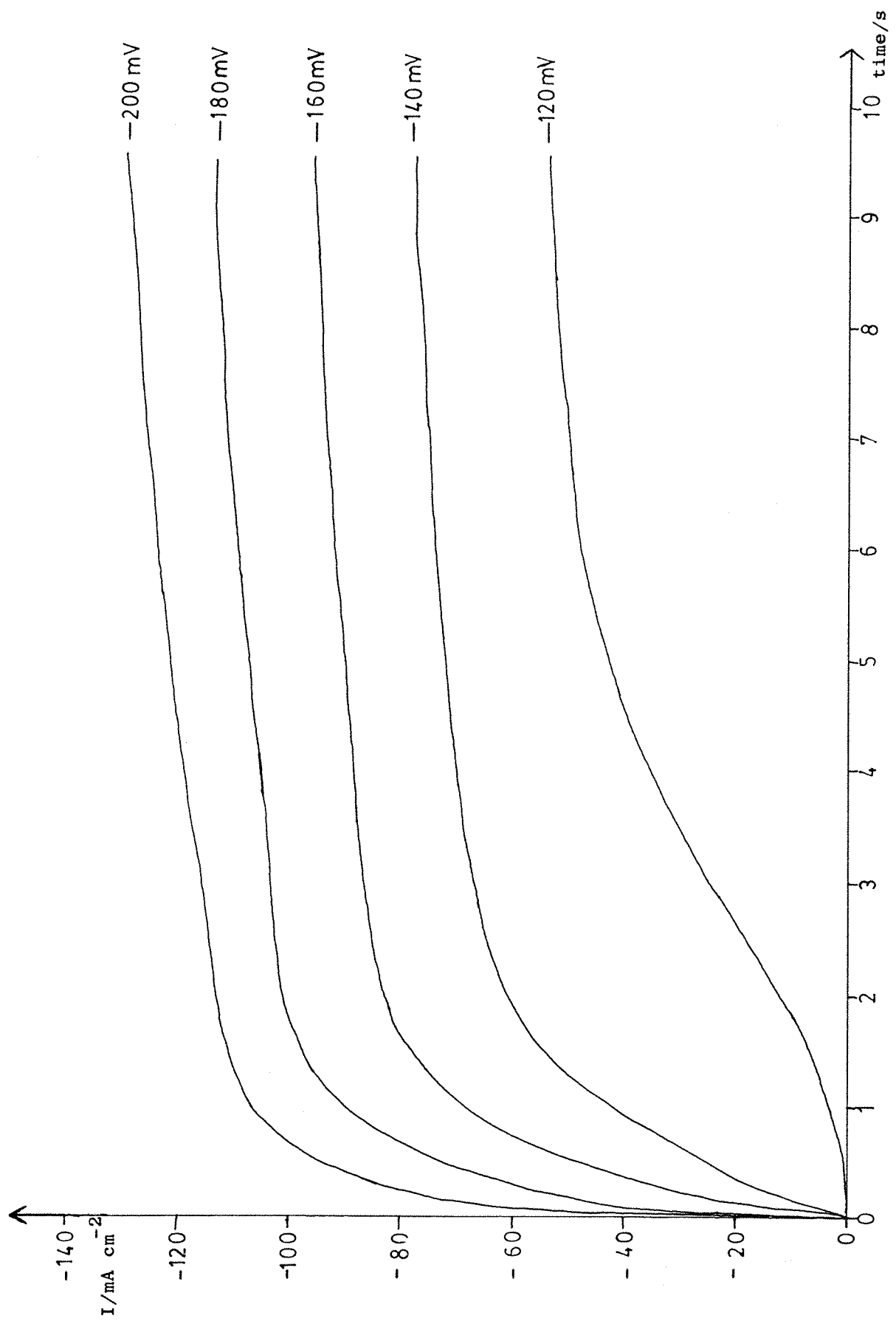


Fig. 3.7 The current time responses to a series of potential steps from 0.0V to the potentials shown (vs  $\text{Li}/\text{Li}^+$ ) using a copper microelectrode ( $A = 5 \times 10^{-5} \text{ cm}^2$ ) in  $\text{THF}/\text{LiAsF}_6$  (0.37 mol  $\text{dm}^{-3}$ ).



**Fig. 3.8** The current-time responses to a series of potential steps from 0.0V to the potential shown (vs Li/Li<sup>+</sup>) using a copper microelectrode ( $A = 5 \times 10^{-5} \text{ cm}^2$ ) in THF/LiAsF<sub>6</sub> (0.82 mol dm<sup>-3</sup>).

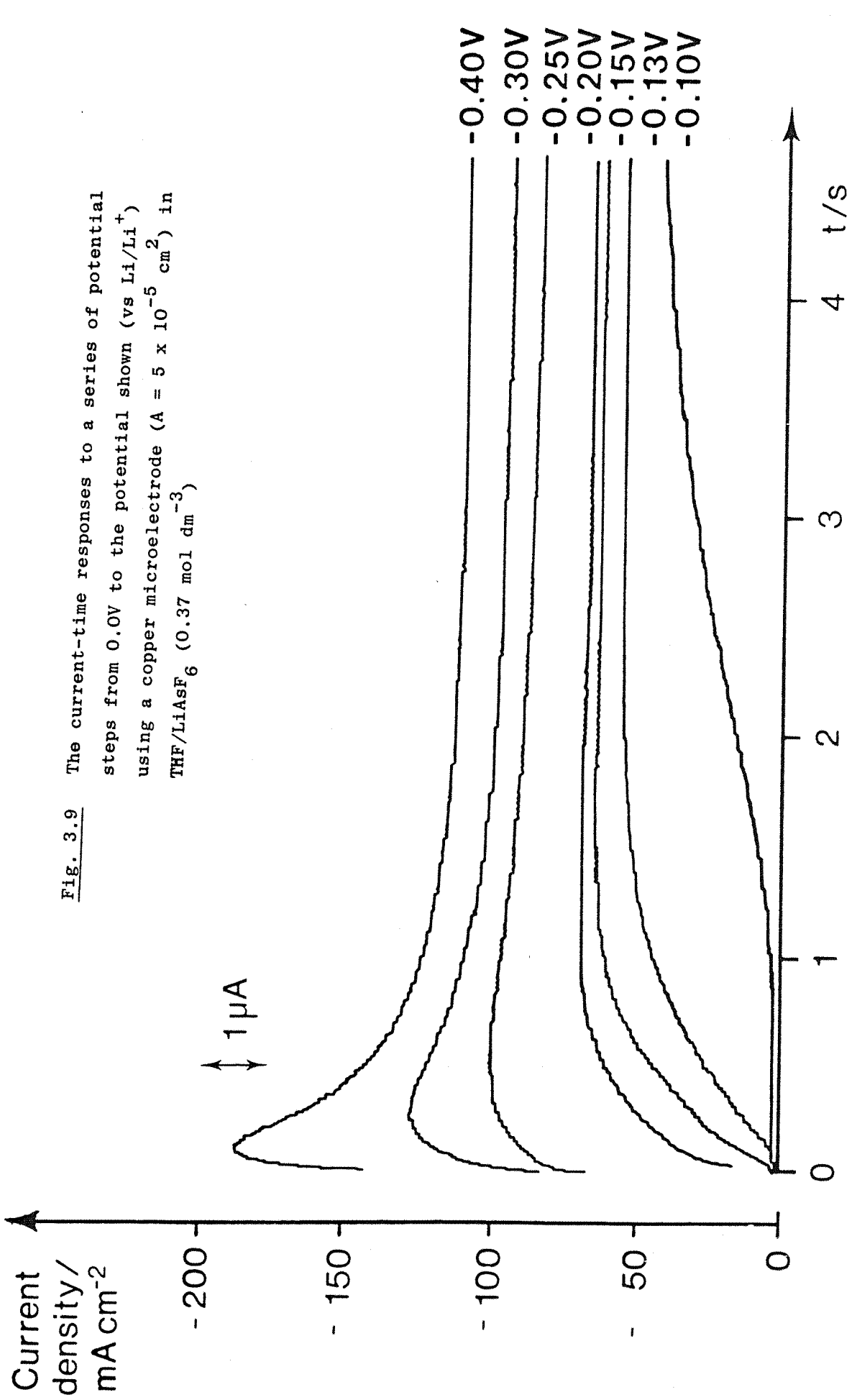


Fig. 3.9 The current-time responses to a series of potential steps from 0.0V to the potential shown (vs  $\text{Li}/\text{Li}^+$ ) using a copper microelectrode ( $A = 5 \times 10^{-5} \text{ cm}^2$ ) in  $\text{THF}/\text{LiAsF}_6$  ( $0.37 \text{ mol dm}^{-3}$ )

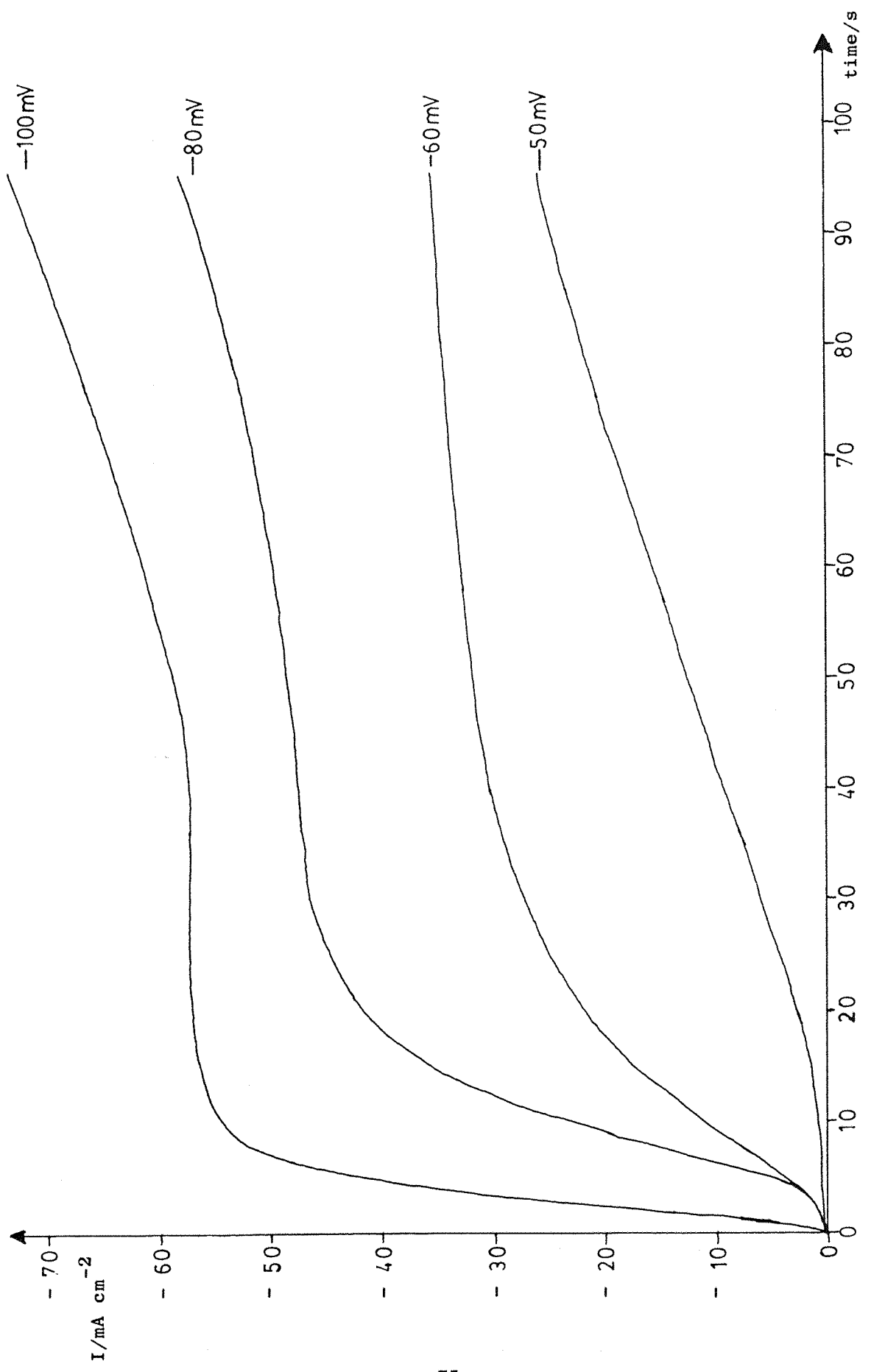
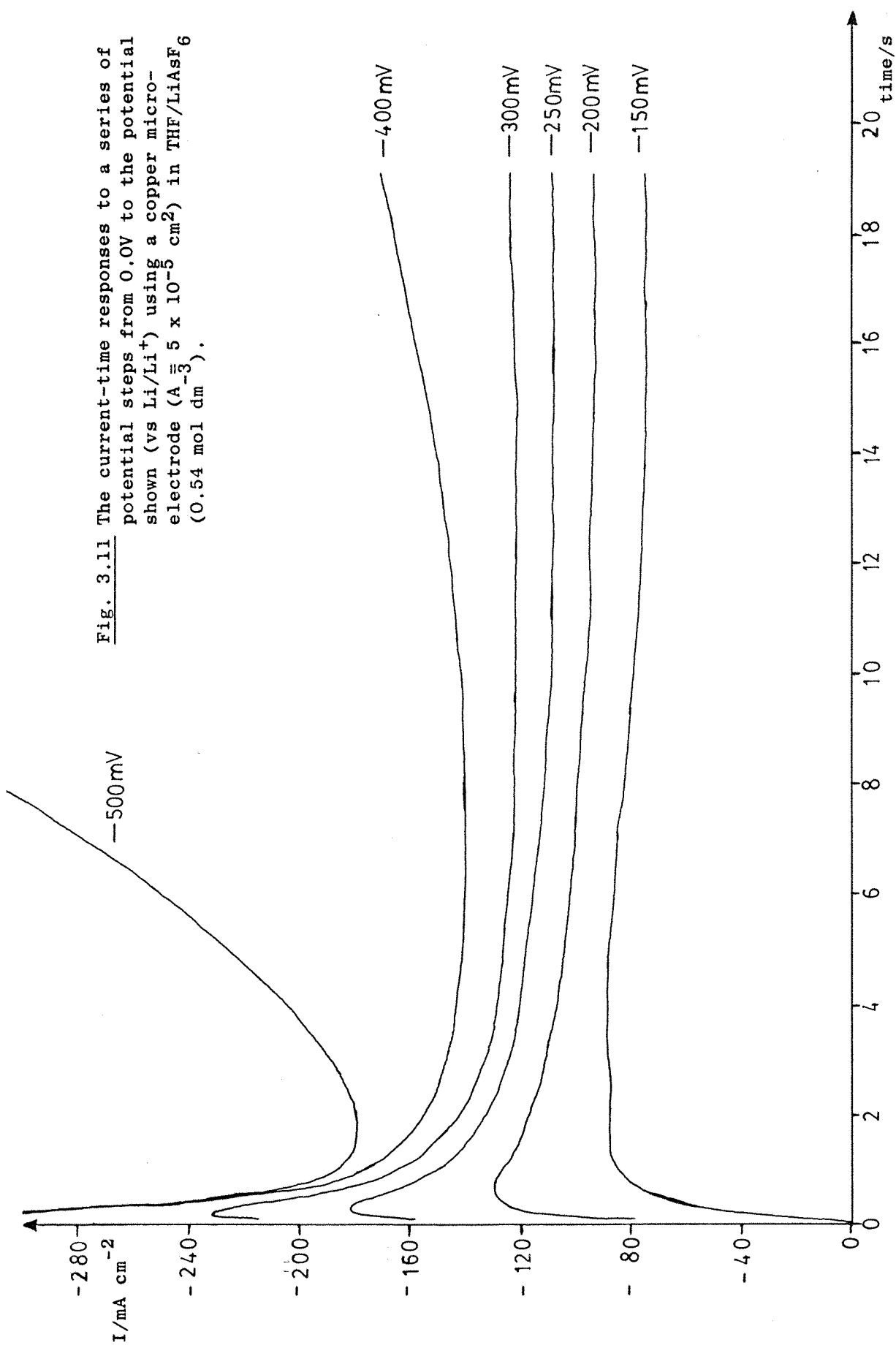


Fig. 3.10 The current-time responses to a series of potential steps from 0.0V to the potential shown (vs Li/Li<sup>+</sup>) using a copper microelectrode ( $A = 5 \times 10^{-5} \text{ cm}^2$ ) in THF/LiAsF<sub>6</sub> (0.54 mol dm<sup>-3</sup>).

Fig. 3.11 The current-time responses to a series of potential steps from 0.0V to the potential shown (vs Li/Li<sup>+</sup>) using a copper micro-electrode ( $A = 5 \times 10^{-5} \text{ cm}^2$ ) in THF/LiAsF<sub>6</sub> (0.54 mol dm<sup>-3</sup>).



time, increase in current also prevents the observation of the steady state currents at low overpotentials. This can be seen from fig. 3.12 which shows the I-t response for a potential step to -40 mV. After nucleation the current rises as expected but instead of reaching a steady state value, it continues to increase over a period of hundreds of seconds to values more characteristic of much higher overpotentials. The steady state plateau has been lost, probably due to overlap of the short time (nucleation and growth) and the long time (increase in electrode area) influences on the current. Because of this long time effect a series of double potential step experiments were performed to investigate the steady state currents corresponding to low overpotentials. In these experiments the potential was stepped from 0.0V to -150mV for four seconds (deposition charge  $0.25 \text{ C cm}^{-2}$ ) and then pulsed back to the potential of interest. Effectively the first pulse is used to deposit a lithium layer on the copper, whilst the second pulse is used to observe the steady state rate of growth of the lithium at the potential of interest. Figures 3.13 and 3.14 show the results of such experiments for overpotentials in the range -10 mV to -80 mV. At each potential it can be seen that the current quickly reaches a steady state value. The data from these experiments are analysed further later.

### 3.1.5 Double potential steps to study the dissolution of Li

The anodic dissolution of lithium metal was studied in more detail by a series of double potential step experiments which had the general potential-time program of that shown in figure 3.15.

In these experiments the first pulse was used to deposit a known and controlled amount of lithium whilst the second pulse was used to study the anodic dissolution of the metal at the potential of interest. Figures 3.16 to 3.19 show the results of such experiments where the potential was stepped to -120 mV for 30s (deposition charge  $1.5 \text{ C cm}^{-2}$ ) and then pulsed back

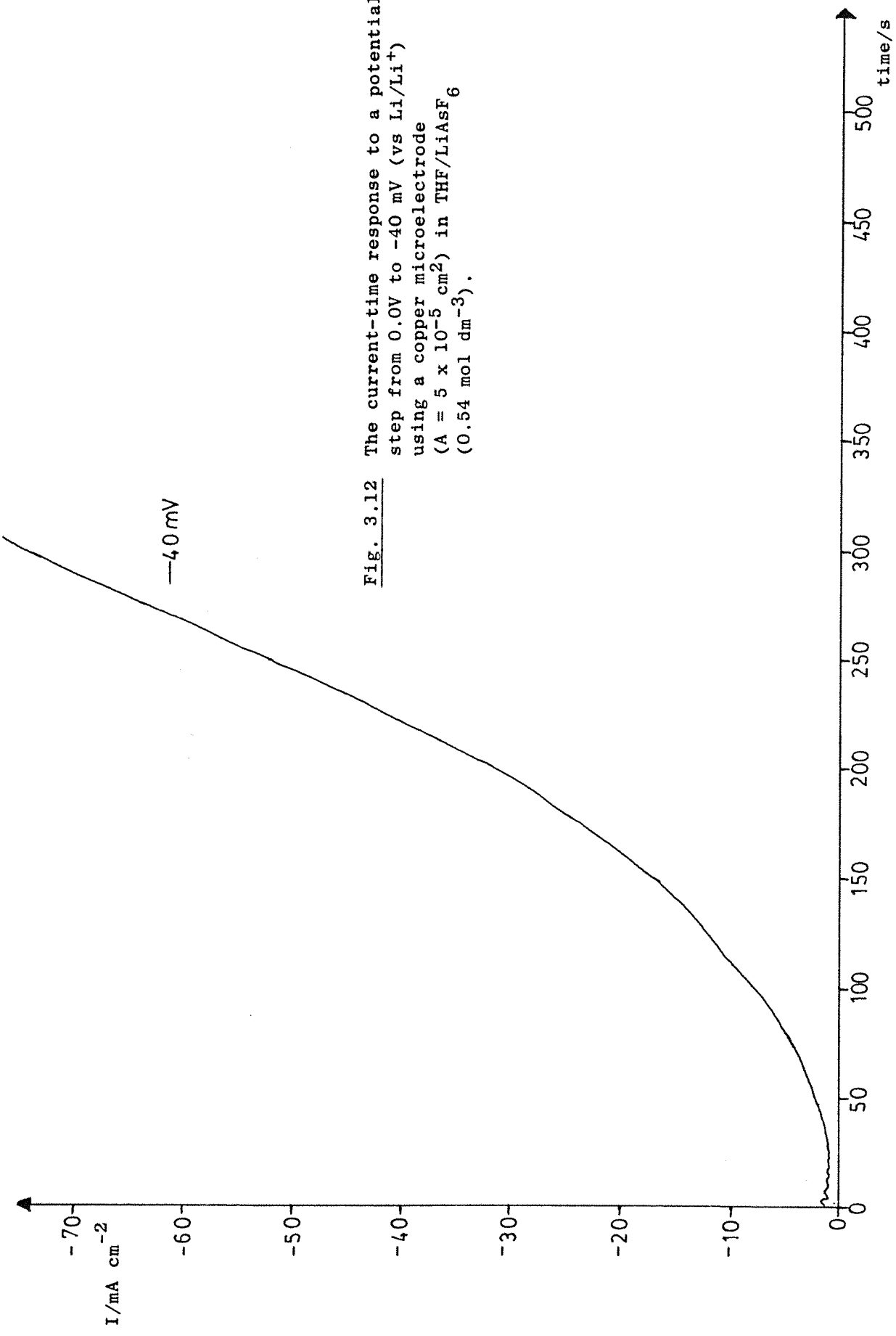
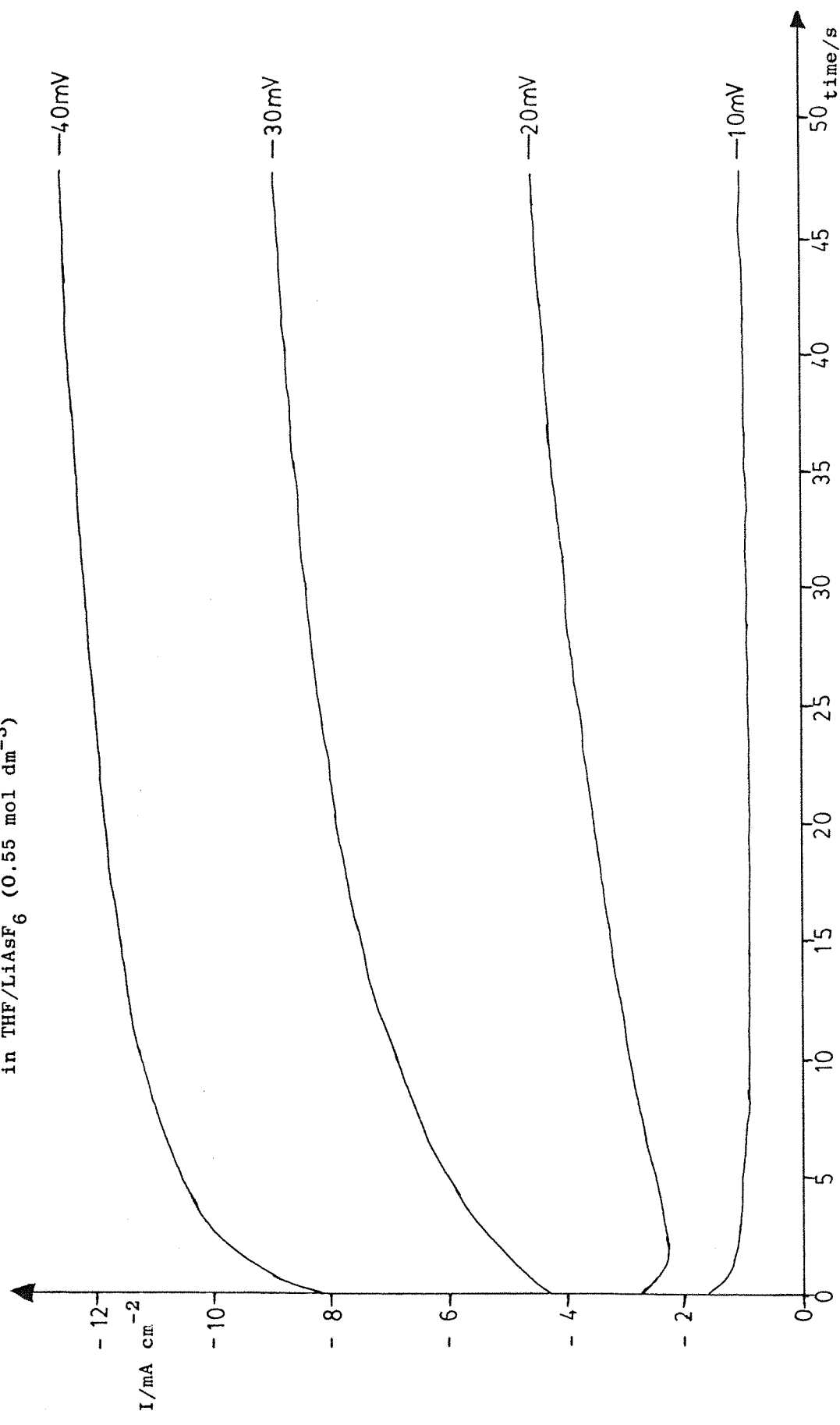
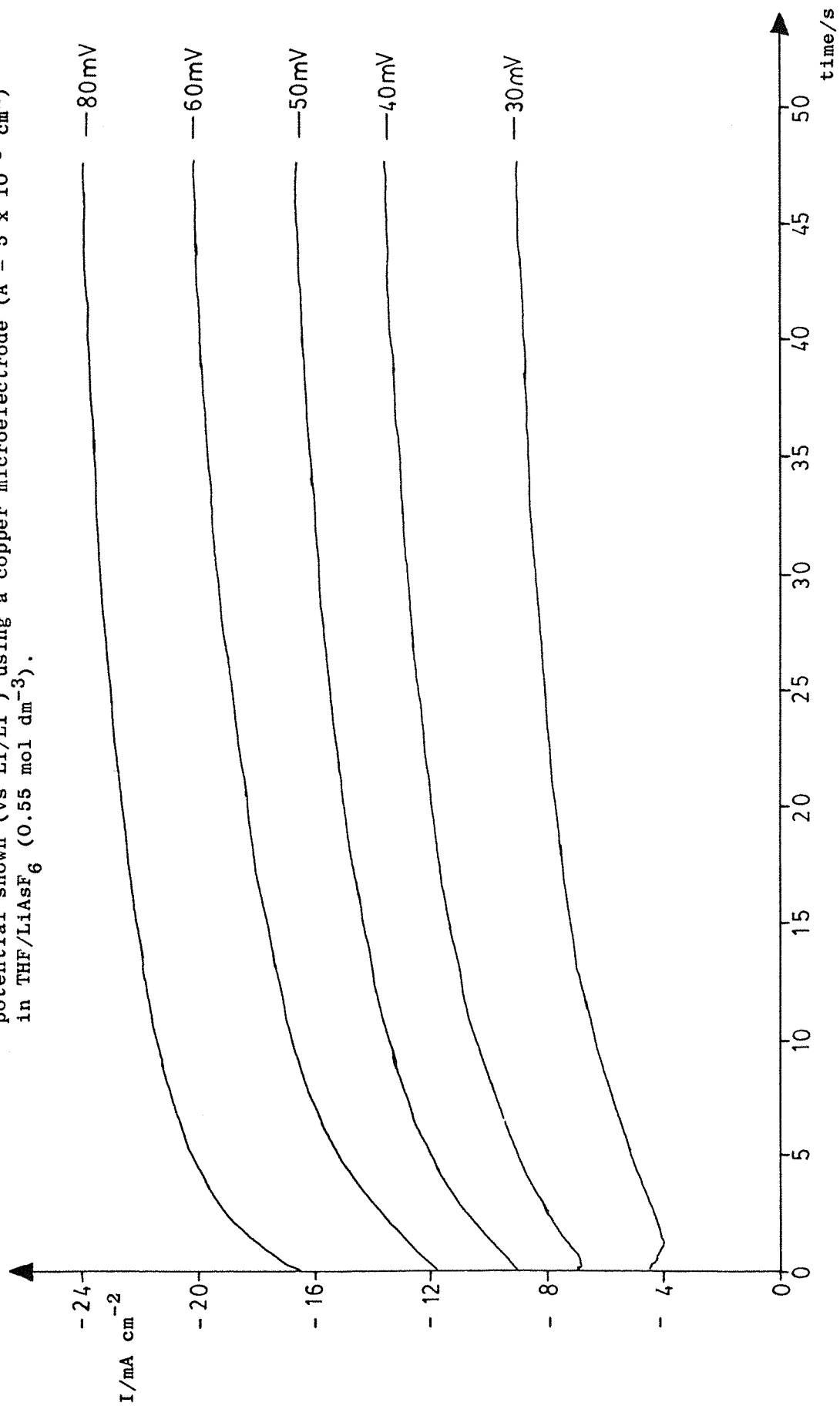


Fig. 3.12 The current-time response to a potential step from 0.0V to  $-40 \text{ mV}$  (vs Li/Li $^{+}$ ) using a copper microelectrode ( $A = 5 \times 10^{-5} \text{ cm}^2$ ) in THF/LiAsF<sub>6</sub> ( $0.54 \text{ mol dm}^{-3}$ ).

Fig. 3.13 The current-time responses for the deposition of lithium metal on a freshly deposited lithium surface. Potential step sequence  $0.0V \rightarrow -150 mV (4s) \rightarrow$  potential shown (vs Li/Li<sup>+</sup>) using a copper microelectrode ( $A = 5 \times 10^{-5} cm^2$ ) in THF/LiAsF<sub>6</sub> (0.55 mol dm<sup>-3</sup>)



**Fig. 3.14** The current-time responses for the deposition of lithium metal on a freshly deposited lithium surface. Potential step sequence  $0.0V \rightarrow -150 mV (4s) \rightarrow$  potential shown (vs Li/Li<sup>+</sup>) using a copper microelectrode ( $A = 5 \times 10^{-5} cm^2$ ) in THF/LiAsF<sub>6</sub> ( $0.55 mol dm^{-3}$ ).



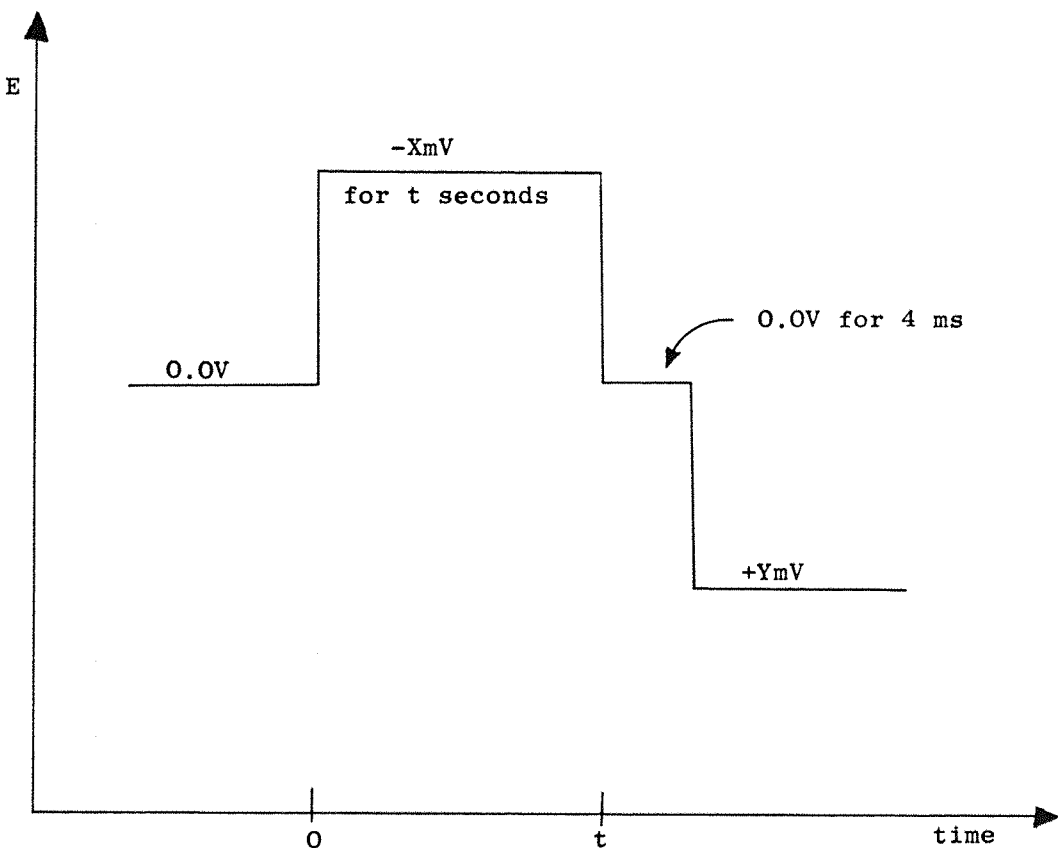


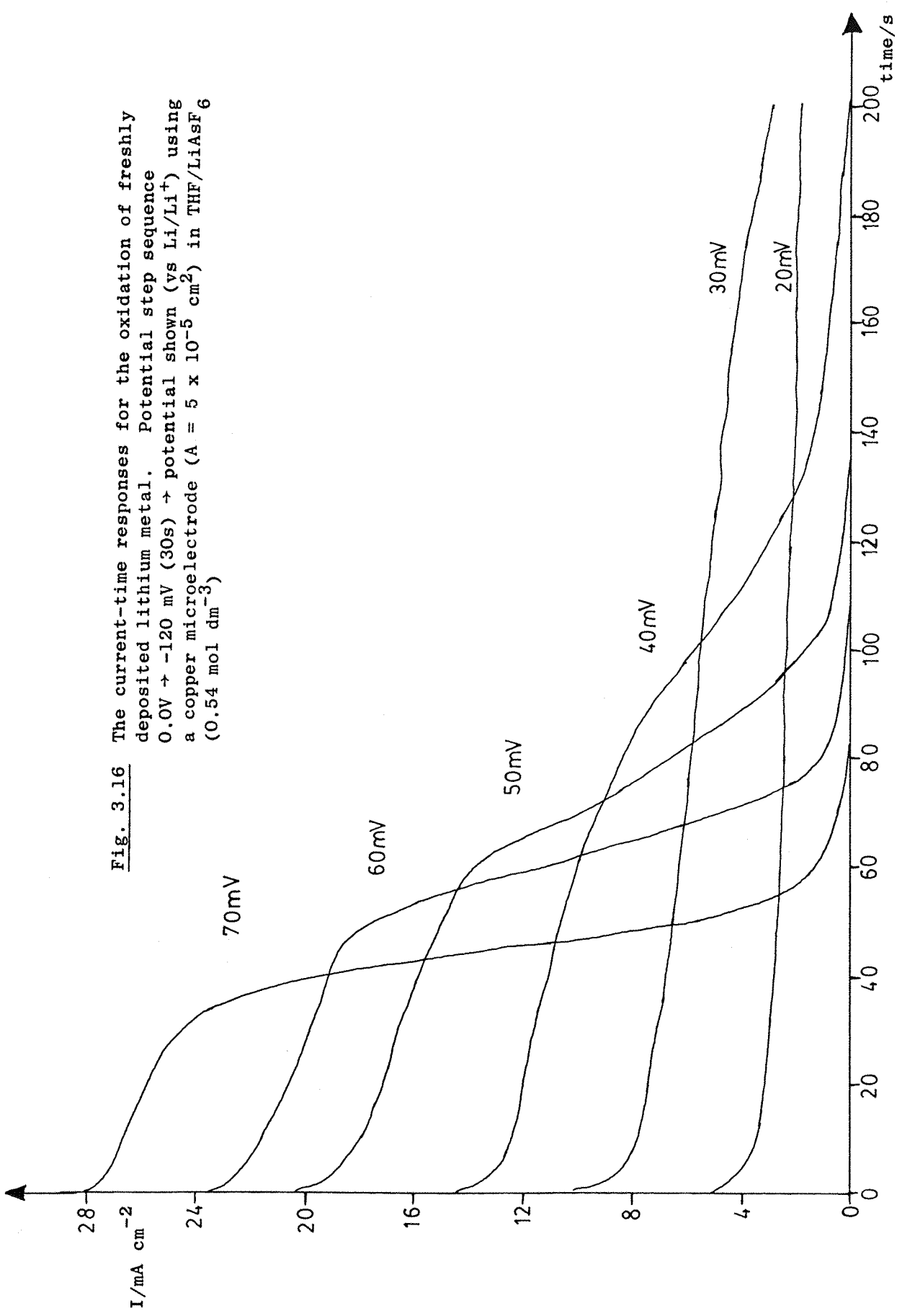
Fig. 3.15 The form of the potential-time program used in the study of the anodic dissolution of lithium metal.

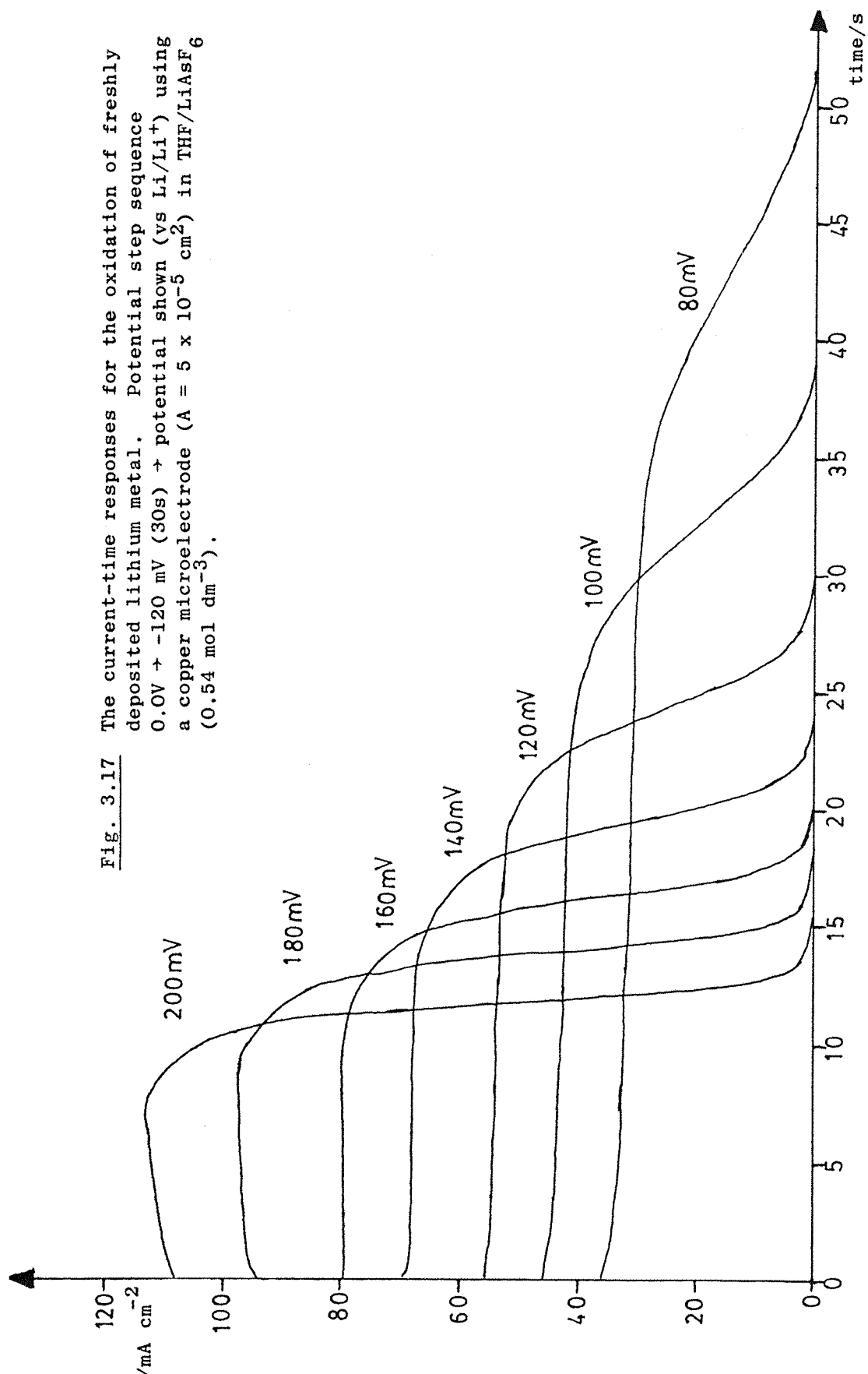
to oxidative overpotentials in the range +20 mV to +1000 mV. Only the  $I-t$  response during the second pulse was recorded. For overpotentials below +200 mV (figs. 3.16 and 3.17) the current maintains a steady value, characteristic of the applied overpotential, until most of the lithium has been removed, when it falls sharply to zero. As expected, the higher the applied overpotential, the faster the lithium can be removed.

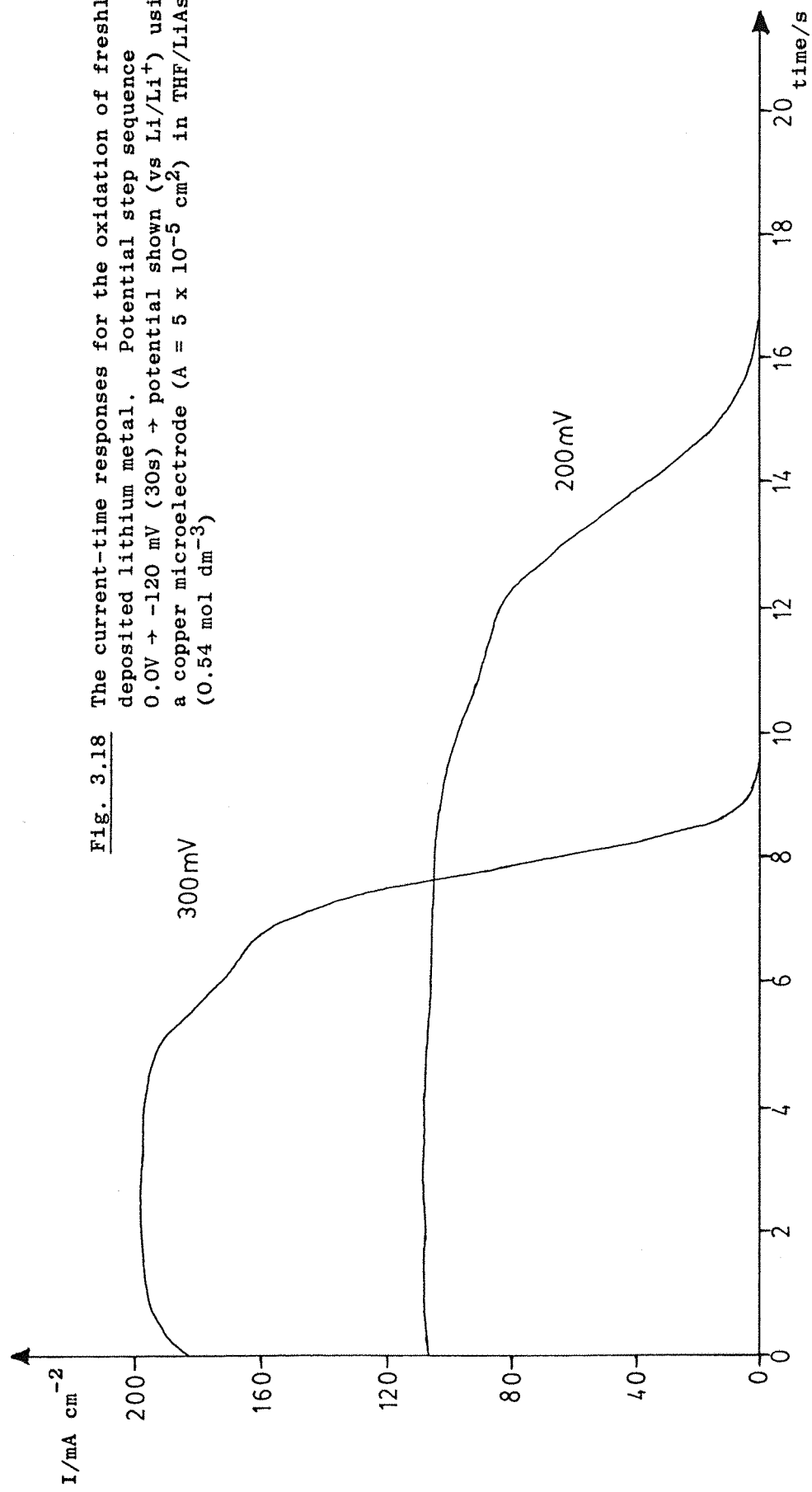
At overpotentials above +200 mV (figs. 3.18 and 3.19) the steady state, current plateau becomes more difficult to identify. The  $I-t$  transients seem to consist of a steady state component and a peak at short times which becomes more pronounced as the overpotential is made more positive.

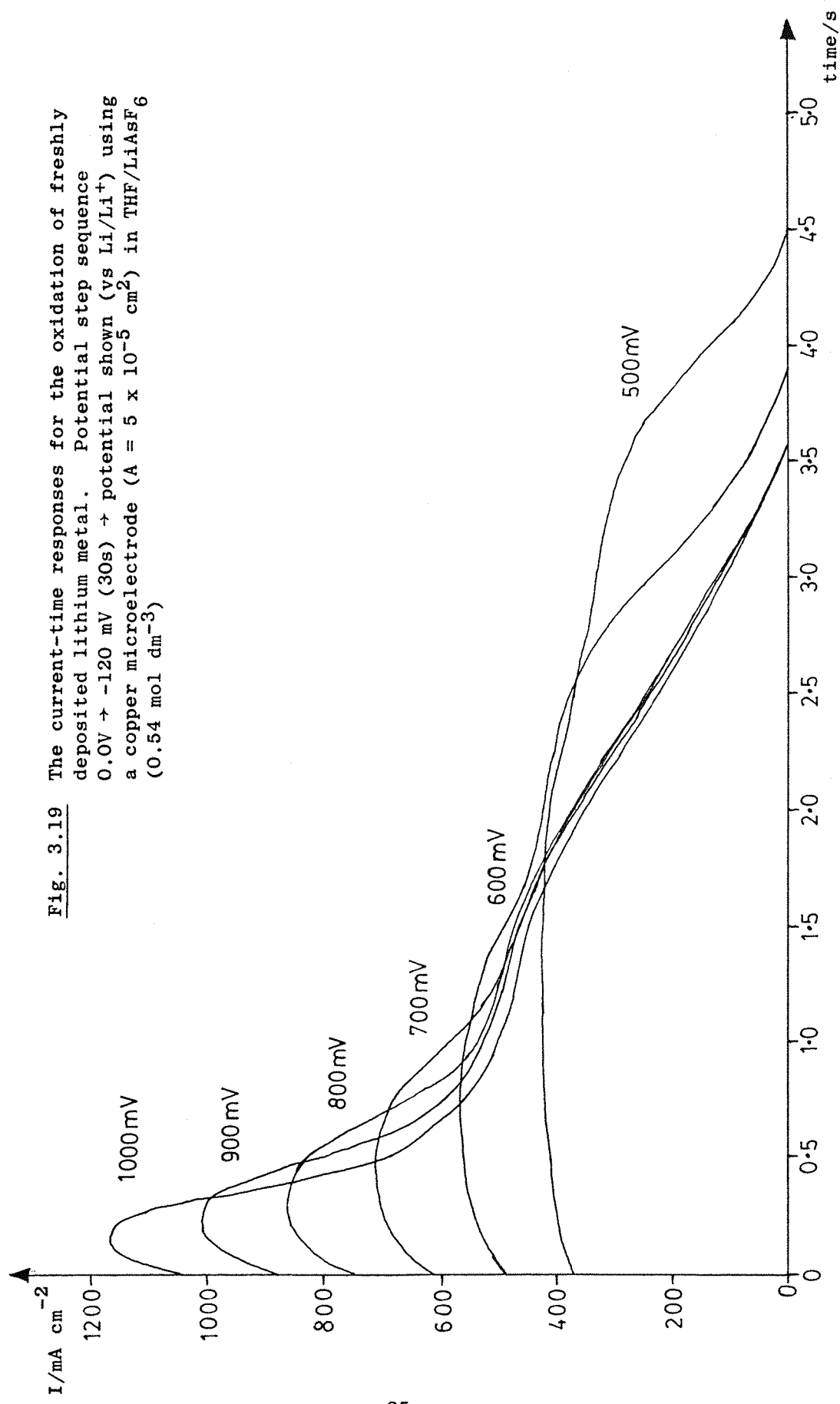
One possible explanation for this initial rapid increase in current might lie in the phenomenon of pitting corrosion. At

**Fig. 3.16** The current-time responses for the oxidation of freshly deposited lithium metal. Potential step sequence  $0.0V \rightarrow -120\text{ mV}$  (30s)  $\rightarrow$  potential shown (vs  $\text{Li}/\text{Li}^+$ ) using a copper microelectrode ( $A = 5 \times 10^{-5} \text{ cm}^2$ ) in  $\text{THF}/\text{LiAsF}_6$  ( $0.54 \text{ mol dm}^{-3}$ )









very high overpotentials the driving force for metal dissolution is extremely strong and instead of being uniform, will occur preferentially at sites of higher activity. This leads to pits and cracks in the metal surface which increases the available area for metal dissolution and so the current increases. Another explanation might be associated with the oxidation of surface films which are known to form on the lithium surface due to reaction with one or more components of the electrolyte.

Whatever the explanation is, the magnitude of this peak current makes the measurement of the steady state current difficult and raises its value above that expected for a mass transport limited system. The steady state value of the current, at overpotentials above +500 mV, does appear, however, to converge at a value of approximately  $420 \text{ mA cm}^{-2}$ .

The steady state currents corresponding to steps to positive overpotentials, along with the steady state results from section 3.1.4 are considered in more detail in section 3.1.6.

### 3.1.6 Analysis of the steady state currents as a function of overpotential

The steady state data from the potential step experiments described in sections 3.1.4 and 3.1.5 has been displayed in two forms:

- (i) Figure 3.20 shows the straightforward current density versus overpotential curve.
- (ii) Figure 3.21 displays the data as a  $\log_{10}|I|$  versus overpotential plot, more commonly known as a Tafel plot.

Figure 3.20 has the expected form of an  $I$  vs  $\eta$  plot in which the current crosses the potential axis at 0.0V, increases rapidly with overpotential until the limiting plateau due to mass

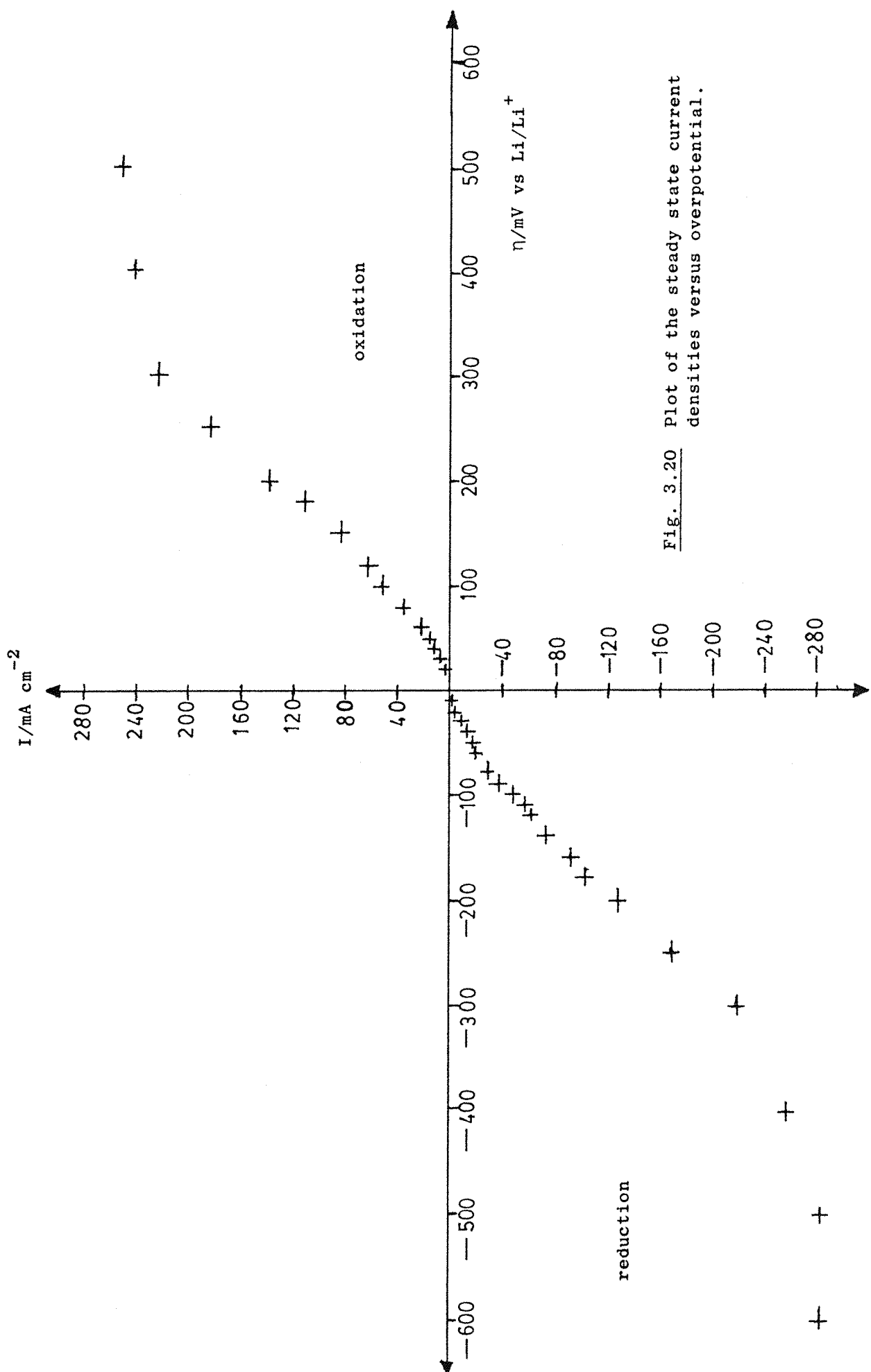


Fig. 3.20 Plot of the steady state current densities versus overpotential.

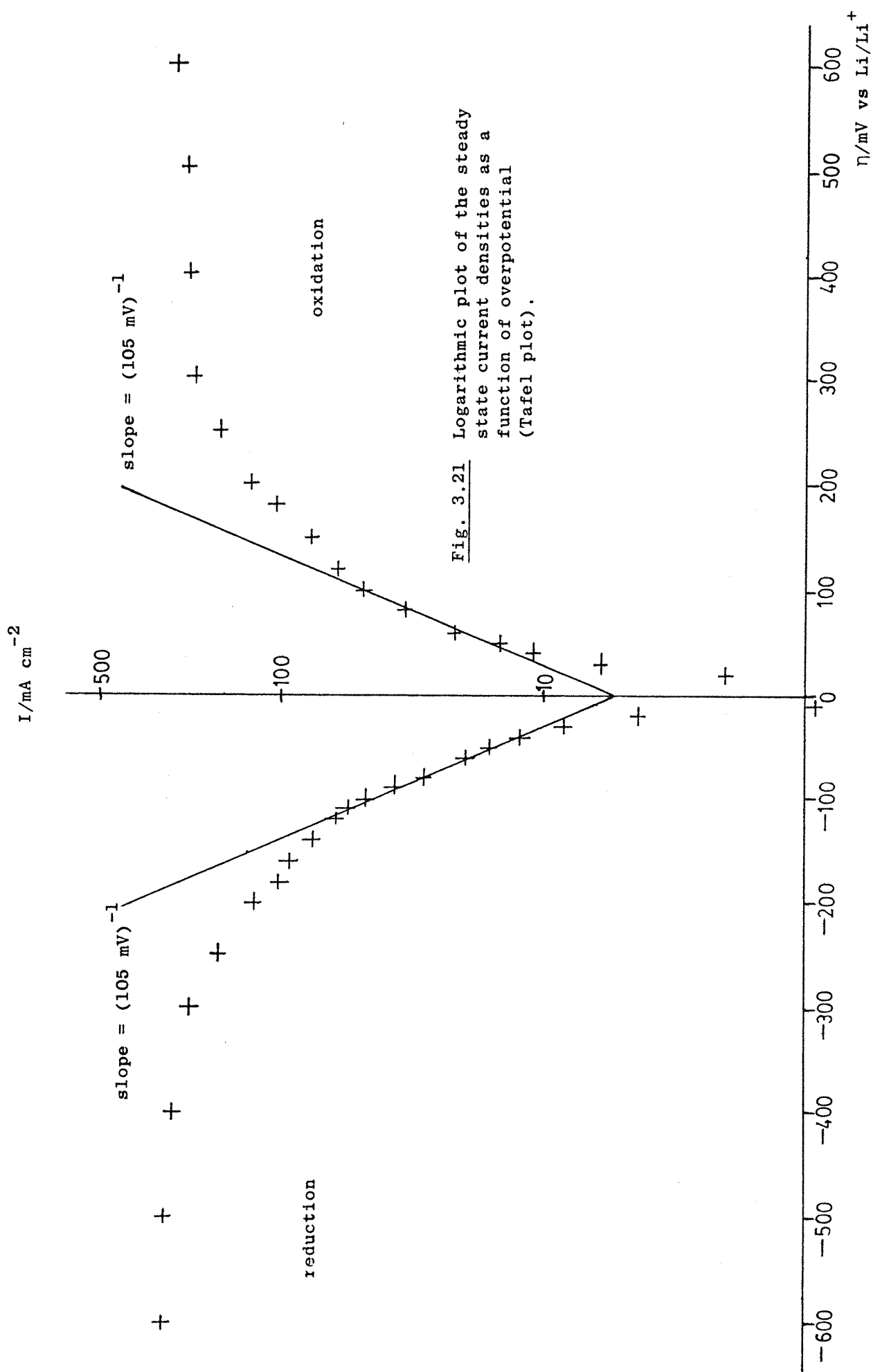


Fig. 3.21 Logarithmic plot of the steady state current densities as a function of overpotential (Tafel plot).

transport control is reached.

The most convenient method for more detailed analysis of this data is to replot it in the form of a Tafel plot (figure 3.21).

Figure 3.21 has the basic features associated with a Tafel plot in which the curve asymptotes to the potential axis at low overpotentials,  $\eta < \pm 50$  mV, and rises to a plateau at high overpotentials. During the rising part of the curve there is no linear region which extends over a prolonged current range. However, a linear region does appear to be present for both the anodic and cathodic currents between 40 and 120 mV, and these have been drawn in on the figure. Both of the lines have the same slope,  $(105 \text{ mV})^{-1}$ , and cross the current density axis at a value corresponding to an exchange current density of  $5.4 \text{ mA cm}^{-2}$ . This high value of the exchange current density, combined with the mass transport limitation on the current density which occurs for only moderate values of  $\eta$ , explains why the linear region only appears to extend over a short current range, i.e. even at relatively low overpotentials (120 mV) the rate of electron transfer is comparable to that of mass transport and deviation from linearity occurs, while below 50 mV the approximation inherent in the Tafel equation is no longer valid. The fact that, under these conditions, the steady state rate of electron transfer is high even at low overpotentials, makes the lithium metal/ion couple ideal for use in batteries.

If the region mentioned above is truly linear, then the Tafel equation (equation 3.2) should apply

$$I = I_o \exp \left[ \frac{\alpha nF}{RT} \cdot \eta \right] \quad (3.2)$$

where  $I$  is the current density at an overpotential  $\eta$ ,  $I_o$  is the exchange current density,  $\alpha$  is the transfer coefficient and the other symbols have their usual meanings. This equation predicts

a slope of  $(120 \text{ mV})^{-1}$  for the lithium system which is in reasonable agreement with the observed value of  $(105 \text{ mV})^{-1}$ . Moreover, the straight line region in figure 3.21 can be used to predict the reverse component of the current densities at low overpotentials and figure 3.22 shows a Tafel plot in which the current densities have been corrected for this back reaction. The use of this corrected data provides a more convincing argument in favour of the existence of a linear region.

Using a combination of the Tafel and Nernst equations, it is possible to derive an equation which relates the exchange current density,  $I_o$ , to the standard rate constant,  $k^\ominus$ , and the activities of the electro-active species (equation 3.3).

$$I_o = nFk^\ominus \left( a_{\text{Li}^+} \right)^{1-\alpha} \left( a_{\text{Li}} \right)^\alpha \quad (3.3)$$

By approximating the activity of  $\text{Li}^+$  to its concentration and assuming that the activity of lithium is 1 mol  $\text{dm}^{-3}$  and that  $\alpha = \frac{1}{2}$ , then using the experimental value of  $I_o$  we obtain a value for the standard rate constant,  $k^\ominus$ , of  $5.6 \times 10^{-5} \text{ cm s}^{-1}$ .

This value is in qualitative agreement with the shape of the  $I-\eta$  curve in figure 3.20 where it can be seen that there is no extended region, where the current is zero although there is a very clear point of inflection at  $\eta = 0 \text{ mV}$ .

Thus the kinetics of the  $\text{Li}/\text{Li}^+$  couple, although fast, are not completely reversible over the whole overpotential range. It will be shown later (section 3.3) that temperature has a considerable influence on the kinetics. For example, figure 3.42 shows that an increase in temperature causes the current, during the reverse sweep of a cyclic voltammogram, to cut through the voltage axis, at 0.0V, at a much steeper angle - indicative of the system becoming more reversible.

One other, very important, point to be emphasised is how

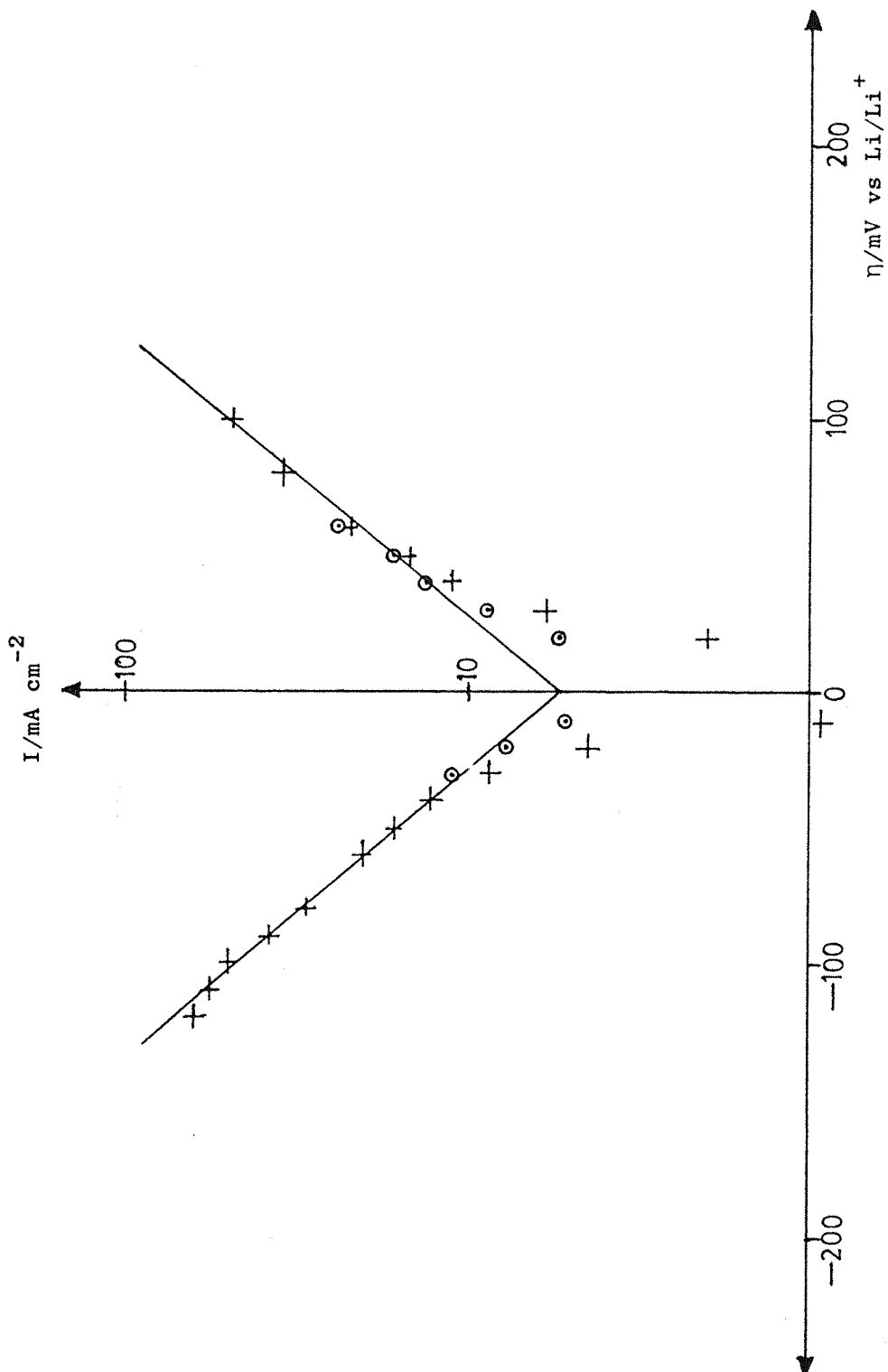


Fig. 3.22 Logarithmic plot of the steady state current densities as a function of overpotential (Tafel plot).

+ : Original data.

○ : Data corrected for the back reaction.

this data differs from that in the literature. Thus, for example, Matsuda<sup>46</sup> obtained a Tafel plot for the  $\text{Li}/\text{Li}^+$  couple in a THF/LiBF<sub>4</sub> (1 mole dm<sup>-3</sup>) medium, which bears little resemblance to the one reported here. Moreover, the few similarities become less convincing when sets of data are transposed onto the same axis scales. The quality of the data obtained during this work suggests that these differences are due mainly to the presence of uncompensated IR drop in much of the work reported in the literature.

### 3.1.7 The nucleation and growth of lithium

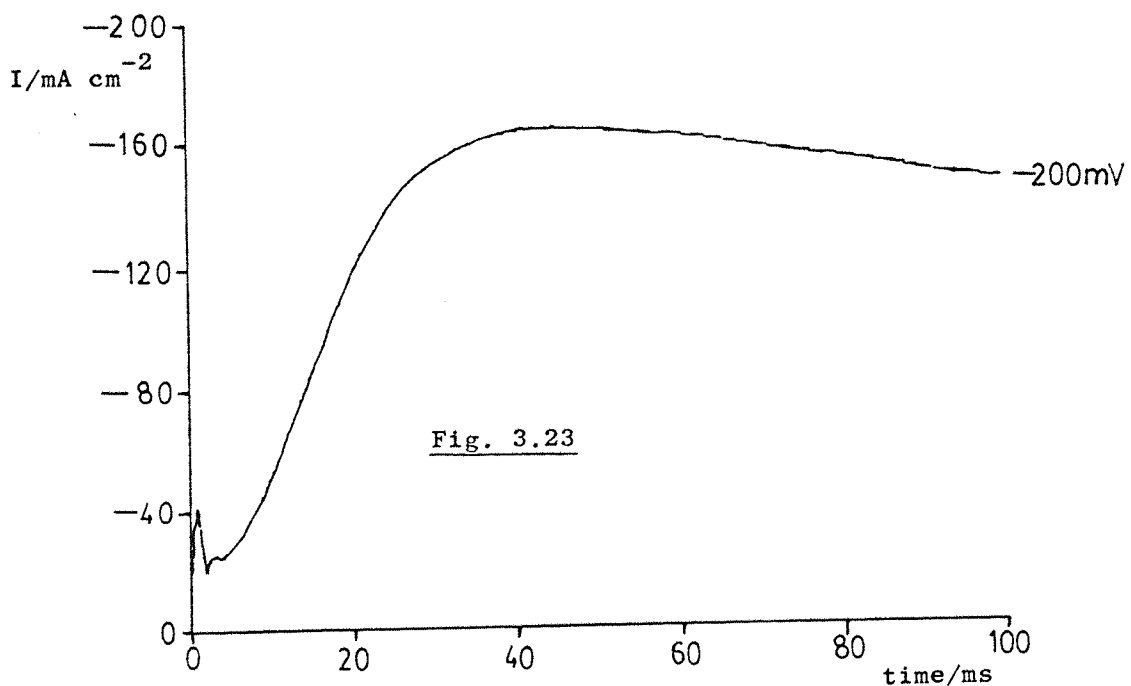
The nucleation and early stages of growth of lithium on copper was probed by a series of potential step experiments similar to those in section 3.1.4, but recorded over a timescale which emphasises the early part of the transient. The I-t transients were stored directly in the BBC microcomputer and in-house software<sup>76</sup> was used to fit the data to an  $I-t^n$  relationship using equation 3.4.

$$(I - I_0) = K(t - \tau)^n \quad (3.4)$$

where  $I$  is the current density at time  $t$ ,  $I_0$  is the current just prior to the rising portion of the transient,  $\tau$  is a fitting parameter which allows for any induction period prior to the start of nucleation, and  $K$  is a constant. Data from the rising part of the transients was fitted for values of  $n$  equal to 3, 2 and  $\frac{3}{2}$ .

Figures 3.23 to 3.25 show the current-time responses for potential steps to -200, -100 and -50 mV. All of these transients have the expected shape which corresponds to the nucleation and growth of lithium centres followed by their overlap to give a layer which thickens by growing into solution under planar diffusion. For the step to -200 mV (figure 3.23) some initial structure is apparently seen at very short times but in fact this is associated with the slow response of the current amplifier.

Figures 3.26 to 3.28 show the best fit  $I-t^n$  curves superimposed

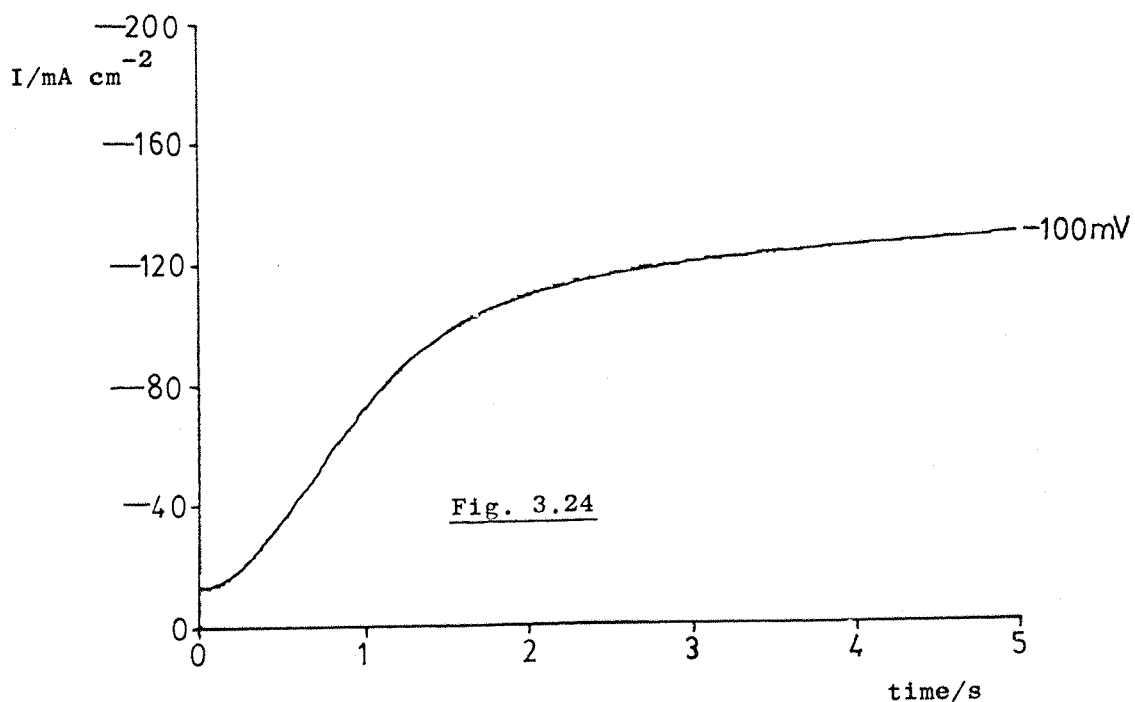


Figs. 3.23 and 3.24

The current-time responses for potential steps from 0.0V to the potentials shown (vs Li/Li<sup>+</sup>) using a copper micro-electrode ( $A = 5 \times 10^{-5} \text{ cm}^2$ ) in THF/LiAsF<sub>6</sub>:

Fig. 3.23:  $0.80 \text{ mol dm}^{-3}$ .

Fig. 3.24:  $0.93 \text{ mol dm}^{-3}$



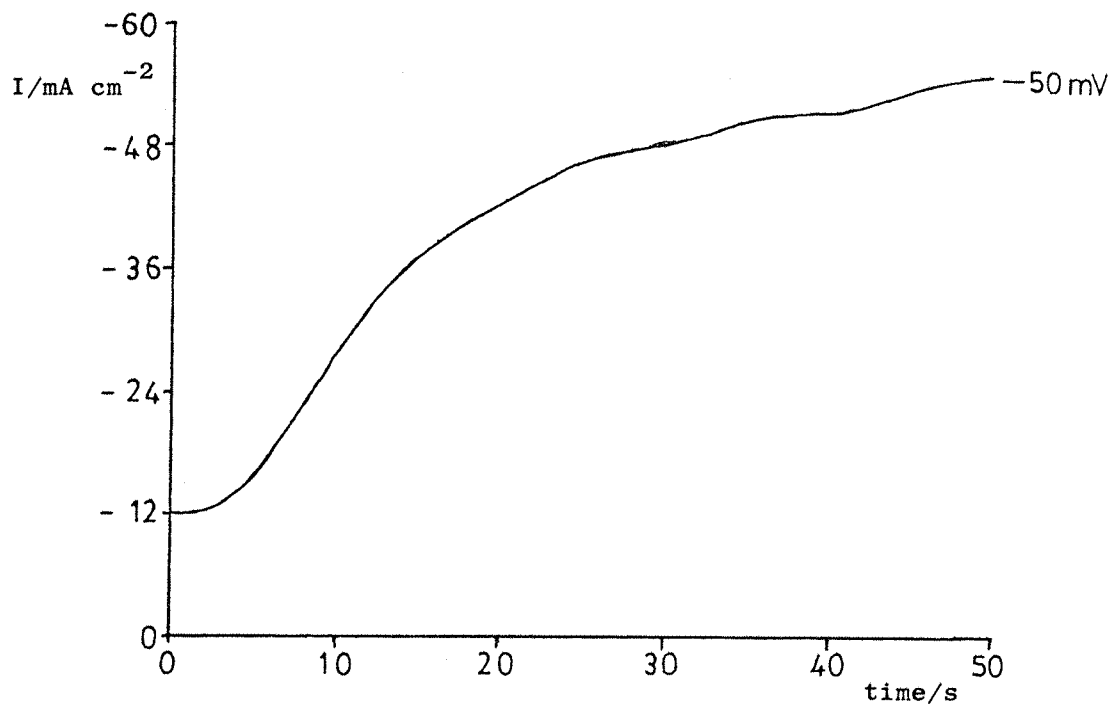
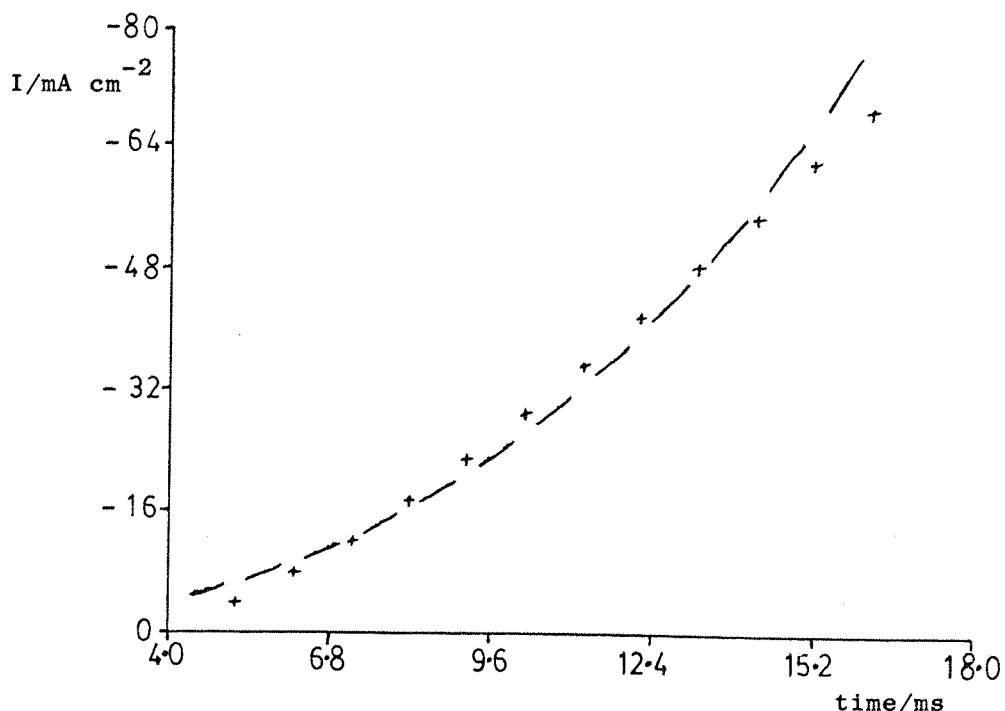


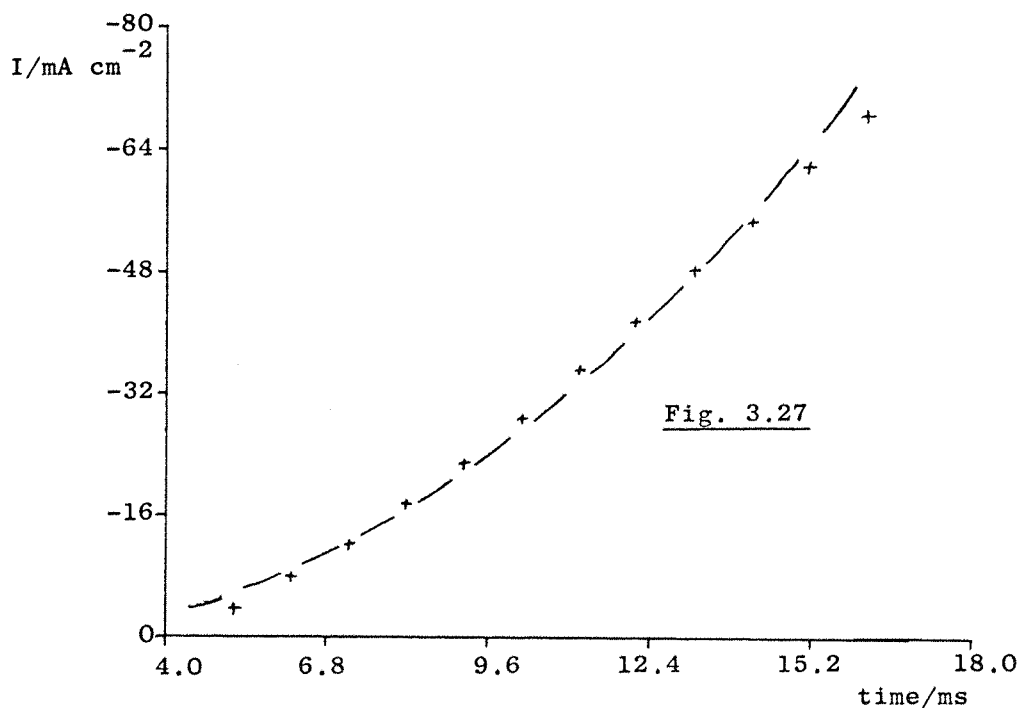
Fig. 3.25 The current time response for a potential step from 0.0V to -50 mV (vs  $\text{Li}/\text{Li}^+$ ) using a copper microelectrode ( $A = 5 \times 10^{-5} \text{ cm}^2$ ) in  $\text{THF}/\text{LiAsF}_6$  (0.80 moles  $\text{dm}^{-3}$ )

Fig. 3.26 Fitting of the rising part of the transient for the potential step to -200 mV (fig. 3.23) to an  $I-t^3$  curve.



+ : Experimental points

— : Theoretical curve

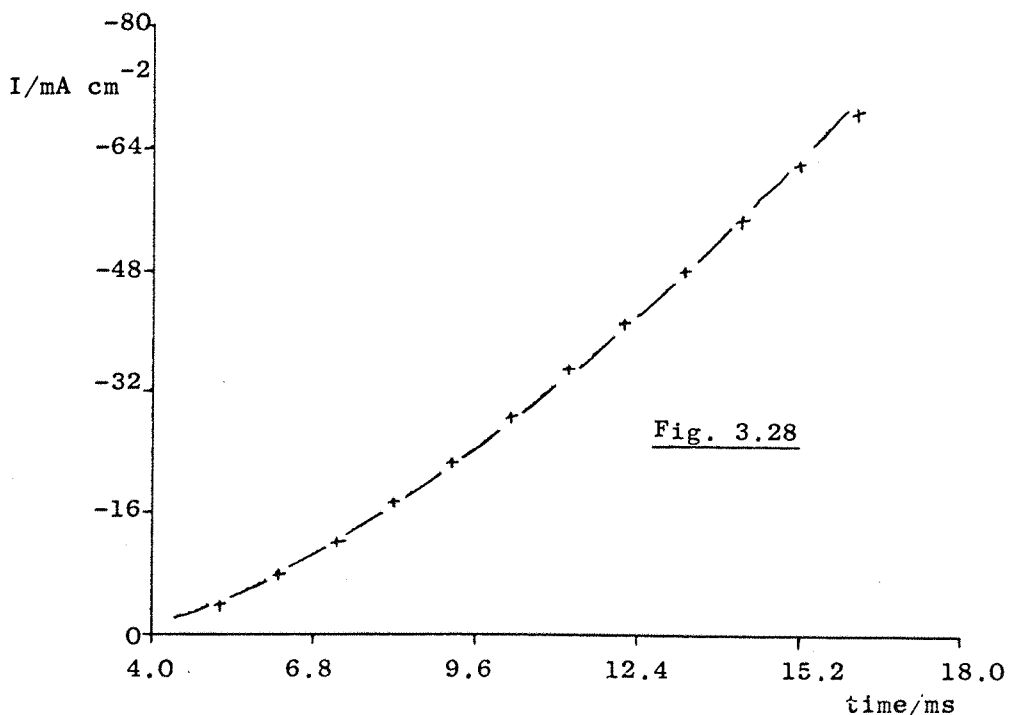


Figs. 3.27 and 3.28

Fitting of the rising part of the transient for the potential step to  $-200$  mV (fig. 3.23) to:

Fig. 3.27: an  $I-t^2$  curve.

Fig. 3.28: an  $I-t^{3/2}$  curve.



+: Experimental points.

— : Theoretical curve

onto the experimental data points for the potential step to -200 mV. In each case the data is fitted between the current minimum and a value approximately half that of the plateau value. Clearly, the most convincing fit (visually) is with the  $I-t^{\frac{3}{2}}$  curve, although the differences are surprisingly small.

The fits are examined more quantitatively in table 3.1 which lists the correlation coefficient for the computer fitting to all of the experimental transients resulting from potential steps to various overpotentials.

Overpotential (mV)	Correlation coefficient for fitting to $I-t^n$		
	<u>n=3</u>	<u>n=2</u>	<u>n=</u> $\frac{3}{2}$
-200	0.9925	0.9972	0.9995
-100	0.9883	0.9956	0.9992
- 50	0.9983	0.9999	0.9979

Table 3.1 The correlation coefficients corresponding to the fitting, by linear regression, of the experimental data points to  $I$  versus  $t^n$  relationships.

The data points from the experimental transients are replotted in the form of an  $I$  versus  $t^n$  plot. If the data truly fits an  $I-t^n$  relationship, then a plot of this type will produce a straight line through all of the points. The correlation coefficient,  $r$ , provides a numerical indication of how accurately the data points lie on the straight line and is calculated using equation 3.5:

$$r = \frac{\left( \sum x_i y_i - \frac{\sum x_i \sum y_i}{m} \right)}{\left( \sum x_i^2 - \frac{(\sum x_i)^2}{m} \right) \left( \sum y_i^2 - \frac{(\sum y_i)^2}{m} \right)} \quad (3.5)$$

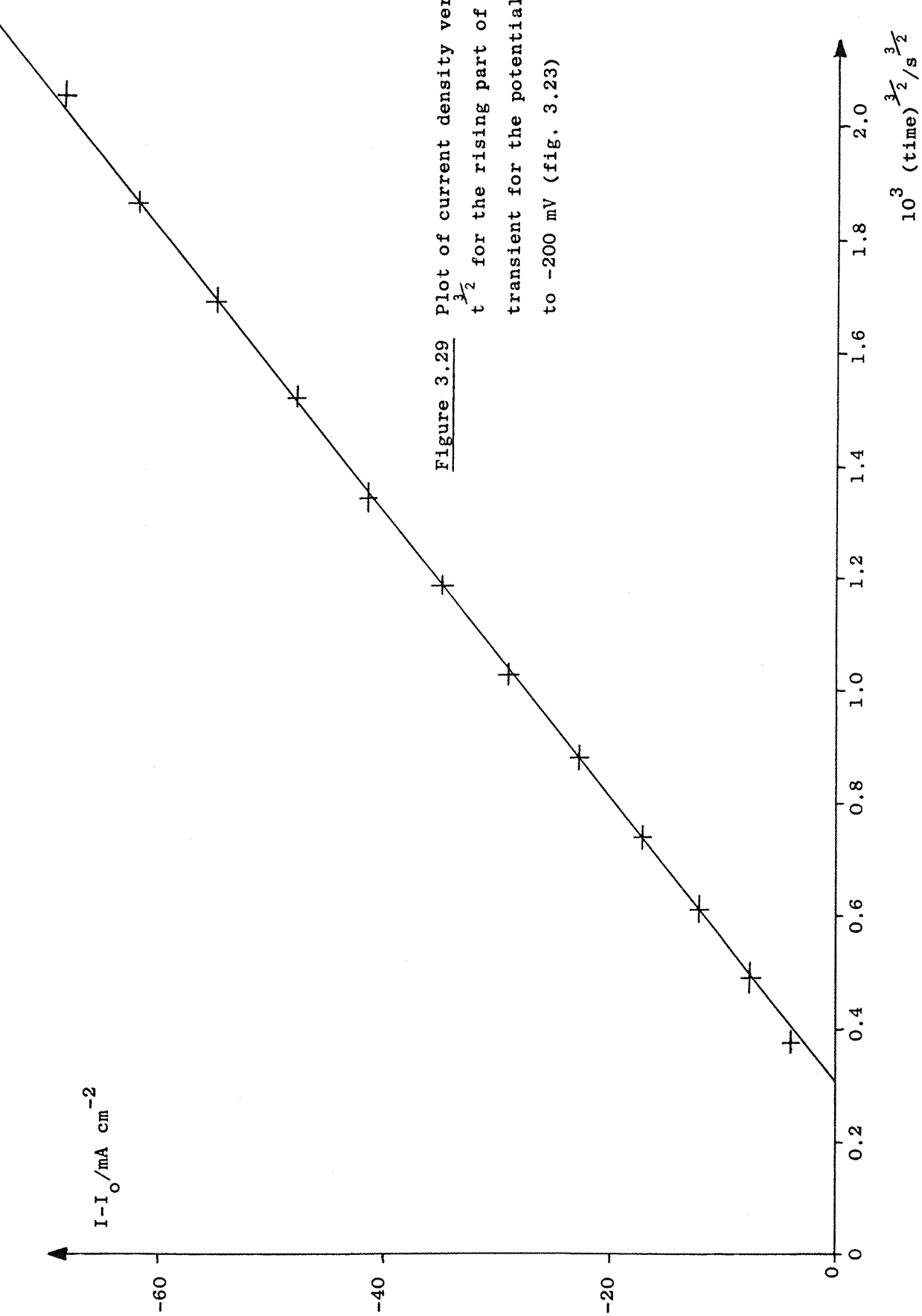
where  $x_i$  and  $y_i$  are the coordinates of a particular point and  $m$  is the number of points. Values of  $r$  equal to 1 indicate a perfect straight line whilst lower values occur due to deviation of the data from that of a straight line.

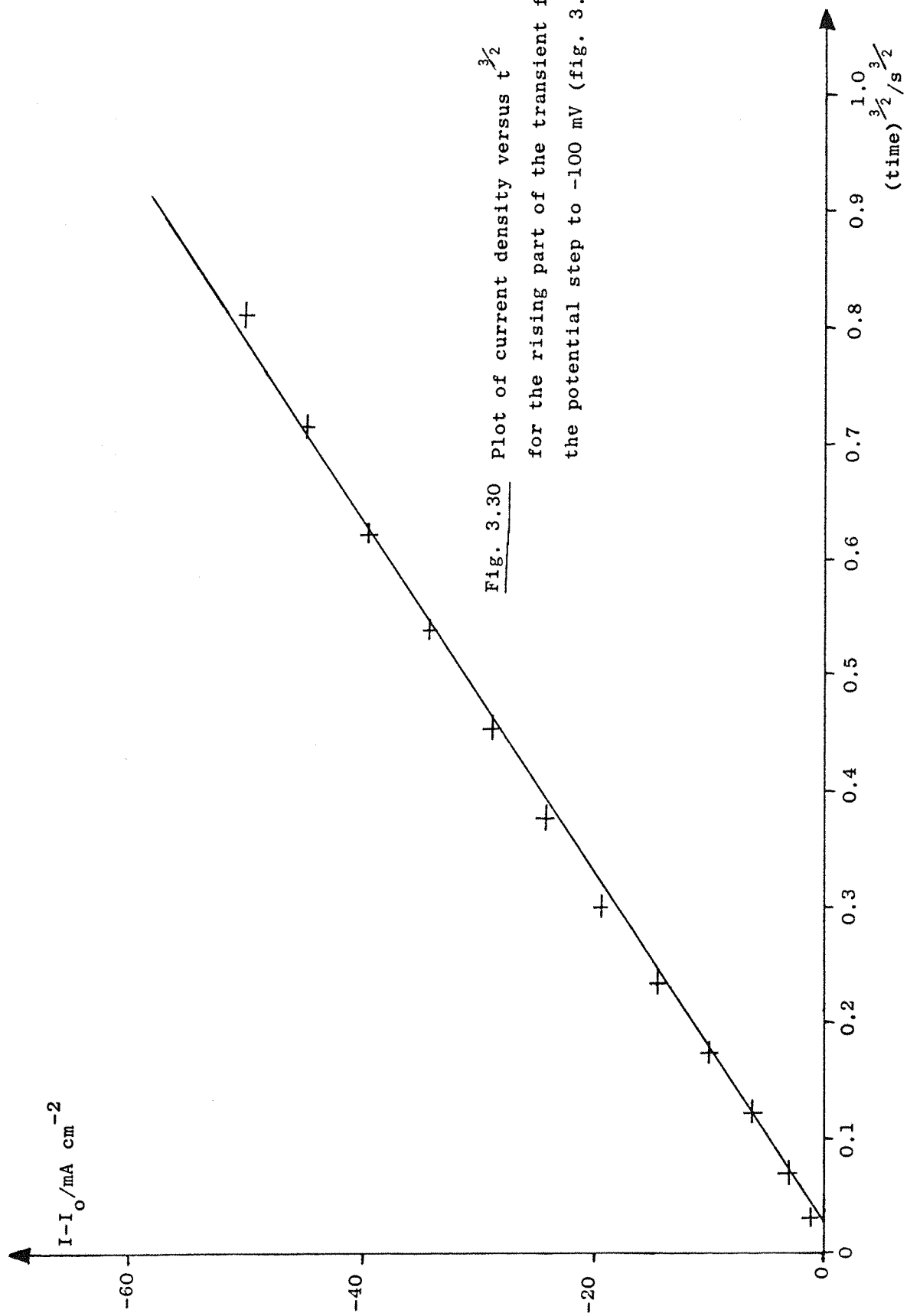
For the steps to -200 and -100 mV the best fit over the whole range of the transient considered is with an  $I-t^{\frac{3}{2}}$  relationship. For the step to -50 mV the best fit appears to be with an  $I-t^2$  relationship. However, an  $I-t^2$  relationship is difficult to accept because a significant value of  $\tau$  has been used to get this fit and this is not compatible with instantaneous nucleation while the overall shape of the transient is not compatible with two dimensional growth.

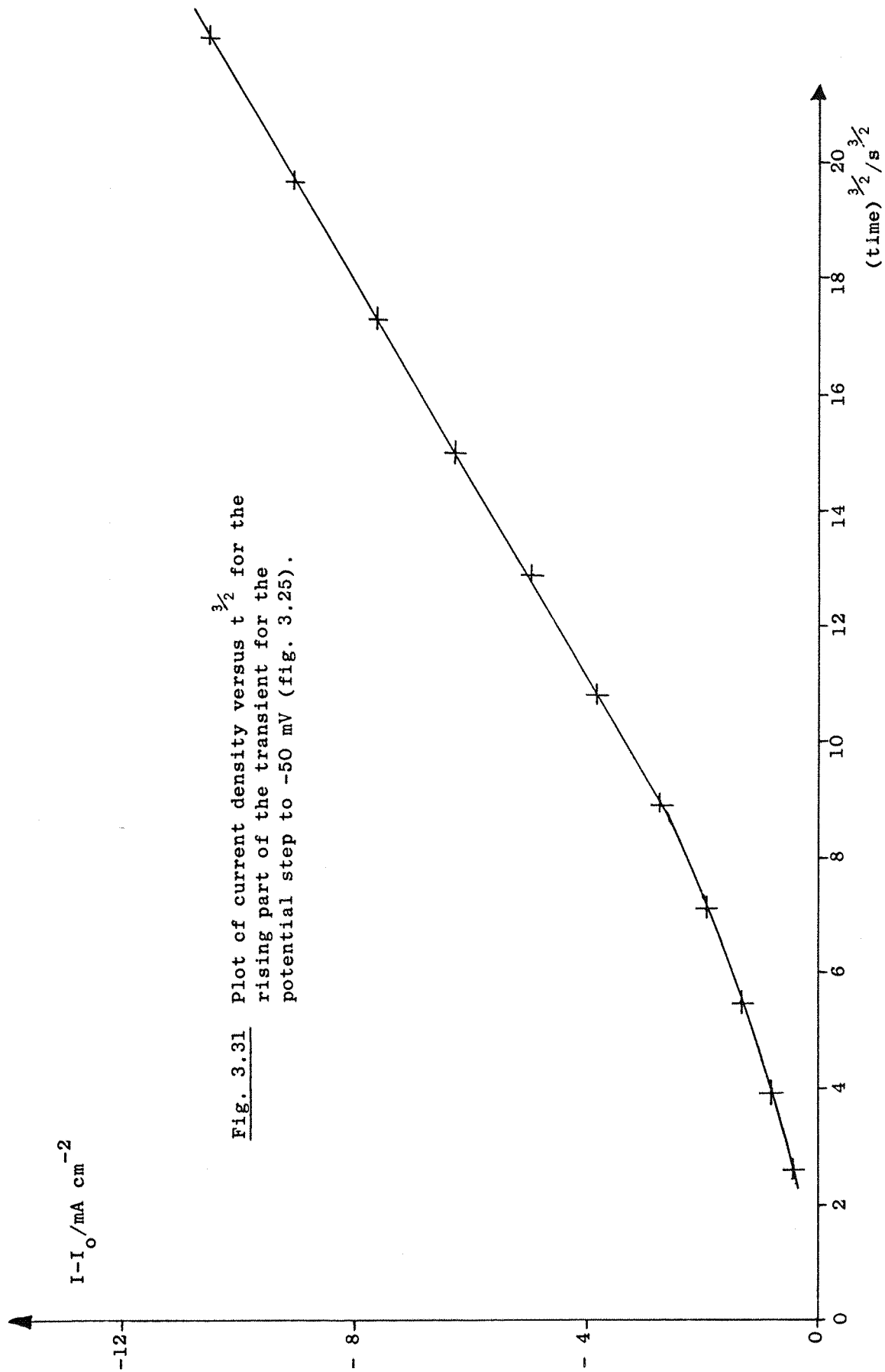
At this point it should be noted that the ability to fit the experimental data to an  $I-t^n$  relationship on the microcomputer does not totally determine the elucidation of the phase growth mechanism. Indeed, this work shows that the correlation coefficients are very reasonable for the  $I-t^{\frac{3}{2}}$ ,  $I-t^2$  or  $I-t^3$  fits and it is therefore essential to take into account all features of the transients.

Overall, the  $I-t^{\frac{3}{2}}$  relationship seems the most convincing and figures 3.29 to 3.31 show the experimental data replotted as a function of time to the power  $\frac{3}{2}$ . Straight lines are obtained over the whole range for the steps to -200 and -100 mV and, over the latter part of the timescale analysed for the step to -50 mV.

These results suggest that the deposition of lithium proceeds via progressive nucleation of metal centres which then grow three dimensionally in space under mass transport (diffusion)







control.

Progressive nucleation is also indicated by the finite and significant value of the nucleation induction period,  $\tau$ , compared to the time scale of the rising transients. Three dimensional growth is supported by the absence of any fine structure in the plateau region of the transients which would indicate two dimensional growth.

The possibility of increased kinetic control at low overpotentials might explain the deviation of the transients, corresponding to the potential step to -50 mV, from the  $I-t^{\frac{3}{2}}$  relationship at short times.

### 3.1.8 Film formation on a freshly deposited lithium surface

It is widely thought that lithium metal, in contact with organic and inorganic electrolytes, reacts with components of the medium to form a surface film.

During this study, a few experiments were carried out to confirm that a film was formed in a THF/LiAsF<sub>6</sub> medium and to show the effect of this film on the dissolution of the bulk metal. A layer of lithium was deposited and then allowed to stand on open circuit for various times before its dissolution was studied at positive overpotentials. The potential-time program shown in figure 3.32 was used. During the first pulse, a layer of lithium of known thickness is deposited. The period at open circuit allows the lithium to react with the THF/LiAsF<sub>6</sub> to form a surface film while the lithium is not cathodically protected or continuously being covered by fresh lithium layers. The cell is then switched back in at 0.0V where no lithium should be deposited or dissolved and then pulsed to the positive overpotential of interest, to observe the rate of dissolution. Figure 3.33 shows the results of such experiments, where the charge of lithium ( $1.5 \text{ C cm}^{-2}$ ) has been allowed to stand at open circuit for periods of 0, 2, 5, 10 and 16 minutes, before being pulsed to +125 mV. It can be seen

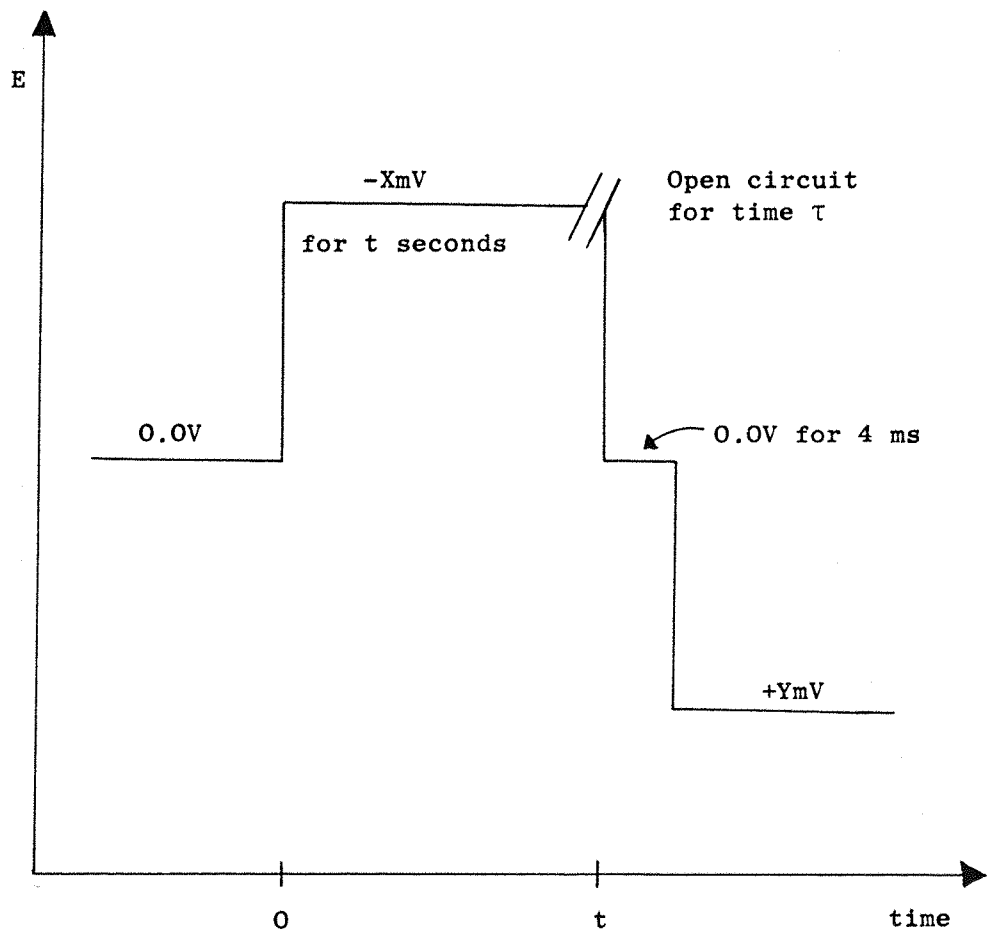
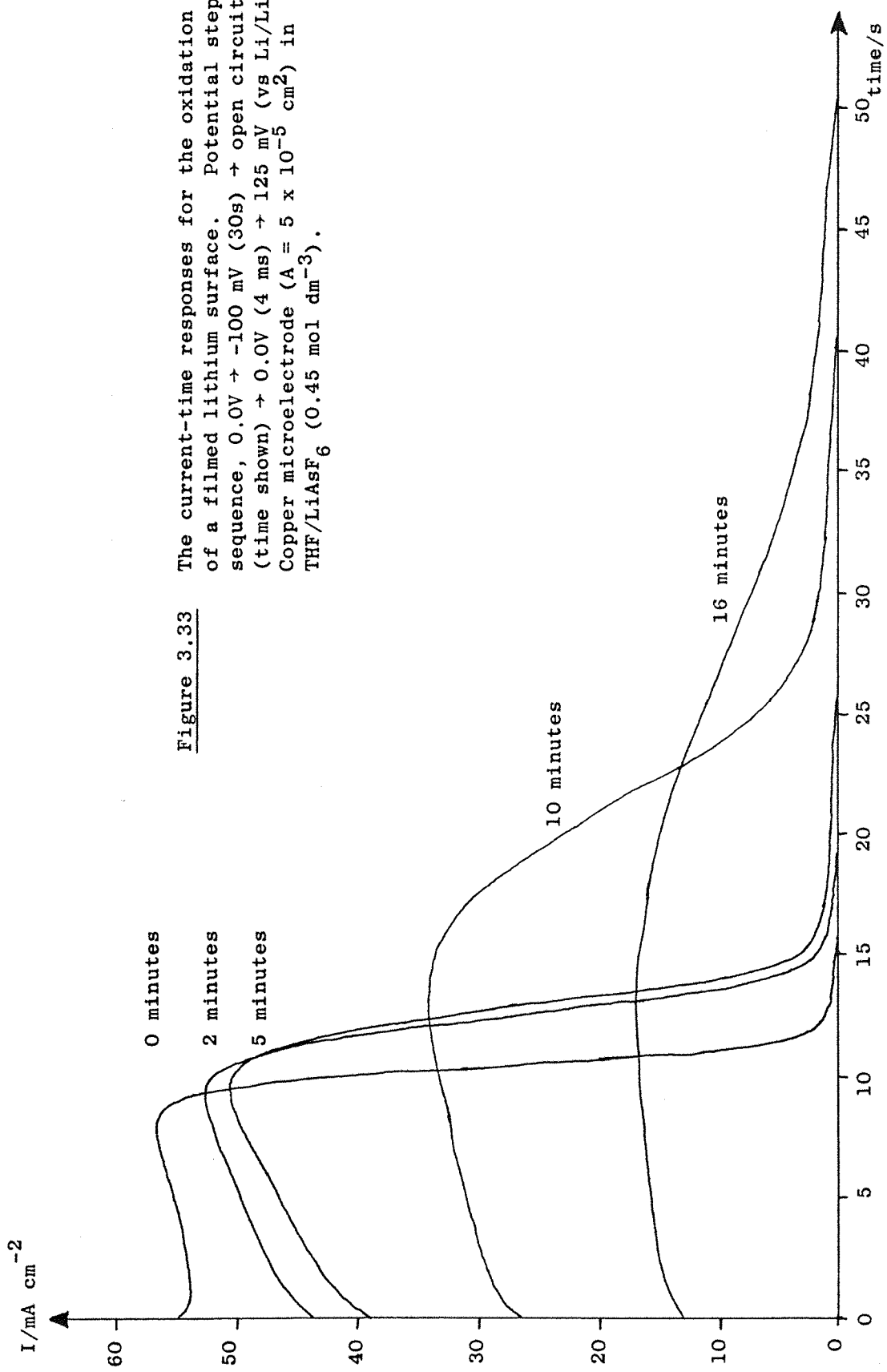


**Figure 3.32** The potential time program used to study the effect of a surface film on the dissolution of lithium metal.

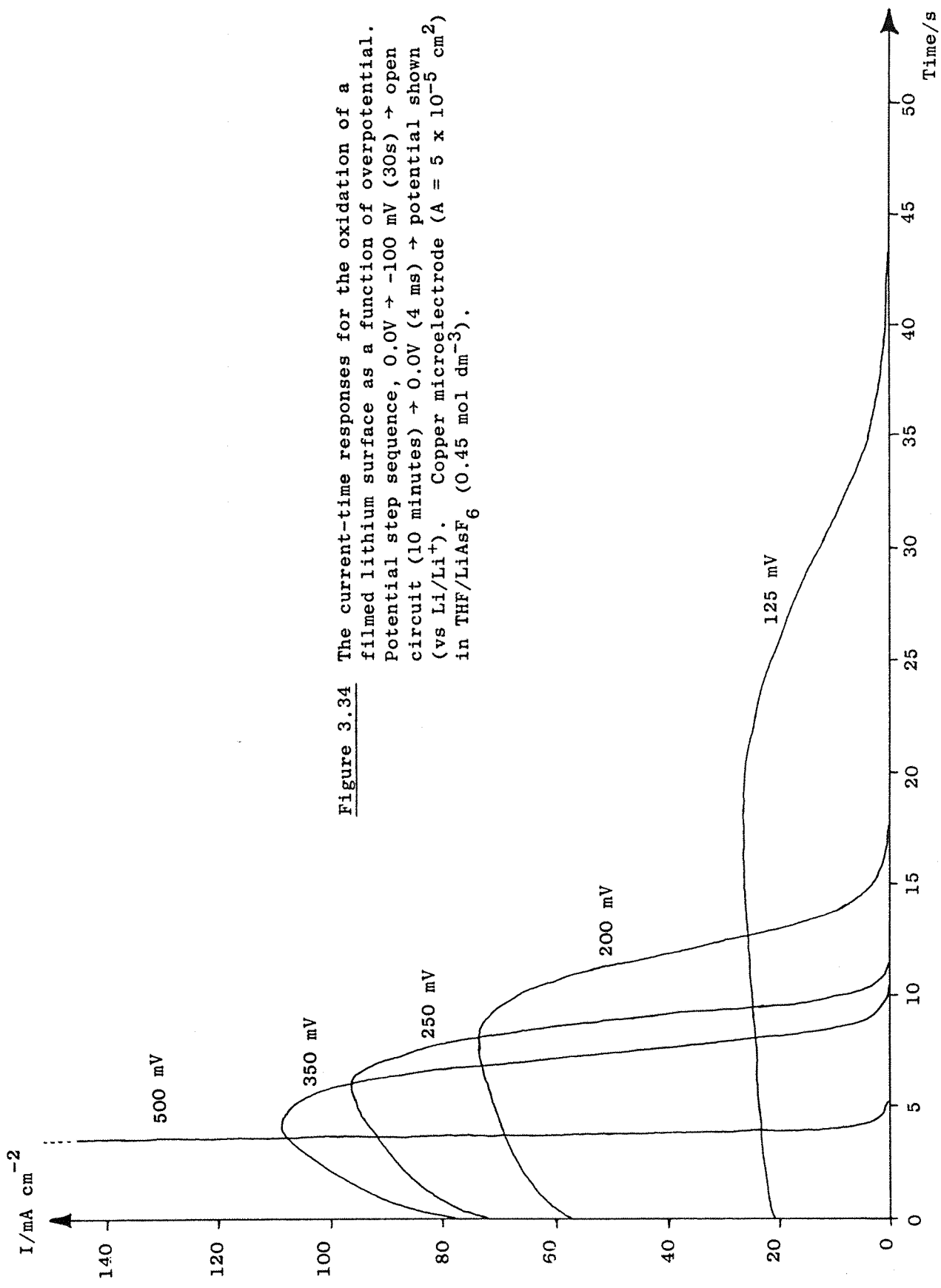


that the I-t response for the deposit stripped immediately after deposition has the same shape as the transients seen in section 3.1.5. and has an initial steady state current density of  $54 \text{ mA cm}^{-2}$  which is the expected value for an overpotential of +125 mV. On standing at open circuit, however, it can be seen that although the transients retain the same basic shape, the plateau current density is reduced, becoming lower with increased time at open circuit. For the deposits left on open circuit for 0, 2, 5 and 10 minutes, the stripping charge was approximately the same ( $0.6 \text{ C cm}^{-2}$ ) whilst for the deposit left for 16 minutes the stripping charge was  $0.5 \text{ C cm}^{-2}$ .

These results confirm that during the period on open circuit the lithium undergoes a slow chemical reaction with one or more components of the electrolyte to produce a surface film which reduces the rate of anodic oxidation of the bulk lithium. This process is initially quite slow, the curves for 0, 2 and 5 minutes on open circuit being quite similar, but after 10 or 16 minutes, the rate of dissolution is markedly diminished. The fact that a relatively steady current density passes even when a film is present suggests that the film is not instantly destroyed and it is more likely that dissolution occurs by a mechanism in which lithium ions pass through the film.

The influence of potential on a filmed lithium deposit was then probed by depositing a known amount of lithium ( $1.5 \text{ C cm}^{-2}$ ), allowing it to stand on open circuit for a fixed time (10 minutes) and then monitoring the current due to lithium dissolution as a function of overpotential. Figure 3.34 shows the results of such an experiment in which the anodic potential was pulsed to +125, +200, +250, +350 and +500 mV versus the  $\text{Li}/\text{Li}^+$  reference electrode.

It can clearly be seen that even when a film is present, the use of a higher overpotential results in a larger dissolution current density. At very high overpotentials (greater than +200 mV) the current density does not exhibit a well defined



plateau region but increases with time until the deposit is depleted. This could be a result of the film being removed or the formation of pores to reveal the "clean" lithium underneath. It was not possible to reproduce exactly the results of these experiments using electrolytes made at various times although the trends observed were always consistent. This is to be expected, however, since it is inevitable that small variations in the electrolyte composition occurred. This is particularly true for reactive impurities such as water, oxygen, nitrogen and carbon dioxide, the concentrations of which were not measured although every care was taken to keep them to a minimum.

The most probable explanation for the reduced current densities with increased time on open circuit is associated with the rate of lithium ion transport in the surface film. The mobility of lithium ion in the surface film will be lower than in solution and so the steady state current may well be determined by diffusion of the  $\text{Li}^+$  ions through the film. The longer the lithium is allowed to stand on open circuit, the thicker the film becomes and the more difficult it is for lithium ions to move through it.

No studies as to the exact origin or nature of the surface film were made and so it is unknown as to whether it is a result of the reaction of lithium with the solvent (THF), hexafluoroarsenate ion ( $\text{AsF}_6^-$ ) or trace impurities such as water. However, Koch has made an extensive study<sup>23</sup> of the lithium film in a  $\text{THF}/\text{LiAsF}_6$  media and has suggested that it consists of a polymer composed of  $(-\text{As}-\text{O}-\text{As}-)_n$  units. In another study in the laboratory<sup>78</sup> it has been noted that the presence of  $\text{AsF}_6^-$  inhibits initiation of the reaction of lithium with alkyl halides. This would also suggest that the film is formed by reaction of the metal and the  $\text{AsF}_6^-$  anion.

### 3.2 Variation of the electrode material and its effect on the THF/LiAsF<sub>6</sub> system

A series of experiments on the medium were carried out to study the effect of the electrode material on the electrochemistry of the system.

#### 3.2.1 25 $\mu\text{m}$ radius aluminium microelectrode

It is well known that lithium metal electrochemically alloys with aluminium<sup>49-57</sup> and there is widespread interest in this alloy as a possible anode in secondary lithium cells. During this work a brief study of the lithium-aluminium alloying process was made using cyclic voltammetry. Figure 3.35 shows a cyclic voltammogram run at 100 mV s<sup>-1</sup> using an aluminium microelectrode ( $r = 25 \mu\text{m}$ ) in THF/LiAsF<sub>6</sub> (0.55 moles dm<sup>-3</sup>), recorded between +1.4V and -0.15V. As for copper, a nucleation overpotential, here 80 mV, is required before the lithium starts to deposit and current begins to flow. The current is still rising at the negative limit and continues to do so at the beginning of the reverse sweep up to a peak value of 53 mA cm<sup>-2</sup>. During the reverse sweep the cathodic current is always higher than on the forward sweep but, unlike copper, reduction continues until +320 mV. The current then crosses the potential axis at +320 mV and an anodic current is seen which increases during the positive scan until a peak is observed at  $E_p = +830 \text{ mV}$ , after which the current falls to zero at around +1.0V. The deposition charge for this voltammogram is 104 mC cm<sup>-2</sup>, whilst the stripping charge is 101 mC cm<sup>-2</sup>, giving a stripping efficiency of approximately 97%. The shape of this voltammogram is due to the alloying of the deposited lithium metal with the aluminium electrode. It was stated (section 1.4.4) that the alloying of metals occurs when it becomes energetically more favourable to form the alloy lattice than the individual metal lattices and this is seen as a shift in equilibrium potential to a more positive potential and sometimes also as a decrease in the overpotential required for the metal ion reduction. This is seen for lithium on aluminium in the

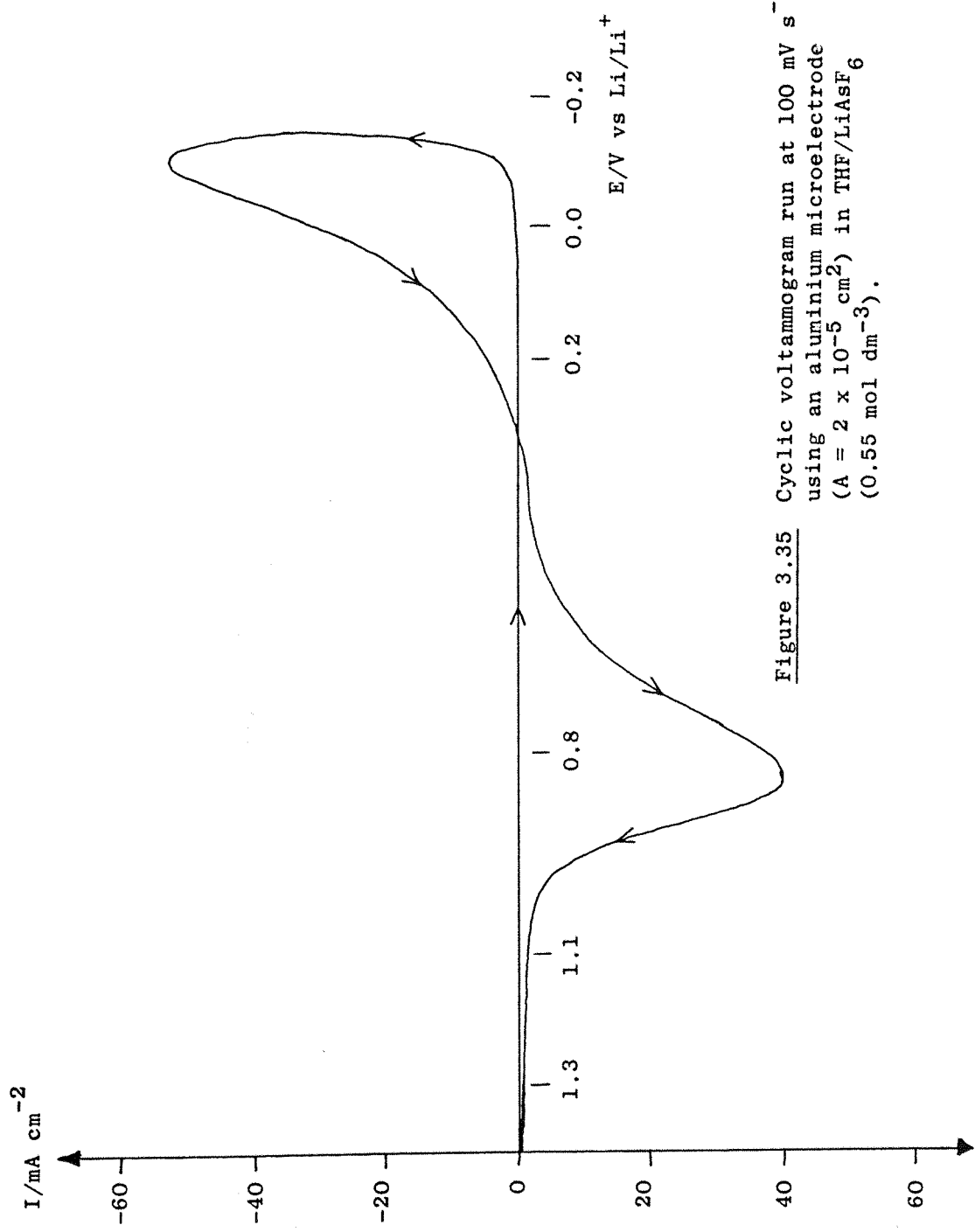


**Figure 3.35** Cyclic voltammogram run at  $100 \text{ mV s}^{-1}$  using an aluminium microelectrode ( $A = 2 \times 10^{-5} \text{ cm}^2$ ) in THF/LiAsF<sub>6</sub> ( $0.55 \text{ mol dm}^{-3}$ ).

cyclic voltammogram already described in figure 3.35, although the decrease in overpotential is not as large as expected. Once the lithium starts to deposit onto the aluminium, it begins to move into the aluminium lattice, forming the alloy. From then on, the lithium ions in solution see a lithium-aluminium substrate and lithium continues to deposit into the aluminium right up to +320 mV versus the Li/Li<sup>+</sup> reference electrode. Several authors<sup>52,54,55</sup> have noted that the open circuit potential of the lithium-aluminium electrode is dependent on the composition of the alloy. However, a value of between +320 and +330 mV is common for the  $\beta$ -LiAl alloy.

The broad stripping peak is in agreement with the work of Besenhard<sup>51</sup> and Frazer<sup>53</sup> and is due to the need for the lithium atoms to diffuse through the aluminium lattice before oxidation can occur. At this point, it must be emphasised that this cyclic voltammogram was not as reproducible as that for lithium being deposited on copper, with, for example, peak currents differing by up to a factor of two and nucleation overpotentials differing by  $\pm 25$  mV from experiment to experiment. There are two possible reasons for this:-

(i) It is well-known<sup>49,54</sup> that the surface of aluminium is always coated with an oxide layer,  $Al_2O_3$ , which is virtually impossible to remove completely. Between experiments the electrode surface was always polished and so it is probable that varying amounts of oxide were present during the experimental work. In an attempt to minimise this oxide formation, the experiment was performed inside the argon filled dry box but the results showed no significant difference from those experiments performed outside of the box.

(ii) It is known<sup>51-53,57</sup> that when the lithium diffuses into the aluminium lattice the lattice has to expand and re-organise itself in order to accommodate the lithium metal. Repeated deposition and dissolution of lithium onto aluminium

results in permanent cracks and pores being formed in the lattice which gives rise to an unknown and variable electrode area. Although polishing should minimise the effect of this on the results, it is probable that some interference remains.

Figure 3.36 shows the effect of sweeping the potential to a more negative limit, here -400 mV, on the same system described for fig. 3.35. The nucleation process is similar to that described earlier and the current continues to increase right up to the end of the forward sweep. On the reverse sweep the current is always higher than on the forward sweep, but instead of crossing the potential axis at +320 mV as expected, it crosses at +60 mV. During the remainder of the reverse sweep two oxidative peaks are seen at  $E_{p_1} = +350$  mV and  $E_{p_2} = +920$  mV. The charge associated with the deposition process is  $1.00 \text{ C cm}^{-2}$  whilst the charge associated with the first stripping peak is  $0.42 \text{ C cm}^{-2}$  ( $E = 42\%$ ) and the second stripping peak approximately  $0.50 \text{ C cm}^{-2}$  ( $E = 50\%$ ). Similar experiments using different negative limits and sweep rates have shown that as the charge under the peak at lower positive overpotentials increases, the charge under the peak at +800 to +900 mV becomes relatively less important. The larger the deposition charge or the faster the sweep rate, the larger this first peak becomes. The point at which the current crosses the potential axis is also dependent on the deposition charge and sweep rate.

These results are similar to those reported by Frazer<sup>53</sup> for a lithium-aluminium electrode in a propylene carbonate/LiClO<sub>4</sub> electrolyte. However, like Fawcett<sup>54</sup>, we do not agree with his suggestion that the peak at lower anodic overpotentials corresponds to the dissolution of various lithium rich alloy compositions. It is more probable that this peak is due to freshly deposited lithium sitting on the alloy surface waiting to move into the alloy lattice. However, no experiments were carried out to test this theory.

The effect of cycling the aluminium electrode can be seen in figure 3.37, which shows the first four cycles, run between

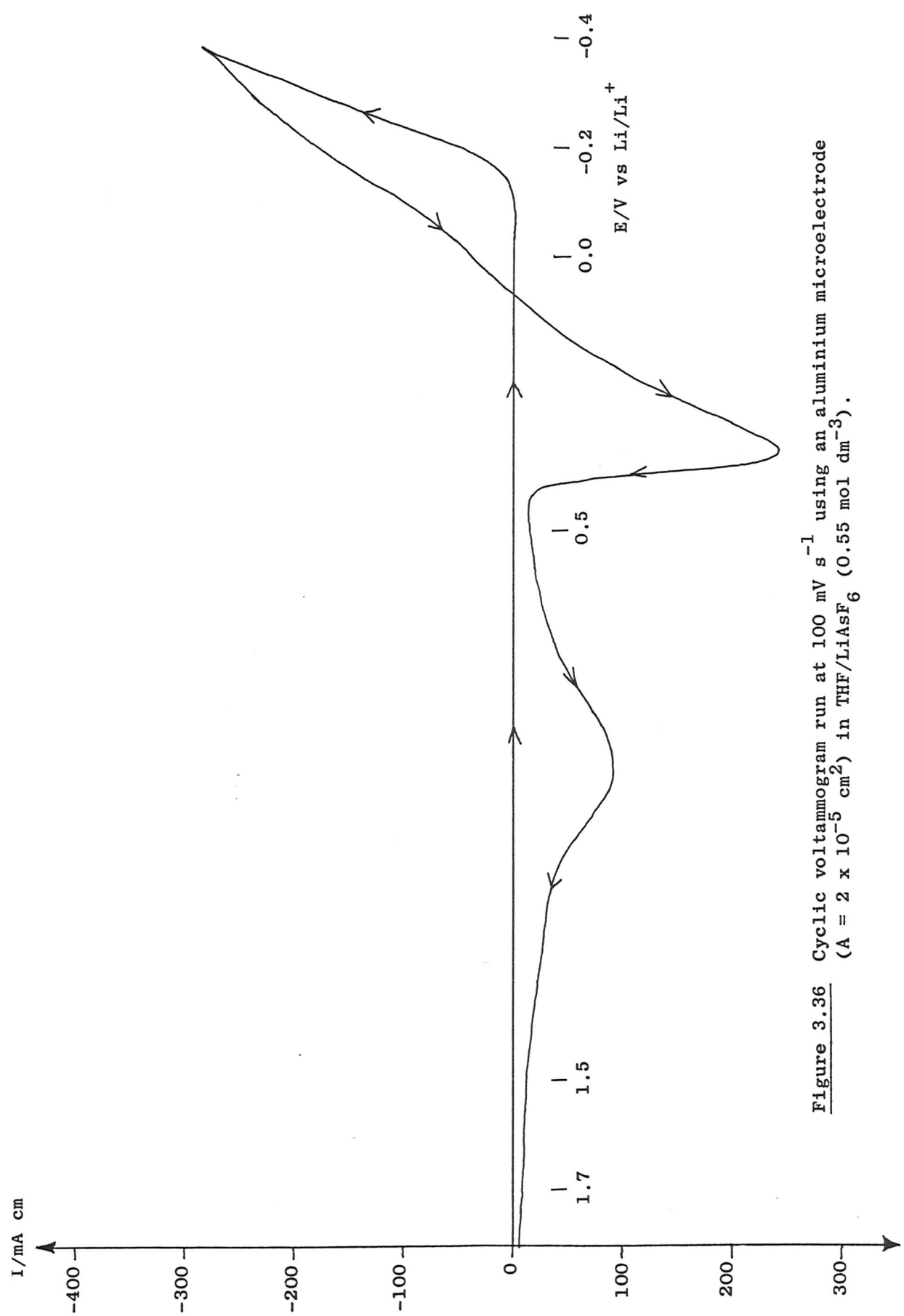
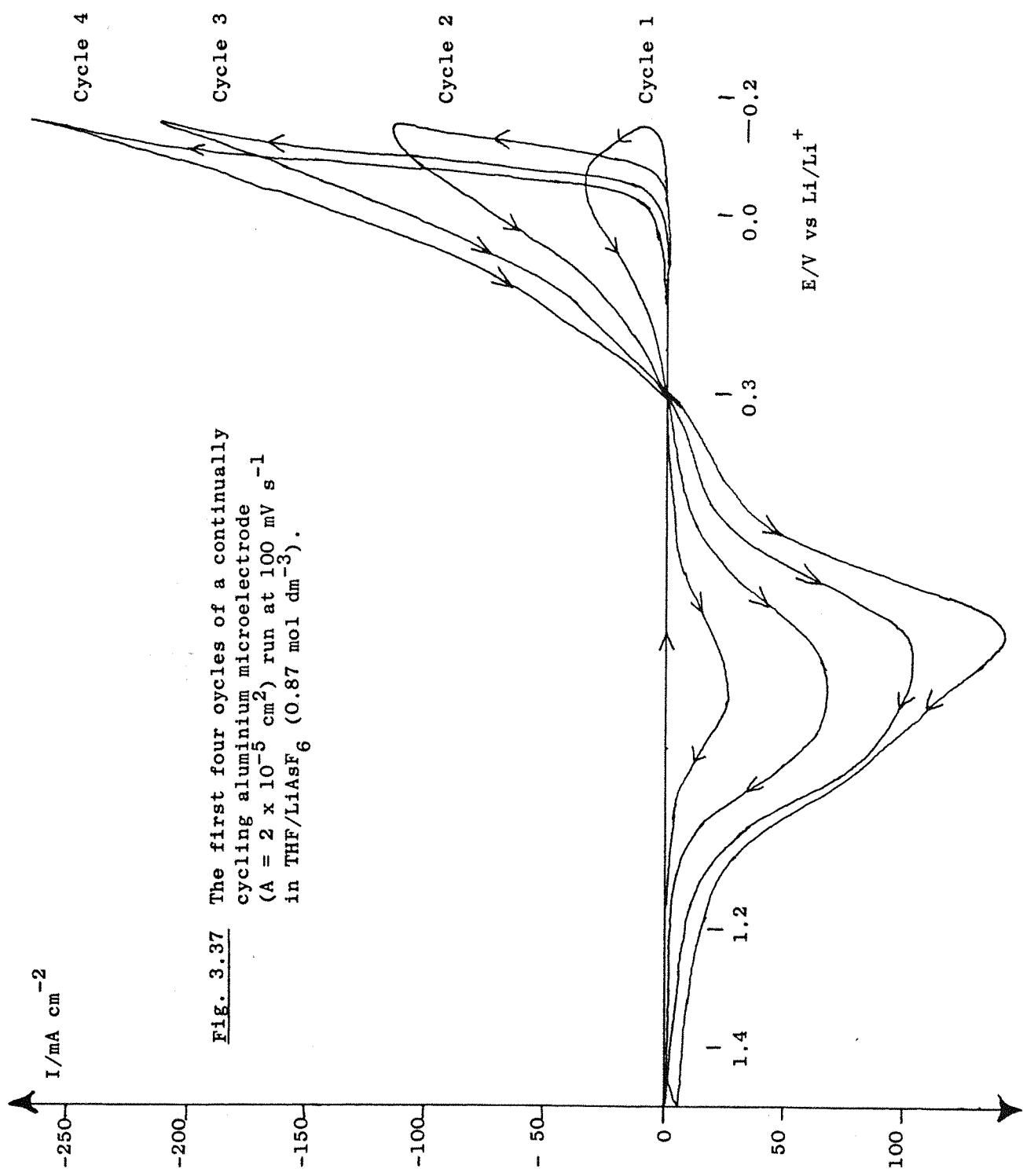


Figure 3.36 Cyclic voltammogram run at  $100 \text{ mV s}^{-1}$  using an aluminium microelectrode ( $A = 2 \times 10^{-5} \text{ cm}^2$ ) in  $\text{THF}/\text{LiAsF}_6$  ( $0.55 \text{ mol dm}^{-3}$ ).



**Fig. 3.37** The first four cycles of a continually cycling aluminium microelectrode ( $A = 2 \times 10^{-5} \text{ cm}^2$ ) run at  $100 \text{ mV s}^{-1}$  in  $\text{THF}/\text{LiAsF}_6$  ( $0.87 \text{ mol dm}^{-3}$ ).

+1.5 and -0.15V in a THF/LiAsF<sub>6</sub> (0.87 moles dm<sup>-3</sup>) electrolyte. The first sweep is similar to the result in fig. 3.35 and shows a cathodic peak at -0.050V of magnitude 37 mA cm<sup>-2</sup> and an anodic peak at +0.800V of magnitude 25 mA cm<sup>-2</sup>. However, successive sweeps show that nucleation occurs at progressively lower overpotentials and by the fourth sweep, nucleation is, in fact, occurring at positive overpotentials. This earlier nucleation results in larger cathodic currents and deposition charges. This process continues to occur until the 35th cycle, figure 3.38, by which time nucleation is occurring at approximately +320 mV (apparently the E<sup>o</sup> value of this LiAl alloy) and the peak cathodic current is 390 mA cm<sup>-2</sup>. A second small oxidative peak is also observed at +150 mV. No further changes occurred in the voltammogram until the 50th cycle at which time the experiment was terminated.

These results are again probably explained by the reduction of the oxide layer during the first few cycles and expansion of the aluminium lattice due to the continued insertion and removal of the lithium from the electrode surface.

Finally, the deposition of lithium into aluminium was briefly studied using a potential step method. Figure 3.39 shows the current-time responses to a series of potential steps to -60, -80, -100 and -130 mV using the aluminium microelectrode ( $r = 25 \mu\text{m}$ ) in a THF/LiAsF<sub>6</sub> (0.6 moles dm<sup>-3</sup>) electrolyte.

The transients are similar to those for lithium deposition on copper and indicate the need for the nucleation and growth of lithium centres on the aluminium. The eventual overlap of these centres to give a uniform surface which grows under mass transport control is suggested by the presence of a plateau in the transients. However, the values of the steady state current densities are higher than those obtained for similar overpotentials on copper. This is not surprising since the radius of the aluminium microelectrode is less than that of the copper one and so a higher steady state rate of diffusion would be expected. Again it must be stated that the results on aluminium were not as reproducible as those on copper.

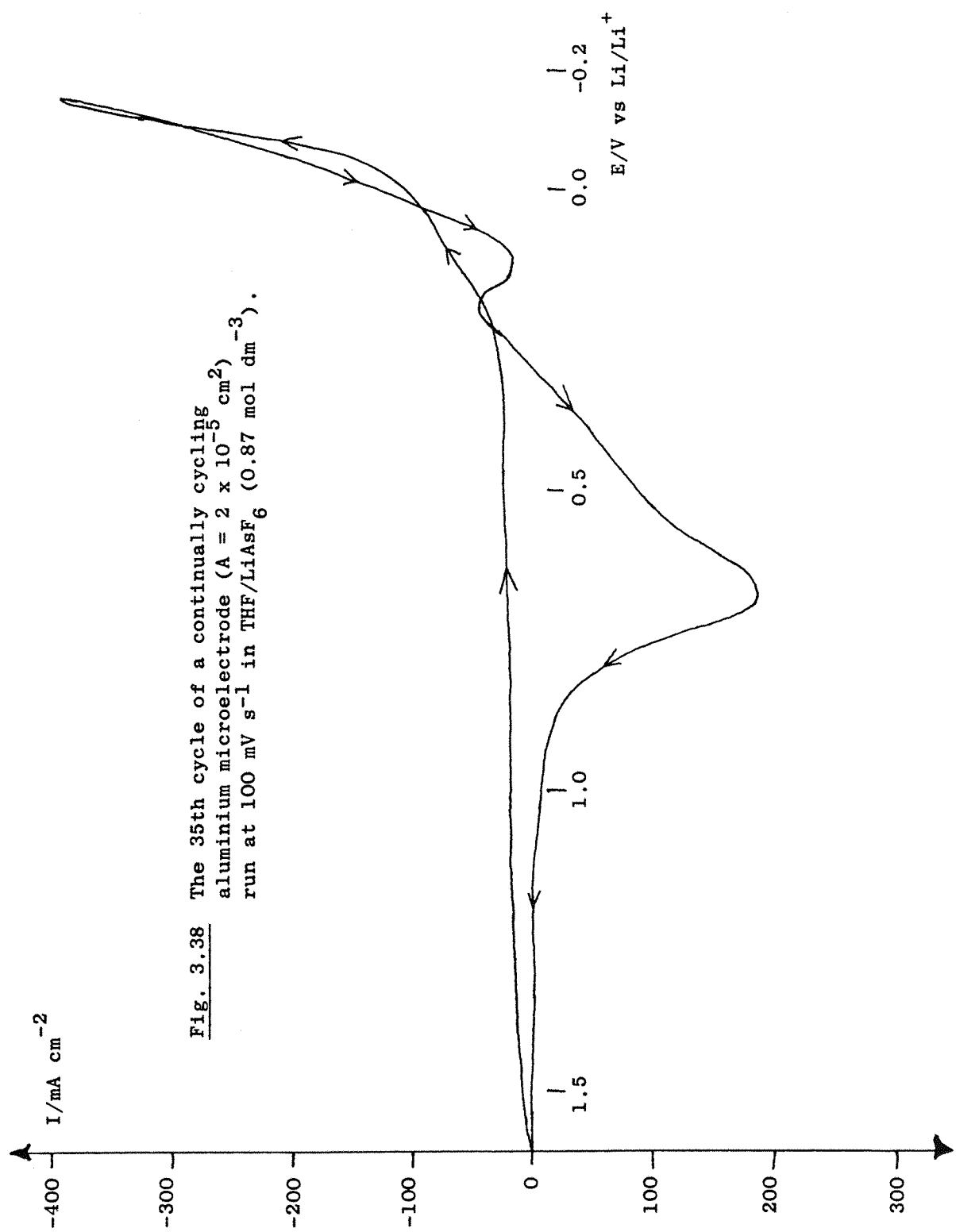


**Fig. 3.38** The 35th cycle of a continually cycling aluminium microelectrode ( $A = 2 \times 10^{-5} \text{ cm}^2$ ) run at  $100 \text{ mV s}^{-1}$  in  $\text{THF/LiAsF}_6$  ( $0.87 \text{ mol dm}^{-3}$ ).

$I / \text{mA cm}^{-2}$

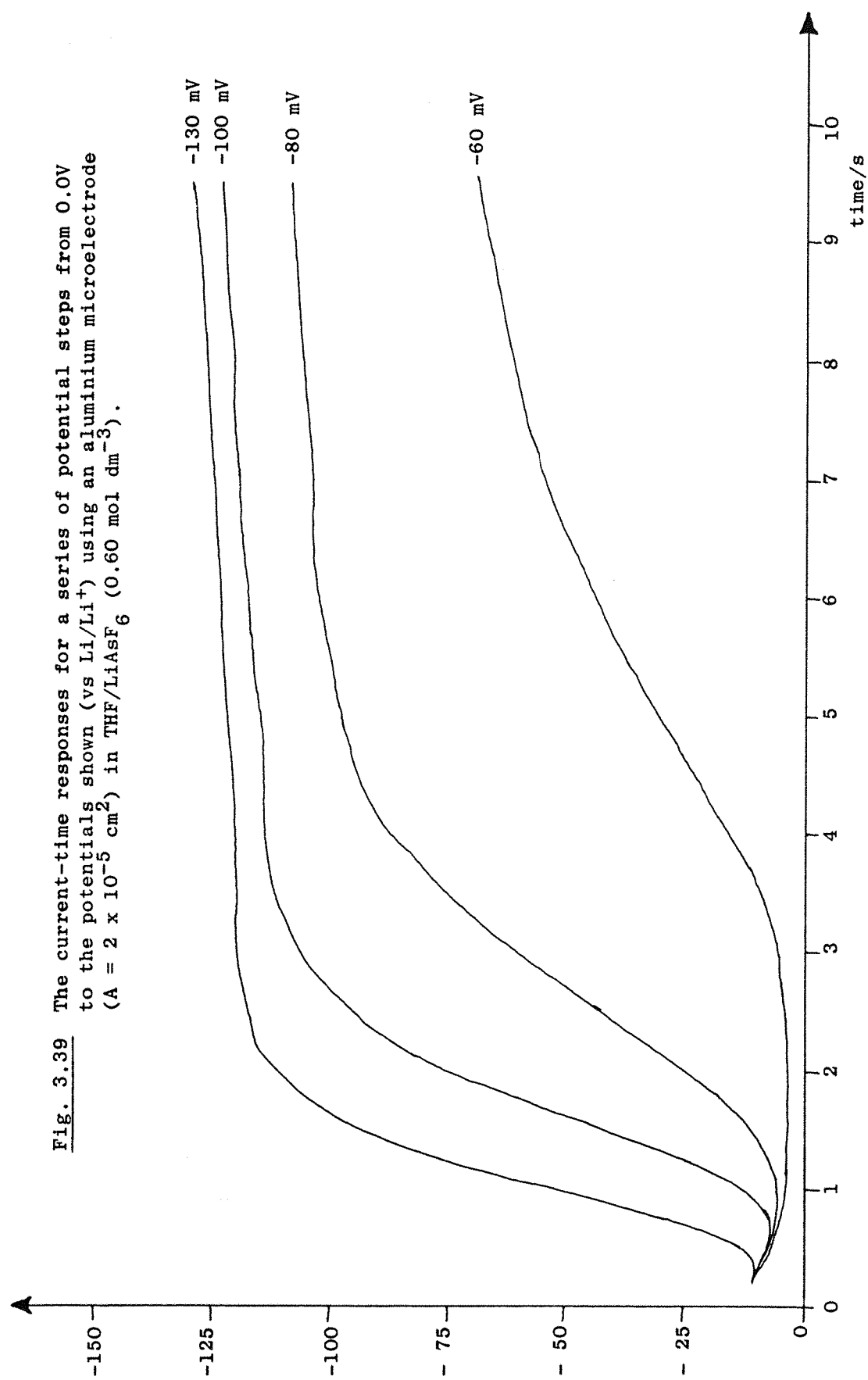


**Fig. 3.39** The current-time responses for a series of potential steps from 0.0V to the potentials shown (vs Li/Li<sup>+</sup>) using an aluminiun microelectrode ( $A = 2 \times 10^{-5} \text{ cm}^2$ ) in THF/LiAsF<sub>6</sub> (0.60 mol dm<sup>-3</sup>).

No further work, using this potential step technique has yet been carried out.

### 3.2.2 25 $\mu\text{m}$ radius nickel microelectrode

Due to its use as a support for the lithium metal in  $\text{Li}/\text{SOCl}_2$  cells, it was decided to investigate the deposition and dissolution of lithium on a nickel electrode. Figure 3.40 shows a cyclic voltammogram run at  $100 \text{ mV s}^{-1}$  using a nickel microelectrode ( $r = 25 \mu\text{m}$ ) in  $\text{THF}/\text{LiAsF}_6$  ( $0.59 \text{ moles dm}^{-3}$ ), recorded between  $+500 \text{ mV}$  and  $-200 \text{ mV}$ . This result is almost identical to that for a copper electrode and is clearly that for a non-alloying substrate. Nucleation occurs at  $-120 \text{ mV}$ ,  $30 \text{ mV}$  more negative than copper; a "nucleation loop" is observed with a maximum cathodic current density of  $63 \text{ mA cm}^{-2}$ . The current crosses the potential axis at  $0.0\text{V}$  and an anodic peak is seen at  $+190 \text{ mV}$  with a maximum current density equal to  $66 \text{ mA cm}^{-2}$ . The deposition charge is  $80 \text{ mC cm}^{-2}$  and the stripping charge is  $74 \text{ mC cm}^{-2}$ , giving a stripping efficiency of 92%.

Varying the negative limit and the sweep rate gave the same results as for a copper substrate. No further work was done using this electrode.

### 3.2.3 4 $\mu\text{m}$ radius carbon microelectrode

A brief study of the deposition and dissolution of lithium on a carbon electrode was also carried out during this work.

Figure 3.41 shows a cyclic voltammogram run at  $100 \text{ mV s}^{-1}$  using a carbon microelectrode ( $r = 4 \mu\text{m}$ ) in  $\text{THF}/\text{LiAsF}_6$  ( $1.1 \text{ moles dm}^{-3}$ ), recorded between  $+600 \text{ mV}$  and  $-295 \text{ mV}$ . A similar result is obtained to those using copper and nickel electrodes. A much larger nucleation overpotential is required, here  $-270 \text{ mV}$ , although once growth has started the current rises very steeply due to the fast rate of electron transfer at such a high overpotential. A "nucleation loop" is seen with a maximum current density of  $60 \text{ mA cm}^{-2}$ . The current

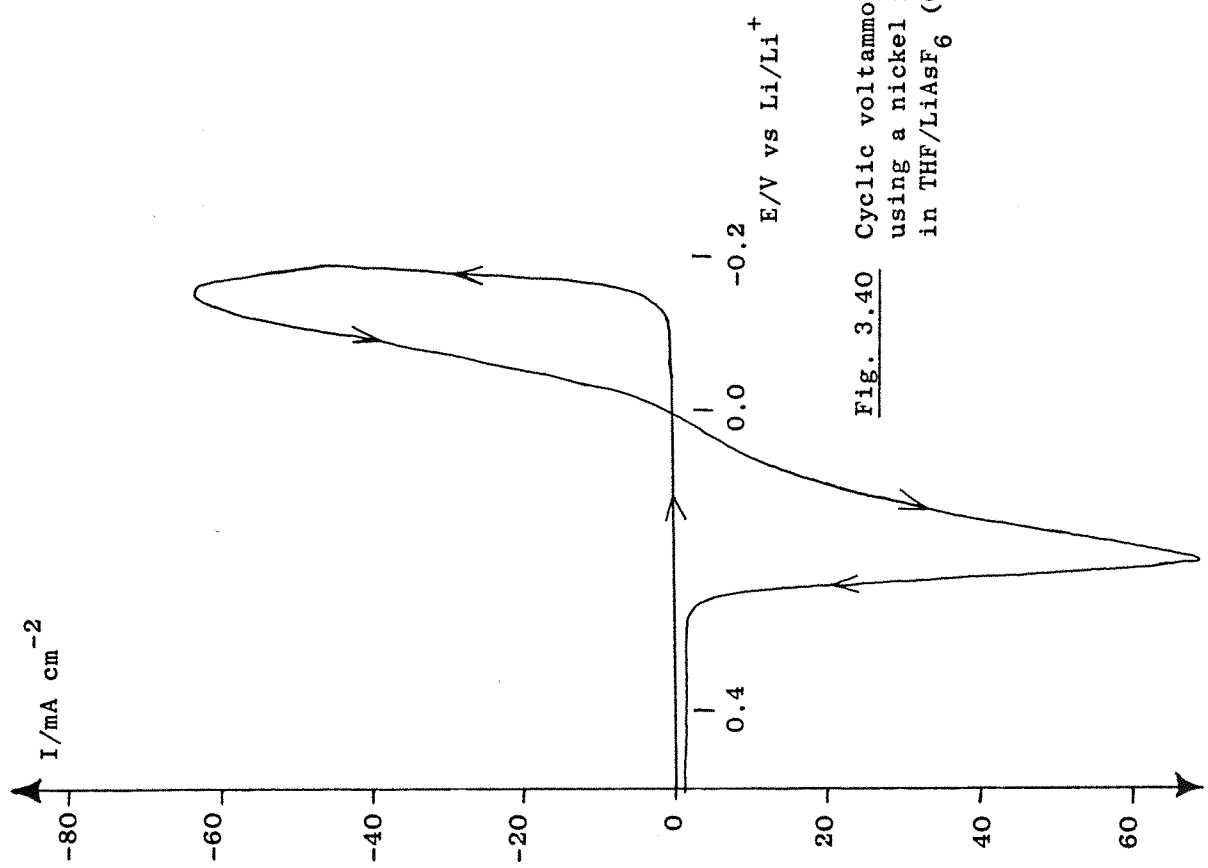


Fig. 3.40 Cyclic voltammogram run at  $100 \text{ mV s}^{-1}$  using a nickel microelectrode ( $A = 2 \times 10^{-5} \text{ cm}^2$ ) in  $\text{THF}/\text{LiAsF}_6$  ( $0.59 \text{ mol dm}^{-3}$ ).

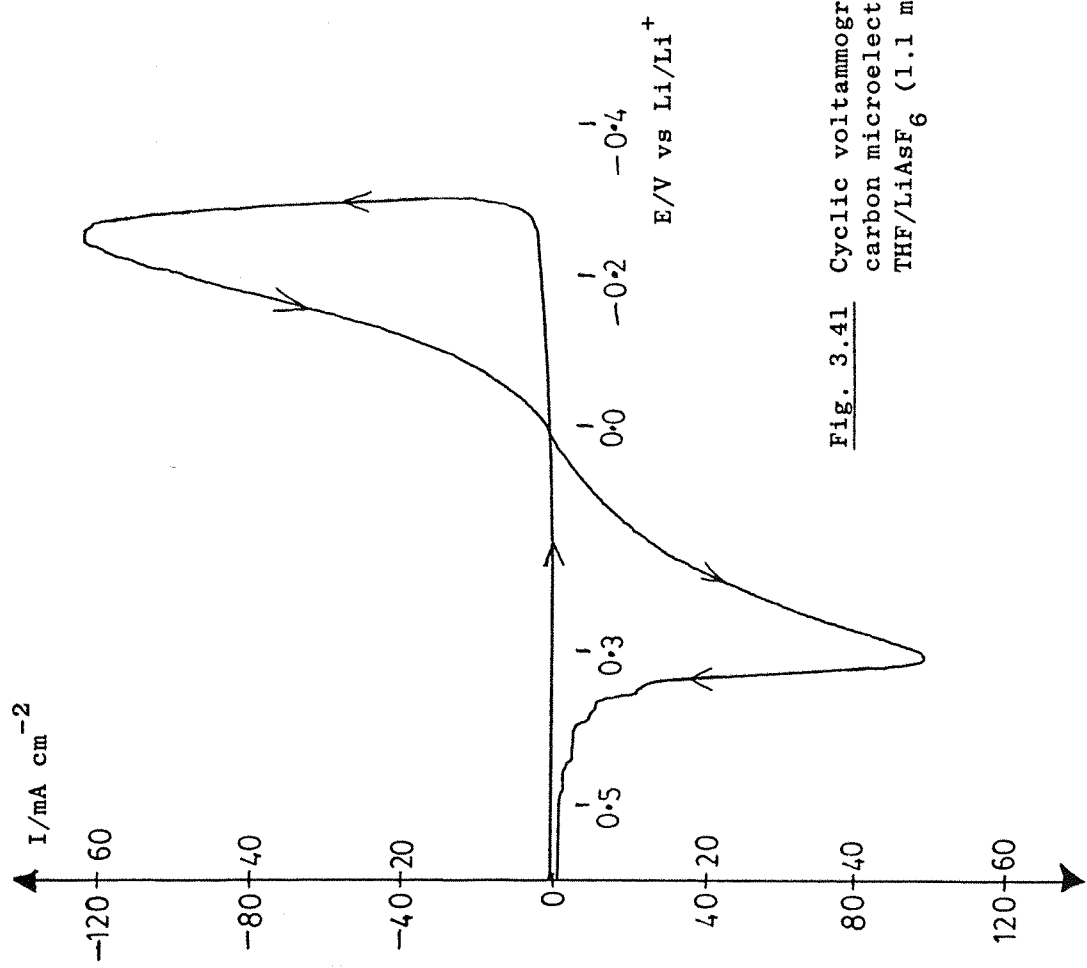


Fig. 3.41 Cyclic voltammogram run at  $100 \text{ mV s}^{-1}$  using a carbon microelectrode ( $A = 5 \times 10^{-7} \text{ cm}^2$ ) in  $\text{THF}/\text{LiAsF}_6$  ( $1.1 \text{ mol dm}^{-3}$ ).

crosses the potential axis at 0.0V and an anodic peak is seen at +320 mV with a maximum current density equal to  $50 \text{ mA cm}^{-2}$ . The deposition charge is  $92 \text{ mC cm}^{-2}$  and the stripping charge is  $82 \text{ mC cm}^{-2}$ , giving a stripping efficiency of 89%. The shape of the stripping peak is similar to those for copper and nickel electrodes as is the angle at which the current crosses through the voltage axis. Thus it appears that the carbon electrode behaves as an inert one with no intercalation of the lithium occurring.

The jagged end of the stripping peak is probably due to noise, an inevitable consequence of using a smaller electrode. No further work was done using this electrode.

In concluding this work on electrode materials, it is important to notice the differences and similarities between the various substrates. As expected the forward sweeps of the cyclic voltammograms show significant differences which are due to the differing nucleation characteristics on the various substrates. For the copper, nickel and carbon electrodes the reverse sweep produces a very similar result because the electrode surfaces have become covered with lithium and the electrode behaves as a lithium electrode. For aluminium, however, the reverse sweep shows significant differences reflecting that the electrode surface is not lithium but a lithium-aluminium alloy.

### 3.3 Influence of temperature on the THF/LiAsF<sub>6</sub> system

A promising feature of lithium batteries is reported to be their ability to operate over a wide range of temperatures. For this reason a study of the effect of temperature on the Li/Li<sup>+</sup> couple was made using the copper and aluminium electrodes.

#### 3.3.1 40 $\mu\text{m}$ radius copper microelectrode

Cyclic voltammograms were run at various temperatures and

the results are summarised in table 3.2.

Figure 3.42 compares the cyclic voltammograms for a copper microelectrode run at  $+60^{\circ}\text{C}$ ,  $+21^{\circ}\text{C}$  and  $-22^{\circ}\text{C}$ . Although all of the voltammograms have the same basic shape, it is clear that temperature has a very strong influence on the kinetics of the  $\text{Li}/\text{Li}^+$  couple. It is clear that as the temperature of the cell is increased, the angle at which the current trace crosses the potential axes becomes much steeper. This indicates that the kinetics of the lithium couple are increasing with temperature.

From table 3.2 it is also clear that as the temperature is reduced, nucleation becomes more difficult and the actual growth rate of the deposit is slowed down, resulting in a lower charge of lithium being deposited. The dissolution rate is also reduced, as seen by the movement of the anodic peak towards higher positive overpotentials. At  $-38^{\circ}\text{C}$ , two waves are seen in the cathodic current although this phenomenon has not been studied further.

### 3.3.2 25 $\mu\text{m}$ radius aluminium microelectrode

Table 3.3 summarises the results of cyclic voltammograms run at  $100 \text{ mV s}^{-1}$  at various temperatures for an aluminium electrode in a  $\text{THF}/\text{LiAsF}_6$  medium. Figure 3.43 compares the cyclic voltammograms at  $21^{\circ}\text{C}$  and  $60^{\circ}\text{C}$ , whilst figure 3.44 shows a voltammogram at  $0^{\circ}\text{C}$ .

For the aluminium electrode, temperature has a much greater influence on the nucleation potential than for the copper electrode. In fact, by  $+40^{\circ}\text{C}$  nucleation starts to occur at positive overpotentials, which leads to much larger lithium charges being deposited by a given potential.

Also, as the temperature is reduced to  $0^{\circ}\text{C}$  (figure 3.44) we observe the disappearance of the single stripping peak and the appearance of the second peak (noted earlier in section 3.2.1) at

Temperature	Concentration of LiAsF <sub>6</sub> (moles dm <sup>-3</sup> )	Nucleation Potential (mV)	Deposition current at -125 mV (mA cm <sup>-2</sup> )	Stripping peak E <sub>p</sub> (mV)	I <sub>p</sub> (mA cm <sup>-2</sup> )
-38	0.74	-500	-	+1200	3.2
-22	0.74	-200	-	+390	3.1
0	0.74	-120	0.5	+260	13
21	0.74	- 90	20	+220	36
30	0.56	-80	30	+160	88
40	0.56	-75	70	+170	140
50	0.56	-70	90	+110	128
60	0.56	-60	100	+110	190

Table 3.2 The influence of temperature on the deposition and dissolution of lithium metal onto copper from a THF/LiAsF<sub>6</sub> solution. Data taken from cyclic voltammograms run at 100 mV s<sup>-1</sup>.

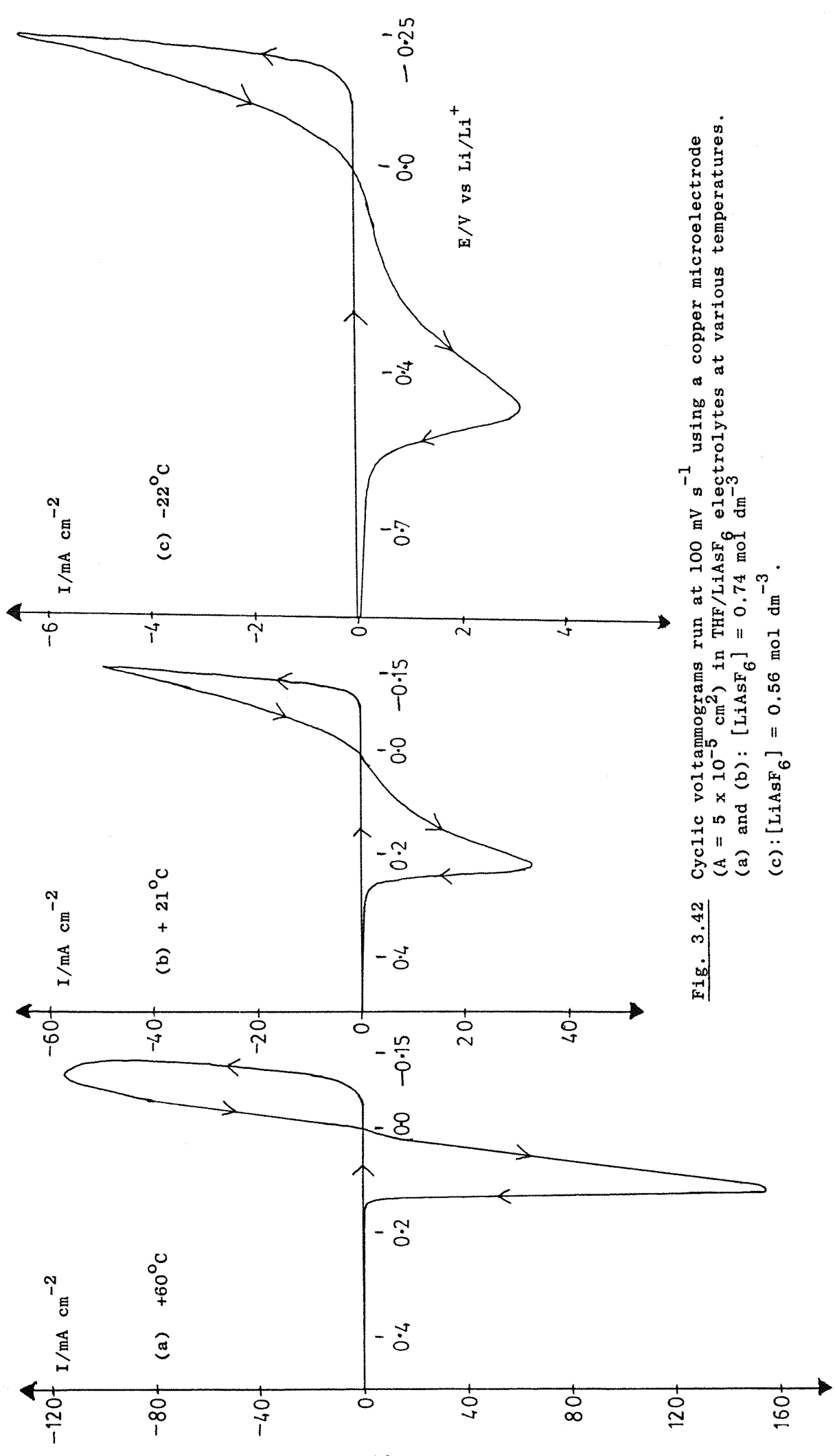


Fig. 3.42 Cyclic voltammograms run at  $100 \text{ mV s}^{-1}$  using a copper microelectrode ( $A = 5 \times 10^{-5} \text{ cm}^2$ ) in  $\text{THF/LiAsF}_6$  electrolytes at various temperatures.  
 (a) and (b):  $[\text{LiAsF}_6] = 0.74 \text{ mol dm}^{-3}$   
 (c):  $[\text{LiAsF}_6] = 0.56 \text{ mol dm}^{-3}$ .

Temperature	Concentration of LiAsF <sub>6</sub> (moles dm <sup>-3</sup> )	Nucleation Potential (mV)	Stripping peak		
			E <sub>p</sub> (mV)	Deposition current at -200 mV (mA cm <sup>-2</sup> )	I <sub>p</sub> (mA cm <sup>-2</sup> )
-42	0.74	-400	-	-	-
-20	0.74	-250	-	600	6
0	0.74	+180	2	340	5
21	0.74	- 65	50	900	13
30	0.56	- 30	215	825	70
40	0.56	0	250	870	160
50	0.56	+ 70	250	780	170
60	0.56	+120	250	680	185
				640	150

**Table 3.3** The influence of temperature on the deposition and dissolution of lithium metal onto aluminium from a THF/LiAsF<sub>6</sub> solution. Data taken from cyclic voltammograms run at 100 mV s<sup>-1</sup>.

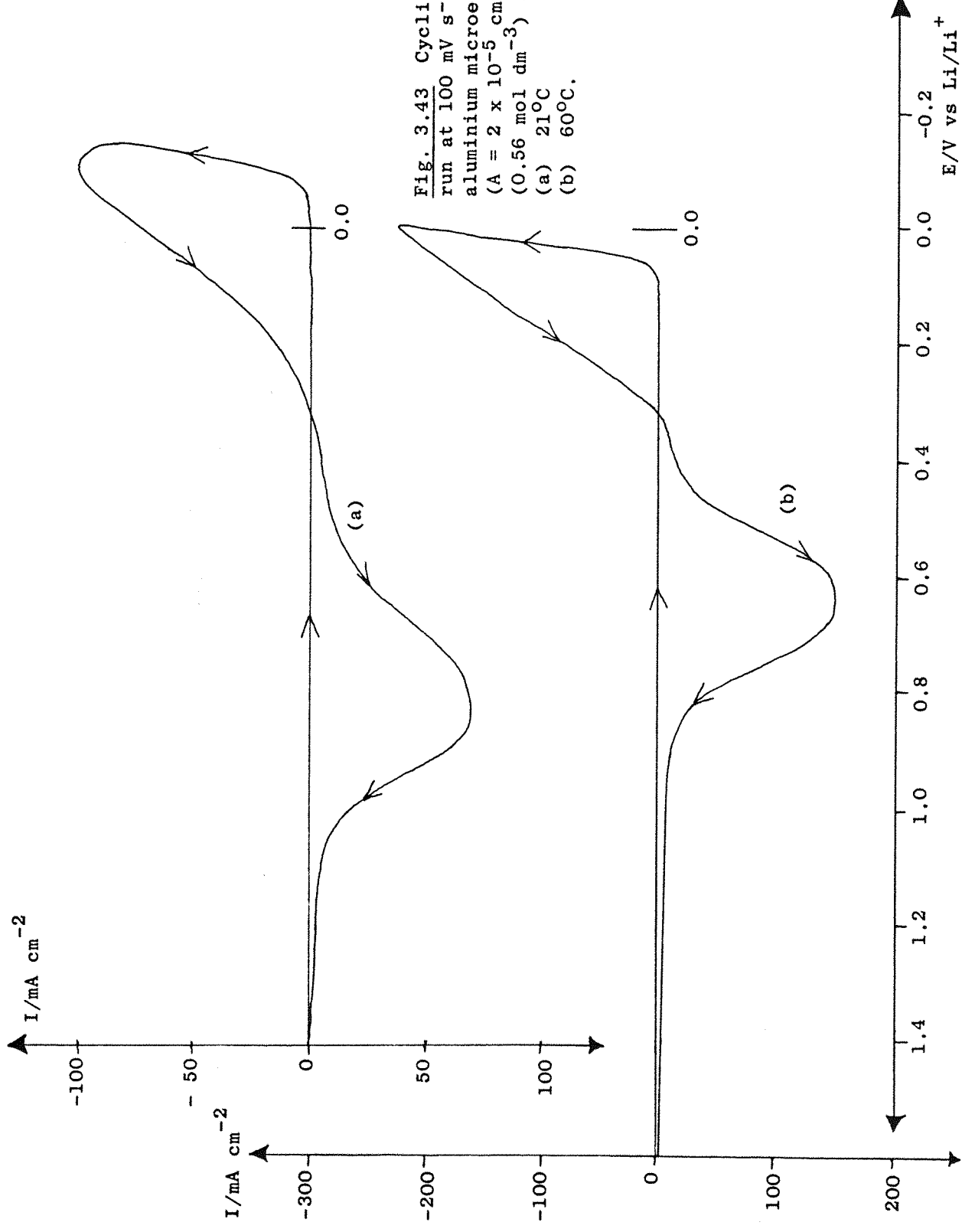


Fig. 3.43 Cyclic voltammograms run at  $100 \text{ mV s}^{-1}$  using an aluminium microelectrode ( $A = 2 \times 10^{-5} \text{ cm}^2$ ) in  $\text{THF}/\text{LiAsF}_6$  ( $0.56 \text{ mol dm}^{-3}$ ) at  
 (a)  $21^\circ\text{C}$   
 (b)  $60^\circ\text{C}$ .

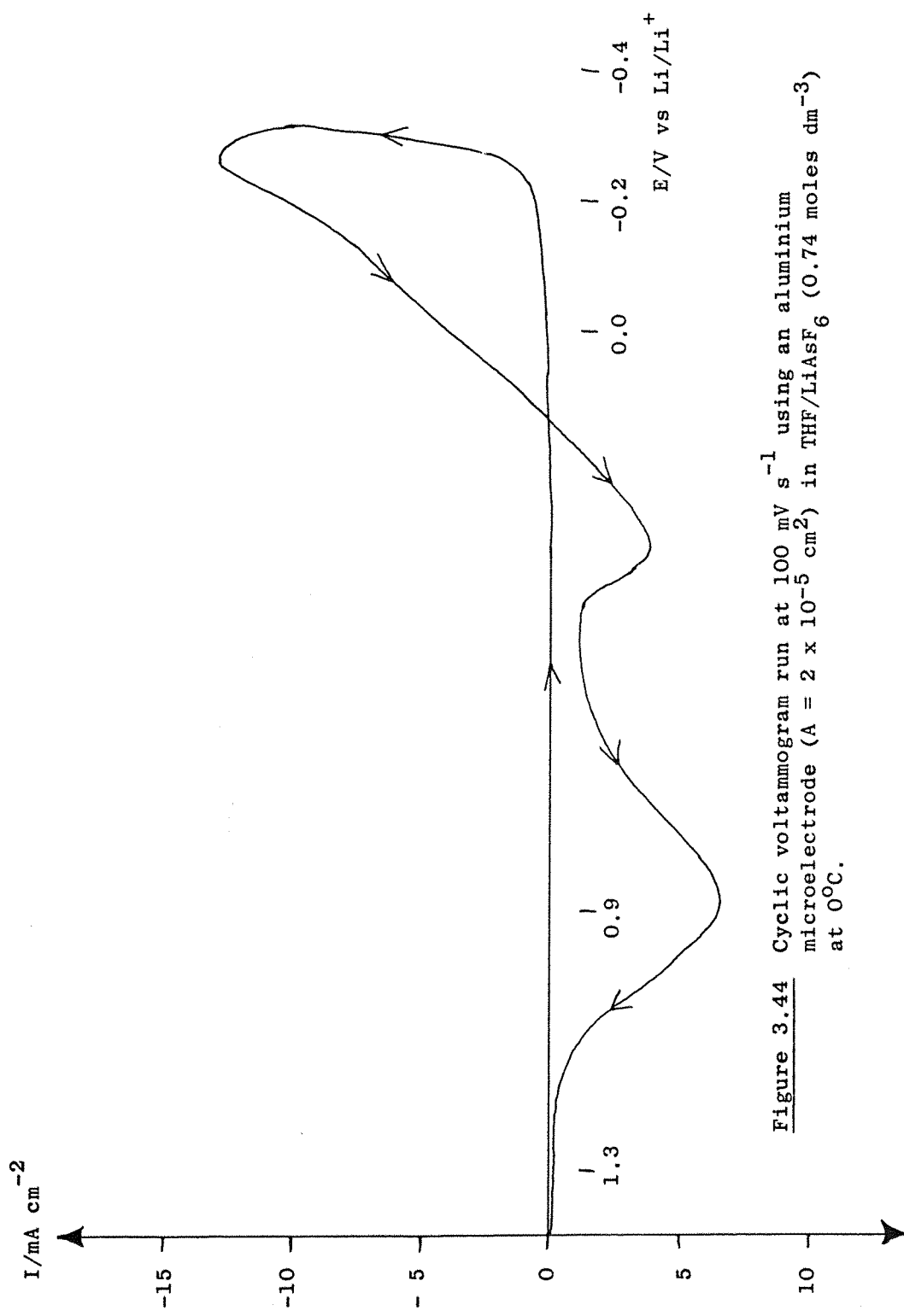


Figure 3.44 Cyclic voltammogram run at  $100 \text{ mV s}^{-1}$  using an aluminium microelectrode ( $A = 2 \times 10^{-5} \text{ cm}^2$ ) in  $\text{THF}/\text{LiAsF}_6$  (0.74 moles  $\text{dm}^{-3}$ ) at 0°C.

low overpotentials.

These results reflect how strongly the mobility of lithium in aluminium is affected by temperature. As the temperature is reduced, the mobility of the lithium in aluminium is greatly reduced and instead of moving quickly into the metal, it sits on the surface, slowly forming the alloy. Thus at intermediate temperatures,  $10^{\circ}\text{C}$  to  $-10^{\circ}\text{C}$ , two peaks are seen: one due to the removal of lithium sitting on the surface of the electrode and one due to removal of the lithium from the alloy. It would be expected that at still lower temperatures, the diffusion of the lithium into the aluminium would be so slow that on the timescale of the cyclic voltammogram, no alloy would be formed and the electrode would behave as an inert one such as copper. Unfortunately, no experiments were done to verify this.

### 3.4 Variation of solvent and electrolyte salt

Many combinations of solvent, electrolyte salt and mixtures of these are used in lithium batteries. In this work several examples were chosen which are commonly in use and these were compared with the THF/LiAsF<sub>6</sub> system.

#### 3.4.1 Variation of solvent

Figure 3.45 compares the cyclic voltammograms, run at  $100 \text{ mV s}^{-1}$ , using a copper microelectrode ( $r = 40 \mu\text{m}$ ), for solutions of LiAsF<sub>6</sub> in propylene carbonate, dioxolane and 2-methyltetrahydrofuran. All of the voltammograms show the same features as the ones run in the THF/LiAsF<sub>6</sub> electrolyte, although, as expected, variations in parameters such as the nucleation overpotential and stripping efficiencies do exist. These solvents have not been studied in detail but one important feature to be noted is that with 2-Me-THF the slope of the I-E response at negative potentials is less than with propylene

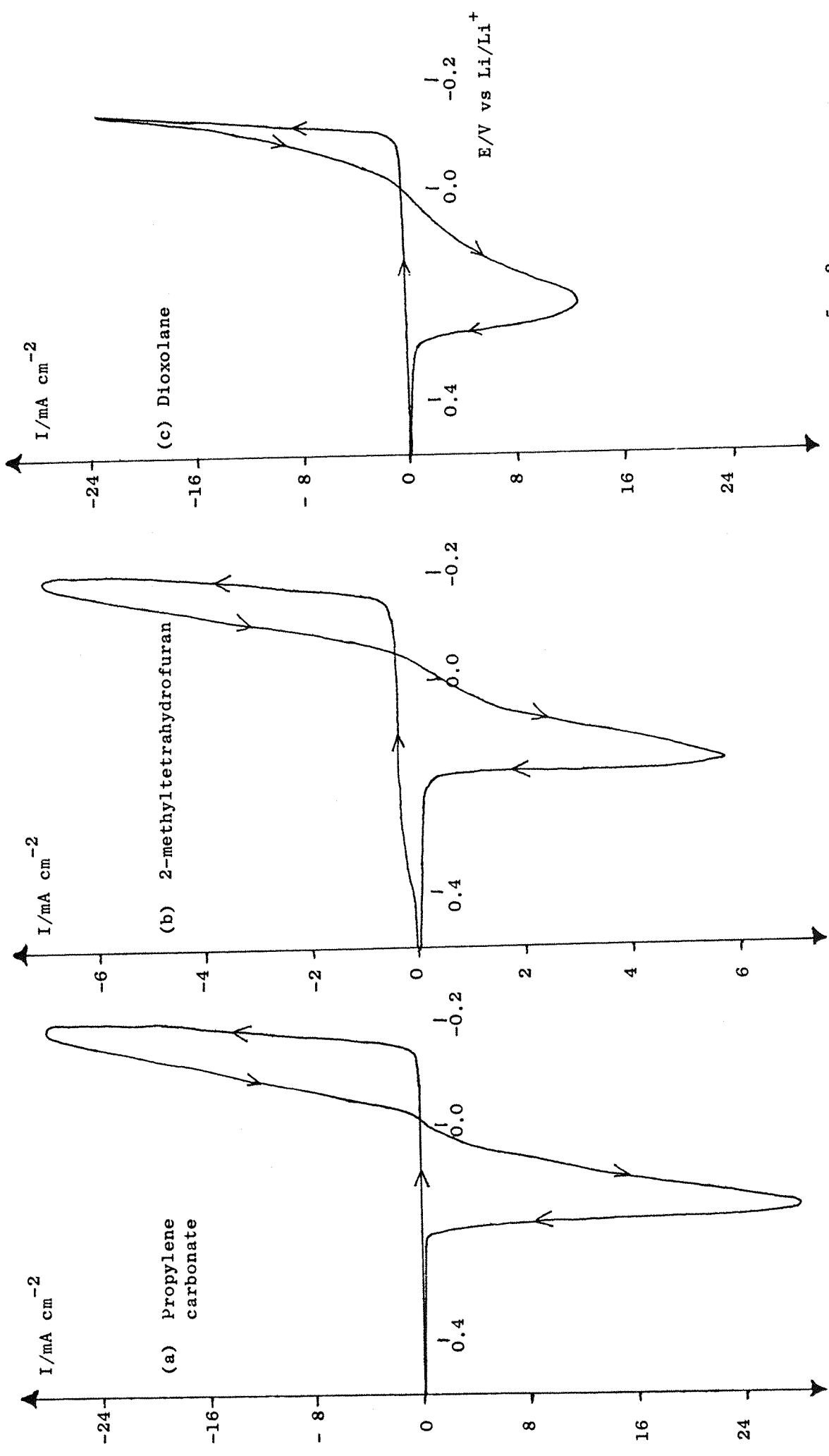


Figure 3.45 Cyclic voltammograms run at  $100 \text{ mV s}^{-1}$  using a copper microelectrode ( $A = 5 \times 10^{-5} \text{ cm}^2$ ) in various solvents.  
 (a)  $[\text{LiAsF}_6] = 0.80 \text{ mol dm}^{-3}$ , (b)  $[\text{LiAsF}_6] = 0.39 \text{ mol dm}^{-3}$ , (c)  $[\text{LiAsF}_6] = 0.81 \text{ mol dm}^{-3}$ .

carbonate, THF or dioxolane and hence the metal deposition charge is less. This may reflect the lower value of the dielectric constant for 2-Me-THF (see table 1.2).

### 3.4.2 Variation of lithium salt

It was the intention of this work to run a series of cyclic voltammograms using electrolytes comprised of various lithium salts dissolved in THF. However, both lithium bromide and lithium hexafluorophosphate ( $\text{LiPF}_6$ ) were found to be insoluble in THF and consequently the only salt, other than lithium hexafluoroarsenate, studied so far was lithium tetrafluoroborate ( $\text{LiBF}_4$ ).

Cyclic voltammograms were run at  $100 \text{ mV s}^{-1}$ , using a copper microelectrode ( $r = 40 \mu\text{m}$ ), in a solution of  $\text{THF}/\text{LiBF}_4$  (0.84 moles  $\text{dm}^{-3}$ ). The voltammograms were identical to those obtained in the  $\text{THF}/\text{LiAsF}_6$  media and showed the expected responses to variations in sweep rate and negative potential limit.

### 3.5 Galvanostatic deposition of lithium onto copper and nickel macroelectrodes

An aim of this work was to define conditions for electroplating a compact layer of lithium of approximately  $50 \mu\text{m}$  thickness onto an electrode of area approaching  $1 \text{ cm}^2$ . Copper and nickel electrodes were chosen for study; details of their construction and physical properties are given in section 2.2(c).

Taking the density of lithium to be  $0.534 \text{ g cm}^{-3}$  and the atomic weight to be  $6.94 \text{ g mole}^{-1}$  and assuming the deposition efficiency to be 100%, means that  $37 \text{ C cm}^{-2}$  of charge are required to provide a  $50 \mu\text{m}$  thick deposit.

Table 3.4 summarises the observations made for deposits formed on both the copper and nickel electrodes at various constant current densities. Unfortunately, it was only possible to assess the deposit quality by eye. All of the deposits were dull grey in

Electrode (surface area)	Concentration of LiAsF <sub>6</sub> (moles dm <sup>-3</sup> )	Constant current density (mA cm <sup>-2</sup> )	Charge density passed (C cm <sup>-2</sup> )	Observation
Copper disc (0.38 cm <sup>2</sup> )	0.59	10.0	34.2	Non-uniform deposit. Centrally smooth but with a very dendritic edge. Dull grey in colour.
	0.98	4.0	40.6	A larger counter electrode was used to try and reduce the dendrites. However, the whole deposit was very dendritic and dull grey in colour. When plunged into water the deposit underwent an explosive reaction.
	0.52	3.1	32.1	Centrally smooth deposit with a dendritic edge. Dull grey in colour.
	0.56	0.2	30.9	Visually smooth over almost all of the electrode. A very thin dendritic edge was present. Dull grey in colour.
	0.38	5.7	32.8	Similar in appearance to the deposit on copper formed at 0.2 mA cm <sup>-2</sup> despite the current density being a factor of 28 higher. Dull grey in colour.
	0.78	10.0	37.0	Dull grey deposit. Centrally smooth but with a dendritic edge.

Table 3.4

Observations of the lithium deposits on copper and nickel macroelectrodes  
in THF/LiAsF<sub>6</sub>.

colour and had to some extent dendritic edges. The use of a larger counter electrode was found to reduce the amount of dendritic growth and provide a smoother deposit. These preliminary studies suggested that smoother deposits are obtained on nickel than on copper for a given current density. As expected, the use of a lower current density always provides a smoother deposit.

In all cases, the immersion of the deposit into a beaker of water produced a violent reaction, which for the more dendritic deposits led to an explosion. This gives a good indication as to how reactive the freshly deposited lithium metal is when it is recalled that a piece of lithium foil undergoes a much milder reaction with water. This high reactivity is probably due to a combination of the absence of a protective film on the lithium deposit and the high surface area of the deposit due to dendritic growth.

Koch<sup>28</sup> has obtained specular, dendrite free, lithium deposits equivalent to  $50 \text{ C cm}^{-2}$  at  $1 \text{ mA cm}^{-2}$  in a blended THF/diethyl ether/LiAsF<sub>6</sub> electrolyte whilst Abraham et al<sup>30</sup> have shown that the addition of 2-methylfuran to a THF/2-Me-THF based electrolyte improves the deposit morphology. As stated in the introduction (section 1.4) many authors are now considering various methods for improving the lithium deposit morphology.

CHAPTER FOUR

CONCLUSIONS

## CONCLUSIONS

It is clear that a much more detailed knowledge of the lithium electrode is required for the future development of secondary lithium cells and the improvement of existing primary batteries. However, the objective of this study was not to solve particular lithium battery problems but rather to demonstrate the range of experiments possible with microelectrodes and the wealth of detailed information about the fundamental electrochemistry of the lithium electrode which may be obtained.

In this respect, the most important conclusion from this work is that meaningful and reproducible experimental data, free from distortion due to  $iR$  effects, using solvents with low dielectric constants (such as ethers which are commonly of interest in rechargeable lithium batteries) may be obtained. Moreover, the experiments employ only a two electrode cell, the electrodes are easily and cheaply manufactured and the control circuit is simple and inexpensive. Such simplicity results from the very low currents passing through the cell: for example, with a working electrode of area  $5 \times 10^{-5} \text{ cm}^2$  the current flowing through the cell is only  $5 \mu\text{A}$  even at a current density of  $100 \text{ mA cm}^{-2}$ . Such low currents result in the minimum of ohmic losses and so are truly representative of any electrochemical processes. The absence of significant IR drop was shown by the use of even smaller electrodes of area  $1.25 \times 10^{-5} \text{ cm}^2$ . Microelectrodes also allow the study of very fast electrochemical processes because they discriminate between the faradaic and charging currents on a much shorter timescale than conventional macroelectrodes and the steady state rate of diffusion to such a small electrode is much higher. In these studies, the freedom from charging currents on the timescale of the experiments is a considerable advantage.

The cyclic voltammetry and potential step experiments have demonstrated that reproducible data may be obtained and explained in terms of the deposition of lithium metal. It has been shown

that under the conditions used to study the lithium electrode the kinetics of the  $\text{Li}/\text{Li}^+$  couple are fast although the couple is not totally reversible. This was proved by running cyclic voltammograms at various temperatures which showed that the kinetics are very strongly influenced by temperature. This is in agreement with the observed deterioration in the performance of lithium batteries, based on ether type solvents, when the temperature is below  $0^\circ\text{C}$ . A value for the exchange current density of  $5.4 \text{ mA cm}^{-2}$  and the standard rate constant,  $k^\circ$ , of  $5.6 \times 10^{-5} \text{ cm s}^{-1}$  for the  $\text{Li}/\text{Li}^+$  couple at room temperature has been determined and this is in quantitative agreement with the observed behaviour of the lithium electrode during cyclic voltammetric studies.

Cyclic voltammetry has also been used in an attempt to study the underpotential deposition of lithium metal onto a copper substrate as this has been reported in the literature<sup>60-62</sup>. However, no convincing results were obtained to suggest that this phenomenon occurs in a THF/LiAsF<sub>6</sub> electrolyte although further studies must be carried out before any definite conclusions can be drawn.

Recently, Moshtev in a review<sup>16</sup> concerning previous studies on the lithium electrode, suggested that the idea of a film free lithium surface was a fictional one. However, the results of this study are contrary to this statement and suggest that film free lithium deposits may, in fact, be formed. The reproducibility and nature of the data suggests that while a freshly deposited lithium surface is maintained at negative overpotentials it does not have time to undergo chemical reaction because it is continually being covered by fresh lithium layers and is cathodically protected.

The observation that the back sweep of the cyclic voltammograms passes exactly through 0.0V on the potential axis is a good indication that the deposit is lithium without a film. (The effect of surface films on the counter electrode are negligible due to the extremely

low current densities at an electrode of such large surface area). Moreover, the fact that the stripping efficiency is 100% for these cyclic voltammograms, supports this hypothesis of a surface free film.

However, the results of section 3.1.8 show that a film does form on the lithium surface relatively quickly on open circuit. No experiments aimed at studying the nature of this film were carried out and it is not known whether it arises from reaction of the lithium with the solvent, lithium salt or trace impurities.

The mechanism of the deposition of lithium onto copper also has been studied using a potential step technique. The reasonable fitting of the data so obtained to an  $I-t^{\frac{3}{2}}$  relationship suggests that lithium deposition occurs via the progressive nucleation of centres which grow three dimensionally under diffusion control. This proposed mechanism is in agreement with the total shape of the transients.

The use of nickel and carbon microelectrodes gave cyclic voltammograms which were similar to those using copper and are clearly those for a non-alloying electrode. The results, however, do indicate the significant differences in the nucleation characteristics of the lithium on these various substrates.

Cyclic voltammetric and potential step techniques were also used to study the alloying process of freshly deposited lithium with an aluminium electrode. It has been shown that the low rate of diffusion of lithium atoms in the aluminium lattice is an important factor in the kinetics of the  $\text{LiAl}/\text{Li}^+$  couple. This was further shown by cyclic voltammograms run at various temperatures which showed that both the kinetics of alloy formation and the mobility of lithium atoms in the aluminium are strongly dependent on temperature. The shape of the transients in response to the potential step experiments clearly indicate the need for the nucleation and growth of lithium centres on the

aluminium as being the initial step in the deposition process.

Preliminary studies on the deposition of lithium using other solvents, namely propylene carbonate, dioxolane, 2-methyl-tetrahydrofuran and salts,  $\text{LiBF}_4$ , have resulted in <sup>Cyclic Voltammograms similar to</sup>  $\text{LiAsF}_6$  those obtained in electrolytes. Thus although there will be some differences, it is probable that very similar deposition mechanisms apply in these electrolytes.

The deposition of relatively thick deposits of lithium, here 50  $\mu\text{m}$ , onto a macroelectrode, has been studied briefly as a function of electrode material and plating current density. These early studies have suggested that the lithium deposits are relatively uneven morphologically as seen by the dendritic edges and dull grey colour. Improvements were made, however, by the use of a larger counter electrode and lower current densities. The high chemical reactivity of the lithium deposits, as seen by their explosive reaction with water, is probably a consequence of the high surface area of the deposit and the absence of thick protective films on the lithium surface. This aspect of these lithium deposits may well find use in the development of very high energy density lithium batteries (both primary and secondary) and in the electro-organic synthesis of lithium alkyl reagents.

### References

1. N.A. Hampson, M. Hughes and S.A.G.R. Karunathilaka, J. Power Sources, in press.
2. W.S. Harris, Thesis, University of California, Berkeley, 1958.
3. E.P. Dousek, J. Jansta and J. Riha, J. Electroanal. Chem., 46 (1973) 281.
4. A.N. Dey, Electrochemical Society Fall Meeting, 1970, Electrochemical Society, Princeton, N.J., Extended abstracts, No.62.
5. I.A. Kedrinskii, S.V. Morosov, G.I. Sukhova and L.A. Sukhova, Soviet Electrochem., 12 (1977) 1094.
6. A.N. Dey, Thin Solid Films, 43 (1977) 131.
7. G.K. Chandler and D. Pletcher, Specialist Periodical Reports on Electrochemistry, 10 (1985) in press.
8. W.R. Fawcett, Soviet Electrochem., 19 (1983) 1044.
9. A. Lundén, J. Power Sources, 11 (1984) 91.
10. A. Hooper and B.C. Tofield, J. Power Sources, 11 (1984) 33.
11. C.A. Vincent, New Scientist, (1984), March 29th issue.
12. J.O. Besenhard and G. Eichinger, J. Electroanal. Chem., 68 (1976) 1.
13. D. Linden, J. Power Sources, 11 (1984) 87.
14. B. Scrosati, J. Power Sources, 11 (1984) 129.
15. "Lithium Batteries", Ed. J.P. Gabano, Academic Press, London, 1983.
16. R.V. Moshtev, J. Power Sources, 11 (1984) 93.
17. M. Fleischmann and H.R. Thirsk, Adv. Electrochem. Electrochem. Eng., 3 (1963) 123.
18. J.A. Harrison and H.R. Thirsk, "Guide to the Study of Electrode Kinetics", Academic Press, 1972.
19. S. Fletcher, J. Chem. Soc., Faraday Trans. 1, 79 (1983) 467.
20. V.R. Koch, J. Power Sources, 6 (1981) 357.
21. R.D. Rauh and S.B. Brummer, Electrochim. Acta, 22 (1977) 75.

22. V.R. Koch and J.H. Young, *J. Electrochem. Soc.*, 125 (1978) 1371.
23. V.R. Koch, *ibid.*, 126 (1979) 181.
24. V.R. Koch and J.H. Young, *Science*, 204 (1979) 499.
25. J.L. Goldman, R.M. Mank, J.H. Young, V.R. Koch, *J. Electrochem. Soc.*, 127 (1980) 1461.
26. K.M. Abraham, J.L. Goldman and M.D. Dempsey, *ibid.*, 128 (1981) 2493.
27. K.M. Abraham, J.L. Goldman and D.L. Natwig, *ibid.*, 129 (1982) 2404.
28. V.R. Koch, J.L. Goldman, C.J. Mattos and M. Mulvaney, *ibid.*, 129 (1982) 1.
29. K.M. Abraham, P.B. Harris and D.L. Natwig, *ibid.*, 130 (1983) 2309.
30. K.M. Abraham, J.S. Foos and J.L. Goldman, *ibid.*, 131 (1984) 2197.
31. R. Jasinski, *Adv. Electrochem. Electrochem. Eng.*, 8 (1971) 253.
32. R. Selim and P. Bro, *J. Electrochem. Soc.*, 121 (1974) 1457.
33. J. Jorné and C.W. Tobias, *J. Appl. Electrochem.*, 5 (1975) 279.
34. E. Peled, *J. Electrochem. Soc.*, 126 (1979) 2047.
35. Y. Geronov, F. Schwager and R.H. Muller, *ibid.*, 129 (1982) 1422.
36. P.G. Glugla, *ibid.*, 130 (1983) 113.
37. J.S. Foos and J. McVeigh, *ibid.*, 130 (1983) 628.
38. J. Butler, D. Cogley and J. Synnot, *J. Phys. Chem.*, 73 (1969) 4026.
39. R. Scarr, *J. Electrochem. Soc.*, 117 (1970) 295.
40. S. Meibuhr, *ibid.*, 117 (1970) 56.
41. M. Garreau, J. Thevenin and D. Warin, *Progr. Batt. Solar Cells*, 2 (1979) 54.
42. J.O. Besenhard, *J. Electroanal. Chem.*, 94 (1978) 77.
43. E.J. Frazer, *ibid.*, 121 (1981) 329.

44. F.E. Dinkevich, V.G. Artamonov, V.Z. Moskovskii and V.A. Barsukov, Soviet Electrochem., 17 (1981) 106.
45. T. Takei, J. Appl. Electrochem., 9 (1979) 587.
46. Y. Matsuda, M. Morita, K-ichi Takata, J. Electrochem. Soc., 131 (1984) 1991.
47. A. Baranski and W.R. Fawcett, J. Electroanal. Chem., 94 (1978) 237.
48. A. Baranski and W.R. Fawcett, J. Chem. Soc. Faraday Trans. 1, 76 (1980) 1962.
49. A.N. Dey, J. Electrochem. Soc., 118 (1971) 1547.
50. B.M. Rao, R.W. Francis and H.A. Christopher, *ibid.*, 124 (1977) 1490.
51. J.O. Besenhard, J. Electroanal. Chem., 94 (1978) 77.
52. I. Epelboin, M. Froment, M. Garreau, J. Thevenin and D. Warin, J. Electrochem. Soc., 127 (1980) 2100.
53. E.J. Frazer, J. Electroanal. Chem., 121 (1981) 329.
54. A.S. Baranski and W.R. Fawcett, J. Electrochem. Soc., 129 (1982) 901.
55. T.R. Jow and C.C. Liang, *ibid.*, 129 (1982) 1429.
56. Y. Geronov, P. Zlatilova and G. Staikov, Electrochim. Acta, 29 (1984) 551.
57. A.S. Baranski, W.R. Fawcett, T. Krogulec and M. Drogowska, J. Electrochem. Soc., 131 (1984) 1750.
58. E. Peled, A. Lombardi and C.R. Schlaikjer, *ibid.*, 130 (1983) 1365.
59. D.M. Kolb, Adv. Electrochem. Electrochem. Eng., 11 (1976) 125.
60. I. Fried and H. Barak, J. Electroanal. Chem., 30 (1971) 279.
61. D.M. Kolb, M. Przasnyski and H. Gerischer, *ibid.*, 54 (1974) 25.
62. I. Morcos, *ibid.*, 66 (1975) 250.
63. D.M. Kolb and H. Gerischer, Surface Science, 51 (1975) 323.
64. Handbook of Chemistry and Physics, CRC Press, 1972.

65. R.M. Wightman, Anal. Chem., 53 (1981) 1125A.
66. M.I. Montenegro, Port. Electrochim. Acta, in press.
67. M. Fleischmann, F. Lasserre, J. Robinson and D. Swan, J. Electroanal. Chem., in press.
68. J.O. Howell, J.M. Goncalves, C. Amatore, L. Klasinc, R.M. Wightman and J.K. Kochi, J. Am. Chem. Soc., 106 (1984) 3968.
69. R. Lines and V.D. Parker, Acta Chemica Scandinavica, B, 31 (1977) 369.
70. A.M. Bond, M. Fleischmann and J. Robinson, J. Phys. Chem., in press.
71. A.M. Bond, M. Fleischmann and J. Robinson, J. Electroanal. Chem., 168 (1984) 299.
72. D. Ilkovic, Coll. Czech. Chem. Comm., 8 (1936) 13.
73. G. Gunawardena, G. Hills and B. Scharifker, J. Electroanal. Chem., 130 (1981) 81.
74. B. Scharifker and G. Hills, ibid., 130 (1981) 99.
75. Solidisk Technology Ltd., Southend-on-Sea, Essex, England.
76. M. Lain and D. Pearce, Electrochem. Group, Univ. Southampton.
77. L.G. Irr, Electrochim. Acta, 29 (1984) 1.
78. J.D. Genders and D. Pletcher, unpublished results.